UNCLASSIFIED

GEMP-106A

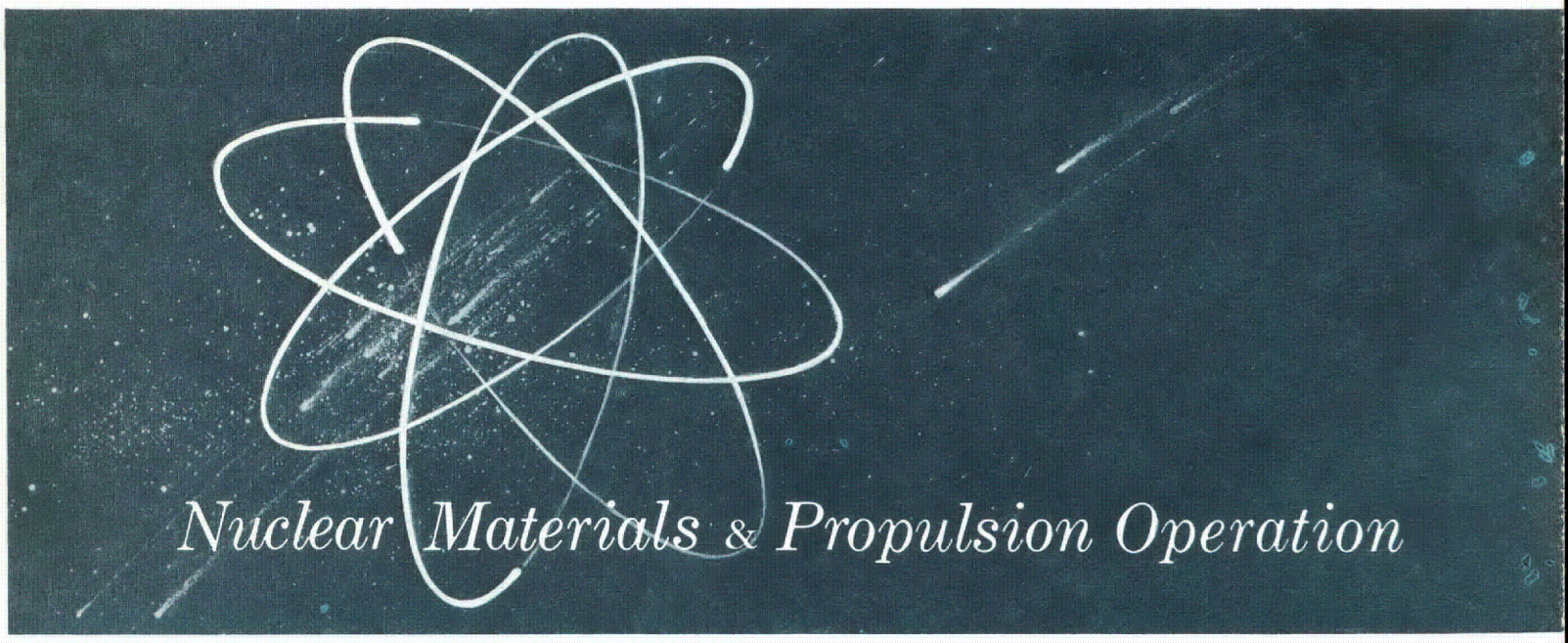

FIRST ANNUAL REPORT - HIGH-TEMPERATURE MATERIALS AND REACTOR COMPONENT DEVELOPMENT PROGRAMS

Volume I - Materials

February 28, 1962

FLIGHT PROPULSION LABORATORY DEPARTMENT
GENERAL ELECTRIC

UNCLASSIFIED

Printed in USA. Price $2.50. Available from the

Office of Technical Services
U. S. Department of Commerce
Washington 25, D. C.

GEMP-106A

UC-25 – Metals,
Ceramics, and Materials
TID-4500 (17th Ed.)

FIRST ANNUAL REPORT - HIGH-TEMPERATURE MATERIALS AND REACTOR COMPONENT DEVELOPMENT PROGRAMS

Volume I - Materials

February 28, 1962

United States Atomic Energy Commission Contract No. AT(40-1)-2847

NUCLEAR MATERIALS and PROPULSION OPERATION
FLIGHT PROPULSION LABORATORY DEPARTMENT

GENERAL ELECTRIC

Cincinnati 15, Ohio

DISTRIBUTION

EXTERNAL

AEC Headquarters
- J. M. Simmons (2)
- F. C. Schwenk
- R. G. Oehl
- G. W. Wensch
- I. Hoffman
- T. W. McIntosh
- G. M. Anderson
- F. C. Moesel

AEC, OROO
- D. F. Cope (3)
- D. S. Zachry, Jr.

AEC, COO
- B. Anderson

AEC, CAO
- C. L. Karl
- J. F. Weissenberg

AEC, NYOO
- M. Balicki
- S. Meyers

AEC, SAN
- G. R. Helfrich

Atomics International
- S. C. Carniglia

General Atomic
- F. B. Eagle
- W. C. Moore

Pratt and Whitney Aircraft (CANEL)
- L. M. Raring (3)

ORNL
- W. D. Manly
- A. J. Miller
- R. E. Clausing
- N. W. Rosenthal
- W. O. Harms
- D. A. Douglas, Jr.
- W. R. Grimes
- R. E. Blanco

BMI
- R. W. Dayton

LASL
- R. D. Baker

Lawrence Radiation Laboratory
- R. E. Batzel
- C. Cline

National Bureau of Standards
- H. S. Parker

INTERNAL

- E. A. Aitken
- W. G. Baxter
- J. R. Beeler
- J. C. Blake
- B. Blumberg
- H. C. Brassfield
- R. W. Brisken
- V. P. Calkins
- C. L. Chase (3)
- D. Cochran
- C. G. Collins
- E. S. Collins
- J. F. Collins
- P. K. Conn
- J. B. Conway
- E. B. Delson
- H. S. Edwards
- E. W. Filer
- M. Goldstein
- L. F. Hardy
- G. Korton
- L. Lomen
- W. H. Long
- R. A. Lutter
- H. F. Matthiesen
- J. A. McGurty
- J. Moteff
- R. Motsinger
- J. W. Morfitt
- G. T. Muehlenkamp
- G. Neumann
- C. E. Niemeyer
- W. E. Niemuth
- G. W. Pomeroy
- W. Z. Prickett
- F. C. Robertshaw
- T. W. Schoenberger
- R. J. Spera
- G. Thornton
- J. I. Trussell
- P. P. Turner
- F. O. Urban
- J. Van Hoomissen
- H. Wagner
- J. F. White
- D. B. Williams
- Library (5)

PREFACE

This report, GEMP-106A, is one of three volumes comprising the first annual report on the High-Temperature Materials and Reactor Component Development Programs (Contract No. AT(40-1)-2847) being conducted at the General Electric Nuclear Materials and Propulsion Operation.

Volumes I (GEMP-106A) and II (GEMP-106B) report the progress made since May 1961 on the unclassified and classified portions, respectively, of the materials program, and Volume III (GEMP-106C) reports the progress on that part of the contract covering controls and instrumentation, fasteners, and Monte Carlo computer programs. A more detailed breakdown of each volume is given below.

Progress made on ceramic fuel materials from November 15, 1961, to January 15, 1962, is included in GEMP-106A and B. This information replaces the eighth monthly progress report, which would have covered that period of ceramic fuel materials work.

GEMP-106A

1. Metallic Fuel Element in Oxidizing Atmosphere
2. High Temperature Non-Fuel Reactor Core Components
   - 2.1 Moderator Materials
   - 2.2 Control Materials
   - 2.3 Structural Materials
   - 2.4 Thermal Insulation
3. Radiation Effects
   - 3.1 Metallic Precipitation Hardening Alloys
   - 3.2 BeO

GEMP-106B

1. High Temperature Fuel Elements
   - 1.1 Metallic Fuel Element in Non-Oxidizing Atmosphere
   - 1.2 Developed Ceramic Fuel Element
   - 1.3 Stabilization of UO_2 in Ceramic Fuel Element
   - 1.4 Graphite Fuel Element in Non-Oxidizing Atmosphere
   - 1.5 Coating for Ceramic Fuel Elements
2. High Temperature Fuel
   - 2.1 UO_2-Y_2O_3
   - 2.2 Coated Fuel Particle
3. High Temperature Neutron Shield Materials
4. Fission Fragment Transport Processes in Ceramic System
5. Materials for Direct Conversion

GEMP-106C

1. Controls and Instrumentation
   - 1.1 Circulating Ball Reactivity Control
   - 1.2 Static Switching
   - 1.3 Capacitance Temperature Sensor
   - 1.4 High Temperature Extension of Conventional Nuclear Sensors
   - 1.5 Development of Nuclear Sensors
2. Fasteners
   - 2.1 High Temperature Fasteners
   - 2.2 Fasteners for Remote Maintenance
3. Monte Carlo Capabilities for Reactor Shield Analysis

CONTENTS

FIGURES

TABLES

INTRODUCTION AND SUMMARY

This report, GEMP-106A, is one of three volumes of the first annual progress report on the GE-NMPO high-temperature materials program conducted during calendar year 1961 under Contract No. AT(40-1)-2847. This volume covers seven unclassified development programs: 1. metallic fuel element materials for greater than 1200°C operation in oxidizing atmosphere; 2.1 moderator materials for use up to 1100°C for 1000 hours; 2.2 control materials capable of operating at 1100° to 1200°C or higher; 2.3 structural materials capable of operating in excess of 850°C for 1000 to 10,000 hours; 2.4 thermal insulation of minimal weight to reduce operating temperature of control and structural components; 3.1 radiation effects in high temperature alloys exposed to neutron environment at temperatures up to 870°C and dosages of 10^{19} nvt; 3.2 radiation effects in BeO as a function of composition, grain size, density, porosity, and irradiation temperature and dosage.

Significant results achieved in these programs are as follows:

The oxidation mechanism of the Fe - 25Cr - 4Al - 1Y cladding alloy has been established up to its limiting temperature of 1425°C. Compatibility with UO_2 up to 1300°C has been improved by the addition of Cr_2O_3 to the UO_2 to form a barrier of alumina to prevent Al-UO_2 reaction.

The yttrium - 5 weight percent Cr alloy, hydrided to an N_H of 5.0 to 5.3, and canned in Fe - 20Cr - 4.5Al alloy can be readily fabricated and has been operated in non-nuclear environments for periods in excess of 1000 hours at 1000°C in both high-pressure static air and 114-feet-per-second dynamic air.

Cermets of europium sesquioxide with palladium, platinum, and iridium used as a control material indicate thermal stability in air for at least 2 hours at 1400°C and above.

Foamed BeO bodies for thermal insulation have been reproducibly fabricated to a density of 1 gram per cubic centimeter and with a thermal conductivity similar to that of solid ZrO_2.

Irradiation to a dosage of about 3×10^{16} nvt ($E_n > 1$ Mev) and at pile reactor ambient temperature decreased the 100-hour stress rupture strength for alloy A-286 from 57,000 to 46,000 psi. This indicates that the apparent threshold of irradiation damage caused by neutron exposure at reactor ambient temperature is less than 3×10^{16} nvt. Irradiation caused notch weakening in contradiction to the results on the unirradiated combination bars, which showed notch strengthening in all cases.

Changes in sintered BeO bodies irradiated to 2×10^{20} neutrons per square centimeter (≥ 1 Mev) at 100°C included a "c" axis expansion seven times that in the "a" axis, approximately 0.6-percent increase in length, approximately 1.6-percent increase in volume, and approximately 1.6-percent decrease in density. At a dosage of approximately 3.5×10^{20}, the length expansion amounted to 2.08 percent. The modulus of rupture of specimens (0.238 inch in diameter by 3.5 inches long) prepared from different grades of BeO ranged from 24 to 33 percent of the unirradiated value at the 2×10^{20} dosage and 2 to 3 percent at 3.5×10^{20}. Thermal annealing of the radiation-induced expansion was dependent on dosage as well as temperature.

1. METALLIC FUEL ELEMENTS IN OXIDIZING ATMOSPHERES (57001)

The objective of this program is to develop combinations of nuclear fuel element materials capable of operating at temperatures above 1200°C, for more than 1000 hours in oxidizing atmospheres, with negligible fission fragment release.

The Fe-Cr-Al-Y alloy is one of the better oxidation-resistant materials and would be useful as a fuel element material at temperatures up to 1300°C under low stress conditions, if the reduction of the UO_2 fuel by the aluminum in the cladding can be prevented. The intermetallic alloy, Nb-Al-Ti, has excellent oxidation resistance in the temperature range from 1250° to 1370°C, and on the basis of initial tests appears to retain fission fragments at 1370°C. The problems of workability and structural stability remain to be overcome. The noble metals are oxidation-resistant to temperatures approaching their melting points but are subject to rapid sublimation of labile oxides in flowing air at high temperatures. Iridium has the highest melting point, 2450°C, and is of the greatest interest as a high-temperature fuel element material if volatilization of the oxide can be arrested.

1.1 Fe-Cr-Al-Y ALLOYS

The objective of the Fe-Cr-Al-Y alloy work is to determine the oxidation characteristics at temperatures ranging from 1200° to 1425°C in air, and to establish the time-temperature limitations of the alloy in combination with various oxide fuels. The ferrous alloy, shown by previous work to have the greatest potential for use above 1200°C, is the Fe - 25Cr - 4Al - 1Y composition. This alloy forms an aluminum oxide film which is protective for well over 1000 hours at temperatures up to 1315°C.

In previous investigations of the Fe-Cr-Al-Y alloy as a fuel element material during the ANP program, it was found that the aluminum in the alloy reduces the UO_2 fuel at temperatures of about 1200°C. Free uranium then diffused to the surface of the fuel element. Investigation of various fuels and fuel additives indicated that excess oxygen added to the UO_2 resulted in the formation of an alumina barrier between the core and the cladding, thereby preventing the Al-UO_2 reaction. This study has been continued to determine the optimum conditions for barrier formation. The successful attainment of this objective will make possible the use of Fe-Cr-Al-Y material as a fuel element cladding in oxidizing atmospheres at temperatures up to 1300°C. Additional studies were made of the oxidation mechanism and the role of yttrium, as well as methods of improving the high-temperature stability of the alloy by the elimination of low melting phases.

HIGH-TEMPERATURE STABILITY

The stability of the Fe-Cr-Al-Y alloy was determined at temperatures up to 1425°C in air for times up to 1000 hours. Specimens of Heat MS-16 (24.2Cr, 3.9Al, 0.8Y, 0.004C, 0.001Si, balance Fe by chemical analysis) 0.170, 0.126, and 0.050 inch in diameter by 0.8

inch long, were tested at 1100°, 1200°, 1315°, and 1425°C in static air. The oxidation data for typical specimens are plotted as (weight change)^2 versus time in Figure 1.1-1. At 1100°, 1200°, and 1315°C, the curves consist of two linear portions showing that a change occurs in the oxidation-controlling mechanism after extensive testing times. The parabolic rate constants, from the equation $W^2 = K_p t$ where W = mg/cm^2, K_p is the parabolic rate constant, and t is the time, are shown for each curve. The parabolic rate constants follow the Arrhenius equation up to about 1300°C.

During oxidation, grain-boundary oxidation occurs initially, together with surface film formation. Depletion of the second phase (YFe_9) occurs during testing. Measurements of external scale thickness, grain-boundary oxidation, and YFe_9 depletion on the 0.170-inch diameter specimens are given in Table 1.1-1. Measurements of YFe_9 depletion in 0.126- and 0.050-inch diameter specimens are given in Table 1.1-2. The growth of the surface oxide and the depletion of the YFe_9 phase both appear to follow parabolic rate laws as shown in Figure 1.1-2. Grain-boundary oxidation occurs rapidly during initial testing; the degree of penetration is not particularly dependent on temperature. Grain-boundary oxidation at 1200°C and 1425°C is shown in Figure 1.1-3. The grain-boundary oxides appear to perform two functions, retaining a fine grain size at the surface and anchoring the surface oxide. The surface oxide grows by diffusion of oxygen ions across the oxide layer to the oxide-metal interface. This is shown clearly in Figure 1.1-3 where, at 1425°C, the surface oxide has grown around a grain-boundary oxide. Platinum wires 0.001 inch in diameter were welded to the surface of a rod specimen and tested in air at 1300°C. The oxide film formed under the wire, again demonstrating that the oxide formed at the oxide-metal interface. The depletion of the YFe_9 phase follows a parabolic relationship with the rate-controlling step being a surface reaction. The rate of YFe_9 depletion increases as the specimen diameter is decreased. The interfacial area between the depleted zone and the matrix decreases while the surface area is constant as the depletion of the YFe_9 phase occurs.

TABLE 1.1-1

OXIDE THICKNESS, GRAIN BOUNDARY OXIDATION, AND YFe_9 DEPLETION IN 0.170-INCH-DIAMETER Fe-Cr-Al-Y SPECIMENS

Specimen No.	Temperature, °C	Time, hr	Oxide Thickness, mils	Grain Boundary Oxidation, mils	YFe_9 Depletion, mils
485	1095	925	0.2	5.7	5.9
486	1200	1	-	0.9	-
487	1200	40	-	2.6	3.5
488	1200	290	0.29	4.8	6.7
490	1200	540	0.47	5.2	8.5
492	1200	768	0.50	6.1	10.6
494	1200	1016	0.60	6.2	11.6
497	1200	1000[a]	0.52	4.9	11.5
498	1315	1	-	0.5	0.7
499	1315	40	0.30	2.9	6.6
500	1315	130	0.52	3.9	9.9
501	1315	290	0.75	4.5	14.7
502	1315	450	0.93	5.9	17.8
503	1315	630	1.40	5.7	18.0
504	1315	768	0.90	6.8	20.4
505	1315	858	1.30	6.8	22.6
506	1315	1016	0.92	7.7	25.0
507	1315	140[a]	0.70	3.5	11.7
508	1315	309[a]	1.00	4.9	17.5
509	1315	575[a]	1.04	6.0	21.8
510	1315	1000[a]	1.51	7.9	28.2
511	1425	1	-	1.0	-
519	1425	588	3.20	6.8	-

[a]Isothermal, other specimens were cycled at either 20- or 100-hour intervals. There was no difference in results and cycle time was not identified.

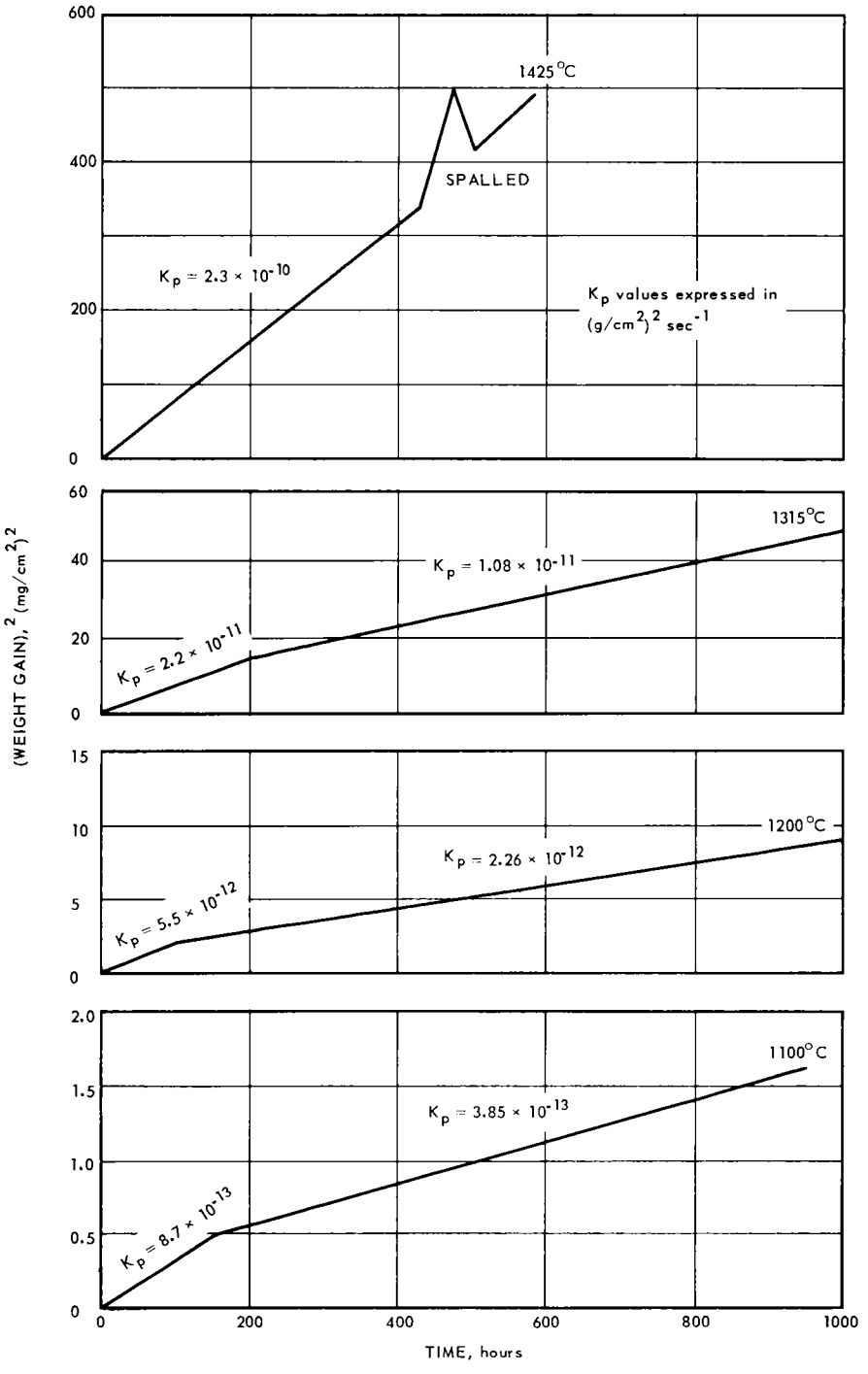

Fig. 1.1-1 – Typical curves of (weight change)^2 versus time showing parabolic nature of oxidation reaction in Fe – 25Cr – 4Al – 1Y alloy at various temperatures

TABLE 1.1-2

MEASUREMENTS OF YFe_9 DEPLETION IN 0.126- AND 0.050-INCH-DIAMETER Fe-Cr-Al-Y SPECIMENS

Specimen No.	Specimen Diameter, mils	Temperature, °C	Time, hr	YFe_9 Depletion, mils
2200-23	50	1200	248	5.1
-26	50	1200	478	7.2
-28	50	1200	638	7.3
-33	126	1200	92	4.2
-35	126	1200	248	6.2
-36	126	1200	638	8.9
2400-23	50	1315	92	9.0
-26	50	1315	318	18.2
-28	50	1315	568	Complete
-31	50	1315	728	Complete
-32	126	1315	92	8.0
-34	126	1315	318	16.0
-36	126	1315	638	21.9
-37	126	1315	728	23.9

Microstructures of tested specimens are shown in Figure 1.1-4. A fine grain size is retained at the surface and in the matrix, but the zone which is depleted of the YFe_9 phase is coarse-grained. The depleted zone is somewhat softer than the matrix but appears to be more brittle, possibly due to the large grain size. Liquation of the YFe_9 phase occurs at 1425°C with diffusion voids located near the center of the grains.

Electron microprobe studies, to determine the compositional changes which occur during oxidation and the role of yttrium in reducing oxidation, are continuing.

COMPATIBILITY WITH UO_2

The reaction between the UO_2 and aluminum in the Fe-Cr-Al-Y alloy had previously been prevented or minimized by the formation of a ceramic Al_2O_3 layer between the fuel and the cladding. To determine the methods of formation and the effects of such barriers on the reaction, simple capsule specimens containing various enriched fuel blends were tested at 1200°C and 1300°C. The Heat MS-16 capsules were machined to a diameter of 0.145 inch with 0.020-inch-thick walls. After loading with approximately 0.5 gram of fuel, the capsules were cold-swaged to compact the fuel. Initial alpha counts were less than 5 counts per minute. The fuel blends, capsule treatments, and alpha counts after 300 hours are given in Table 1.1-3. Except for Number 1 (UO_2), the fuel compositions contained excess oxygen added in the form of U_3O_8 and/or Cr_2O_3. The selection of Cr_2O_3 was based on its free energy of formation, which is lower than that of Al_2O_3 or UO_2. For this reason, the reaction between aluminum and a fuel containing Cr_2O_3 should result in the reduction of the Cr_2O_3 rather than the UO_2. Nine capsules were loaded with each of seven fuel blends. Of each group of nine specimens, four capsules were preoxidized by heating in 1200°C air for 16 hours prior to loading.

The alpha count results shown in Table 1.1-3 indicate that preoxidation of the capsule wall, the addition of U_3O_8, and the various chromium or Cr_2O_3 additions are all effective in preventing reduction of the fuel. X-ray examination showed that, in some cases, poor contact was maintained between the core and the cladding; this was particularly true of the preoxidized specimens. To obtain increased core density and maintain good contact, one specimen of each blend was alternately heated to 1300°C and cold-swaged three times, and

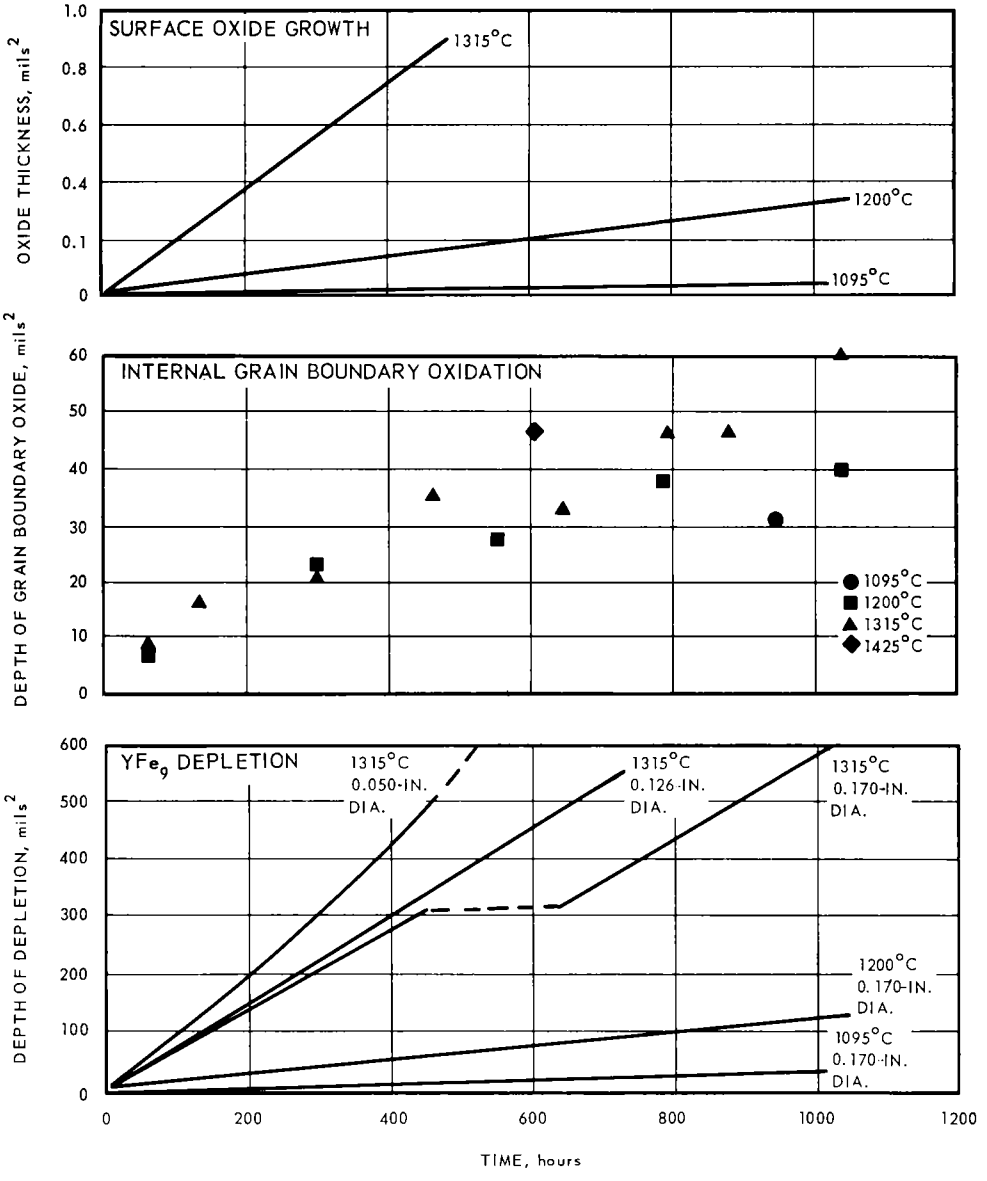

Fig. 1.1-2 – Surface oxide growth, internal oxidation, and YFe_9 depletion as a function of time for Fe-Cr-Al-Y alloy (MS-16) at various temperatures

AFTER 40 HOURS AT 1200°C

Neg. No. 564, As Polished 500 X

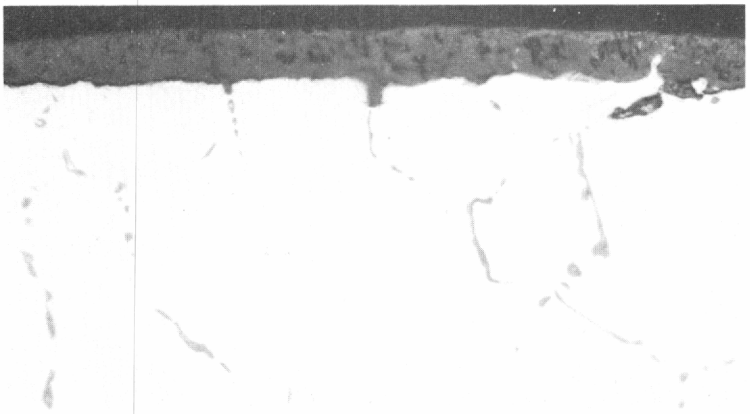

AFTER 1016 HOURS AT 1200°C

Neg. No. 565, As Polished 500 X

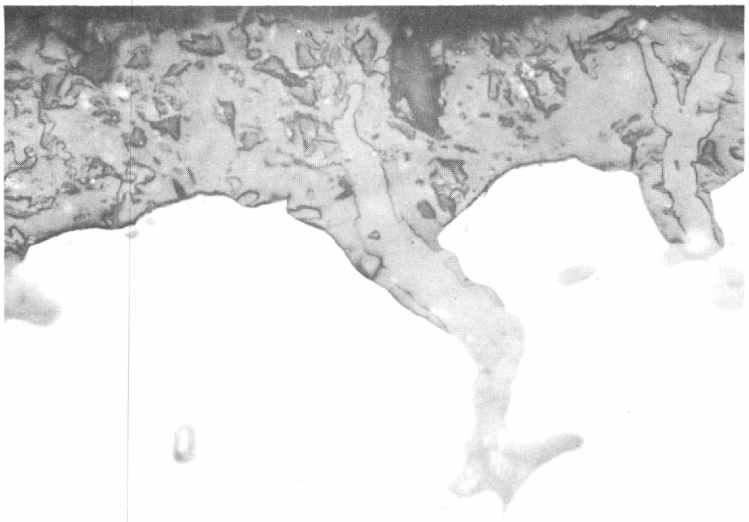

AFTER 588 HOURS AT 1425°C

Neg. No. 569, As Polished 500 X

Fig. 1.1-3 - Grain boundary oxidation in Fe-Cr-Al-Y alloy at 1200°C and 1425°C

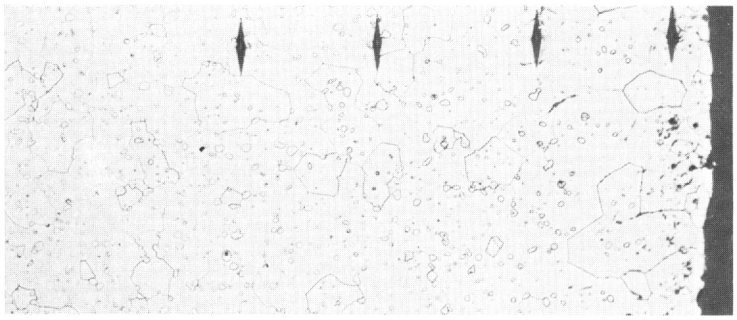

AFTER 925 HOURS AT 1095°C

Neg. No. 571 100 X

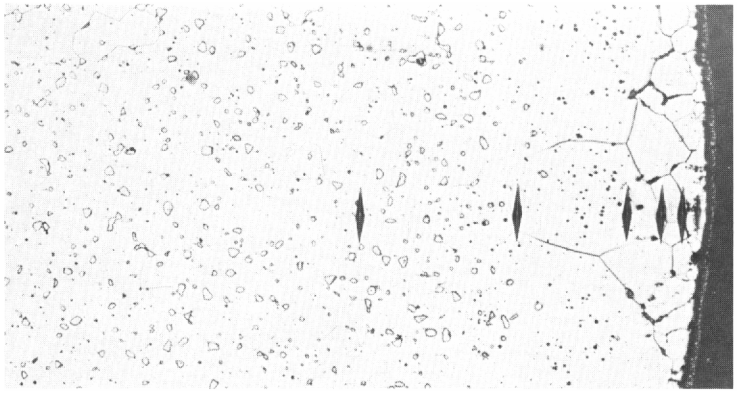

AFTER 1016 HOURS AT 1200°C

Neg. No. 572 100 X

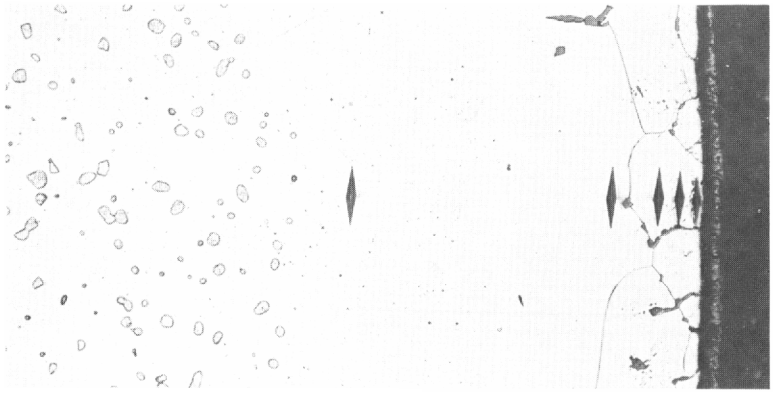

AFTER 1016 HOURS AT 1315°C

Neg. No. 573 100 X

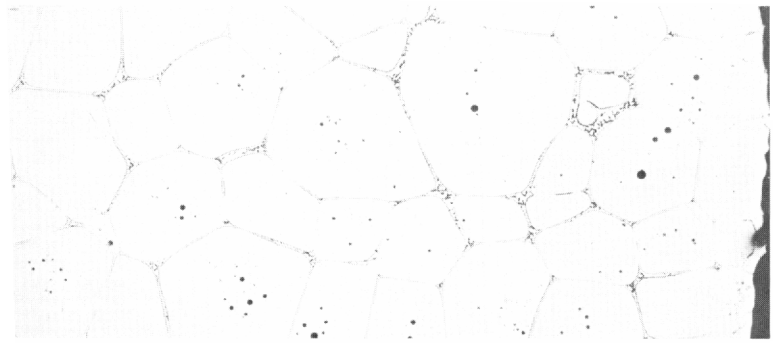

AFTER 1 HOUR AT 1425°C

Neg. No. 574 100 X

Fig. 1.1-4 – Microstructures of Fe-Cr-Al-Y specimens oxidized at temperatures of 1095° to 1425°C in static air

TABLE 1.1-3

ALPHA COUNT DATA AFTER 300 HOURS TESTING TIME FOR FUELED Fe-Cr-Al-Y (MS-16) CAPSULES AT 1200°C AND 1300°C

Fuel Blend	Specimen No.	Capsule Treatment[a]	Temperature, °C	Alpha Counts, cpm/in^2		Contact (Core-Clad)
				Total	Core Only[c]	
UO_2	1-G	1	1200	14,410	130	Good
UO_2	1-D	2	1200	30	20	Poor
UO_2	1-B	3	1200	100	30	Good
UO_2	1-H	1	1300	19,990	18,930	Good
UO_2	1-A	2	1300	60	10	Poor
1 UO_2·1 U_3O_8	2-B	1	1200	39,350	9,610	Good
1 UO_2·1 U_3O_8	2-F	2	1200	30	20	Good
1 UO_2·1 U_3O_8	2-A	3	1200	100	40	Good
1 UO_2·1 U_3O_8	2-H	1	1300	18,190	9,810	Good
1 UO_2·1 U_3O_8	2-C	2	1300	30	20	Good
U_3O_8	3-B	1	1200	70	10	Poor
U_3O_8	3-A	2	1200	20	0	Poor
U_3O_8	3-F	3	1200	20	10	Poor
U_3O_8	3-H	1	1300	30	0	Good
U_3O_8	3-D	2	1300	0	0	Poor
3 UO_2·3 U_3O_8·4 Cr	4-B	1	1200	270	10	Good
3 UO_2·3 U_3O_8·4 Cr	4-E	2	1200	10	0	Good
3 UO_2·3 U_3O_8·4 Cr	4-G	1	1300	250	10	Good
3 UO_2·3 U_3O_8·4 Cr	4-D	2	1300	50	20	Poor
3 U_3O_8·4 Cr	5-D	1	1200	720	20	Good
3 U_3O_8·4 Cr	5-E	2	1200	120	0	Poor
3 U_3O_8·4 Cr	5-B	3	1200	120	10	Good
3 U_3O_8·4 Cr	5-G	1	1300	3,300	0	Good
3 U_3O_8·4 Cr	5-C	2	1300	3,140	70	Good
9 UO_2·2 Cr_2O_3	6-I	1	1200	710	0	Good
9 UO_2·2 Cr_2O_3	6-F	2	1200	80	0	Good
9 UO_2·2 Cr_2O_3	6-G	3	1200	180	10	Good
9 UO_2·2 Cr_2O_3	6-A	1	1300	30	20	Poor
9 UO_2·2 Cr_2O_3	6-B	2	1300	120	0	Poor
9 UO_2·2 Cr_2O_3[b]	7-I	1	1200	100	40	Poor
9 UO_2·2 Cr_2O_3	7-G	1	1300	40	40	Good
9 UO_2·2 Cr_2O_3	7-D	2	1300	20	10	Good

[a]Capsule Treatment - (1) As-machined and -swaged.
(2) Oxidized at 1200°C, 16 hours.
(3) Oxidized and swaged.

[b]Fired in air at 1250°C.

[c]End plugs masked.

then tested at 1300°C for a total of 270 hours. Specimens from Blends 1, 3, and 7 were eliminated due to cracking during swaging. The data for the remaining four specimens are given in Table 1.1-4.

Metallographic examination of these specimens indicated that considerable sintering of the cores occurred initially and that good core-clad contact was maintained. Figure 1.1-5 shows cross sections of these specimens. The U_3O_8-UO_2 core-aluminum reaction resulted in internal grain-boundary oxidation of the cladding rather than formation of a continuous Al_2O_3 barrier. A continuous Al_2O_3 barrier formed at the interface of the other three specimens, even where cracks had occurred during swaging. The oxide barriers were relatively thick, measuring 0.6 to 0.7 mil. Apparently the rate of diffusion of oxygen through Cr_2O_3 is lower than through U_3O_8, thus permitting Al_2O_3-layer formation at the core-clad interface.

Because barriers of Al_2O_3 are apparently effective in preventing the core-clad reaction, depending on the form and amount of the excess oxygen and on the core geometry, these tests are being continued for longer testing times and with more cold-swaging operations to insure core-clad contact.

TABLE 1.1-4

ALPHA COUNT OF HEATED AND COLD-SWAGED SPECIMENS

Specimen No.	Fuel Blend	Alpha Count After 270 Hours At 1300°C (Core Only), cpm/in.^{2}
2-G	$1UO_2 \cdot 1U_3O_8$	25,260
4-F	$3UO_2 \cdot 3U_3O_8 \cdot 4Cr$	60
5-F	$3U_3O_8 \cdot 4Cr$	100
6-C	$9UO_2 \cdot 2Cr_2O_3$	50

1.2 Nb-Al-Ti ALLOYS

The objective of this investigation is to determine the potential of an alloy system based on the titanium-aluminum intermetallic compound, for application as a high-temperature fuel element material. From initial work, based on oxidation resistance at 1370°C, the more promising alloys were those containing niobium in solution in Ti-Al. The oxidation resistance increased with increasing niobium up to the solubility limit of 40 weight percent niobium. The oxidation rate for 500 hours at 1370°C was found to be approximately cubic, where $W^3 = kt$ (W = weight gain, t = time) with a total weight gain of about 8 mg/cm^2. The optimum composition was found to be 34Ti - 28.3Al - 37.7Nb.

This type of alloy is interesting for nuclear applications because of its relatively low density (4.41 gm/cm^3) and its thermal neutron macroscopic cross section of only 0.11 barns. Initial UO_2-alloy compatibility tests indicated that no reaction occurs between the aluminum in the alloy and the UO_2. This is attributed to the high stability of the titanium-aluminum compound. Furthermore, initial in-pile tests of UO_2 clad with Nb-Al-Ti indicated fission product release equal to or lower than that of unalloyed niobium. Among the disadvantages of this type of alloy are a relatively low melting point (1510°C) and poor fabricability due to the ordered face-centered tetragonal structure of Ti-Al.

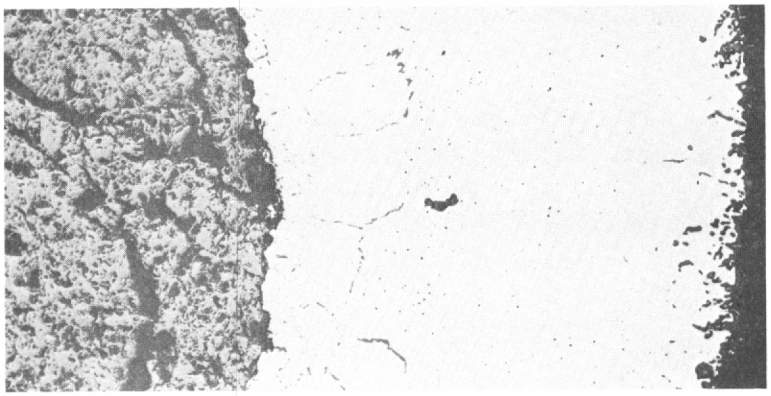

Neg. No. 620, Unetched 100 X

$1\ UO_2 \cdot 1\ U_3O_8$
NO Al_2O_3 BARRIER FORMATION
ALPHA COUNT – 25,260 CPM/IN.^{2}

Neg. No. 621, Unetched 100 X

$3\ UO_2 \cdot 3\ U_3O_8 \cdot 4\ Cr$
Al_2O_3 BARRIER FORMED
EVEN IN CRACKS
ALPHA COUNT – 60 CPM/IN.^{2}

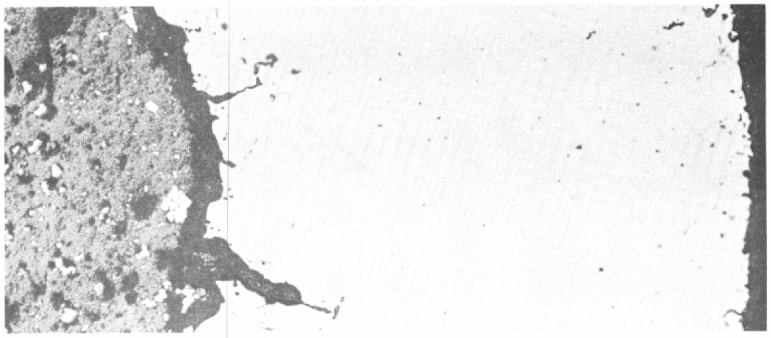

Neg. No. 622, Unetched 100 X

$3\ U_3O_8 \cdot 4\ Cr$
Al_2O_3 BARRIER FORMED
ALPHA COUNT – 100 CPM/IN.^{2}

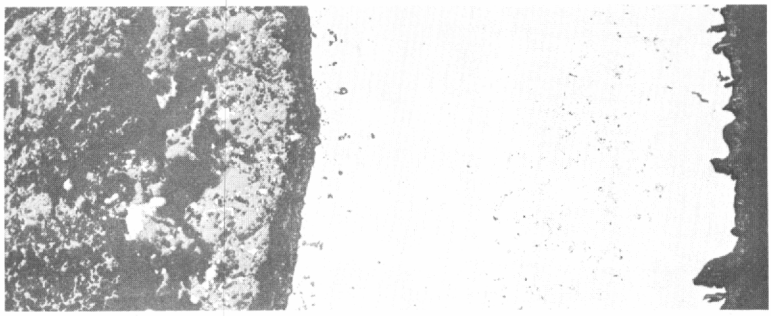

Neg. No. 623, Unetched 100 X

$9\ UO_2 \cdot 2\ Cr_2O_3$
Al_2O_3 BARRIER FORMED
ALPHA COUNT – 50 CPM/IN.^{2}

Fig. 1.1-5 – Fe-Cr-Al-Y-UO_2 compatibility specimens after 270 hours at 1300°C

HIGH-TEMPERATURE OXIDATION RESISTANCE

The Nb-Al-Ti alloy is unusual, in that its oxidation resistance improves with higher temperatures, and is excellent at 1425°C. This is illustrated in Figure 1. 2-1, which shows the oxidation rates for the 36. 7Nb - 33. 7Ti - 29. 6Al alloy at temperatures from 1150° to 1370°C. The weight losses are attributed to spalling of the oxide as the specimens cooled. A continuous weight-gain test at 1200°C performed with the use of a thermobalance demonstrated that the oxidation rate is linear, indicating the formation of a nonprotective oxide. The oxide on this specimen also spalled on cooling.

In an effort to improve the intermediate-temperature oxidation resistance, a number of alloying elements were added to the ternary composition. Chromium demonstrated the most pronounced beneficial effect on the oxidation resistance. The oxidation rates of alloys containing 3 and 6 weight percent chromium are shown in Figure 1. 2-2. The effect of chromium on improving oxide retention is obvious since the 6 weight-percent addition is much more effective than the 3 weight-percent addition of chromium.

Other studies to improve the oxidation behavior at lower temperatures consisted of preoxidation treatments at high temperatures. A series of specimens prepared from induction-melted alloys were preoxidized for 4 hours at 1370°C, and then tested with as-cast specimens at 1040°, 1150°, and 1260°C. No measurable improvement in the Nb-Al-Ti alloys was noted but the Nb-Al-Ti-Cr alloys containing low aluminum levels (27 wt.%) exhibited improved oxidation resistance. This is shown in Figure 1.2-3 for two compositions tested at 1150°C. Also shown are data for specimens that were surface-ground after preoxidation, demonstrating that the effect is due to preoxidation rather than to the thermal treatment or structural changes.

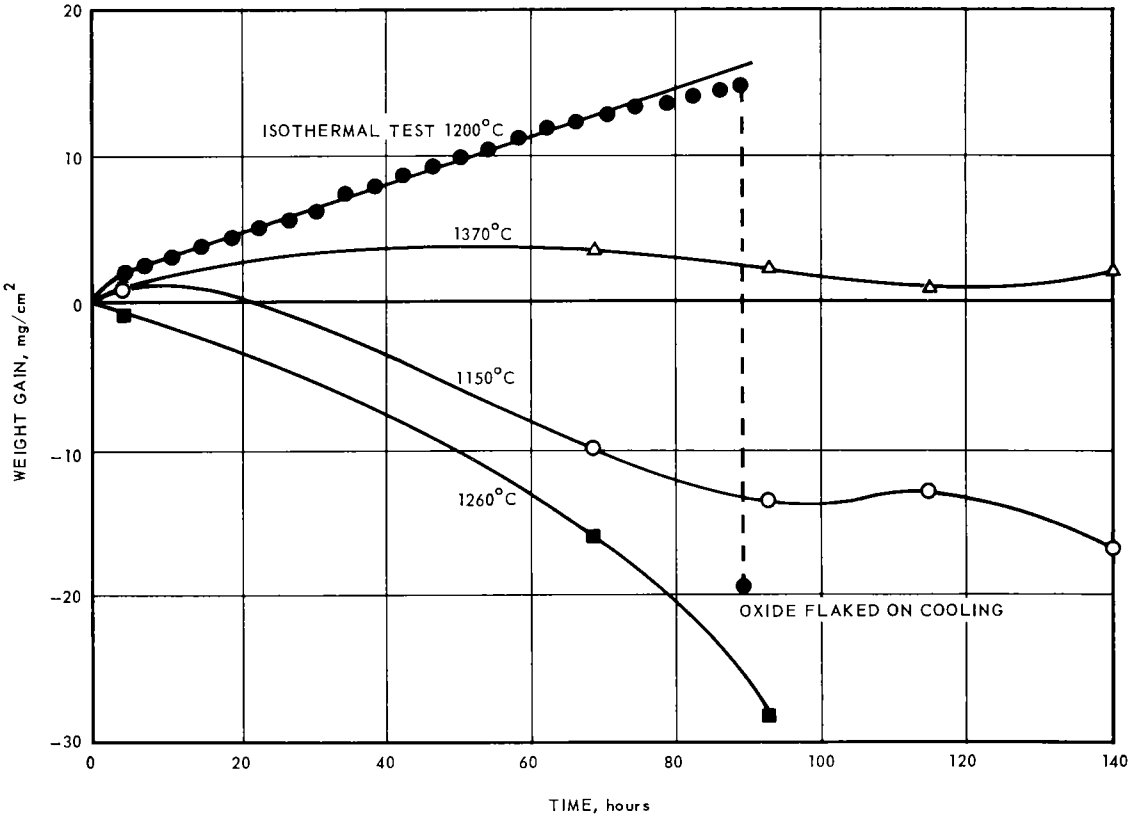

Fig. 1.2-1 – Oxidation rates of 36.7Nb – 33.7Ti – 29.6Al alloy

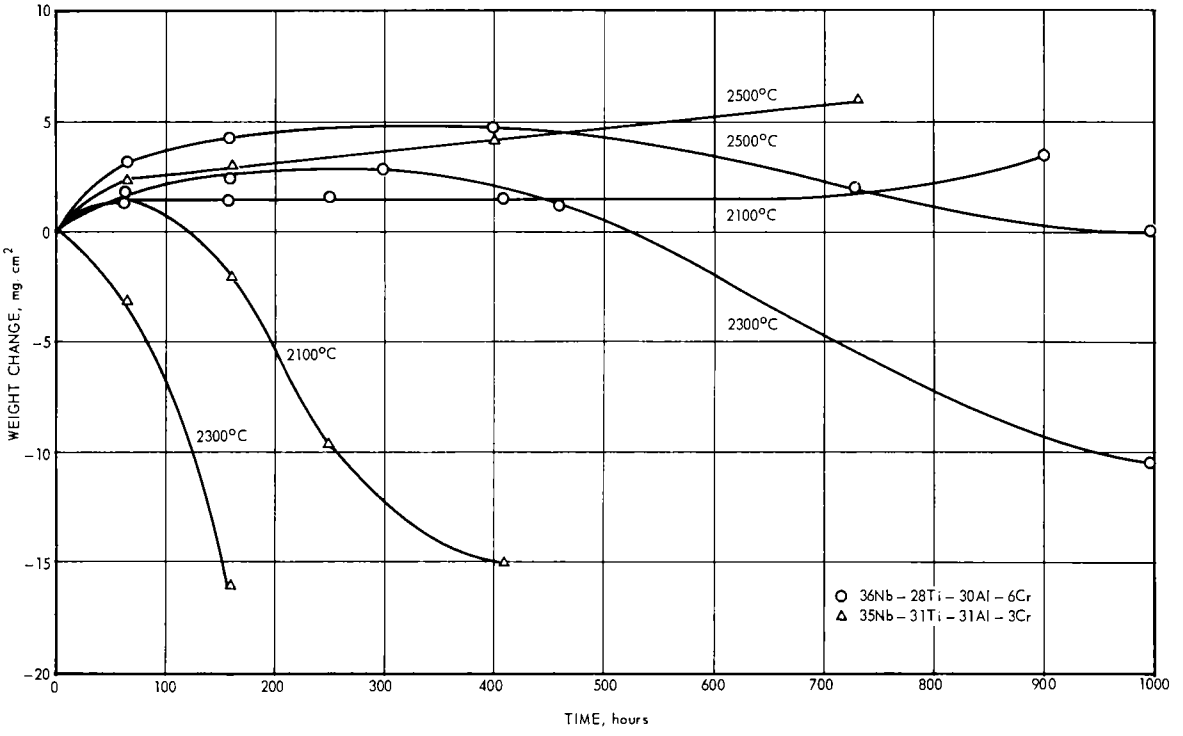

Fig. 1.2-2 – Oxidation behavior of two Nb-Al-Ti-Cr alloys in still air

While improving the oxidation behavior, the addition of chromium to the alloys precipitated a second phase which increased the brittleness of the alloy. As a result, studies were made to determine the mechanism by which chromium improves the oxidation behavior in the hope that more desirable elements than chromium could be found, which would have the same effect as chromium on oxidation resistance without increasing the brittleness.

To determine the oxidation mechanism of chromium, comparisons were made between Nb-Al-Ti and Nb-Al-Ti-Cr alloys. Metallographic analyses of specimens oxidized at 1200°, 1315°, and 1425°C demonstrated that a two-phase oxide is obtained in the Nb-Al-Ti alloy at 1200°C and 1315°C, as shown in Figure 1.2-4. The results of X-ray diffraction and electron microprobe analyses, shown in Table 1.2-1, identified the oxides as $TiO_2 + Al_2O_3$. At 1425°C, however, a continuous layer of Al_2O_3 is formed adjacent to the matrix with a two-phase oxide, $TiO_2 + Al_2O_3$, at the surface. It was also observed that a change in the structure of the matrix occurs at 1425°C because of aluminum depletion. The metallic layer adjacent to the oxide in the 1200°C and 1315°C specimens is probably Nb_3Al which forms due to depletion of aluminum and titanium. Its relatively poor oxidation resistance is therefore responsible for the lowered oxidation resistance in the 1100° to 1300°C temperature range.

The electron microprobe analyses of the alloys containing chromium additions are also given in Table 1.2-1. The microstructures of these alloys are shown in Figure 1.2-5. An Al_2O_3 scale is formed at 1200°, 1315°, and 1425°C. No titanium, niobium, or chromium was found in the oxide. At 1200°C, the second phase present in the matrix is $NbCr_2$ containing substantial amounts of titanium and aluminum. The metallic layer under the oxide is apparently Nb_3Al containing a large amount of chromium. It is apparent that the chromium increases the oxidation resistance of the Nb_3Al layer which permits preferential oxidation of the aluminum to form a continuous Al_2O_3 layer. At 1315°C, incipient melting of the

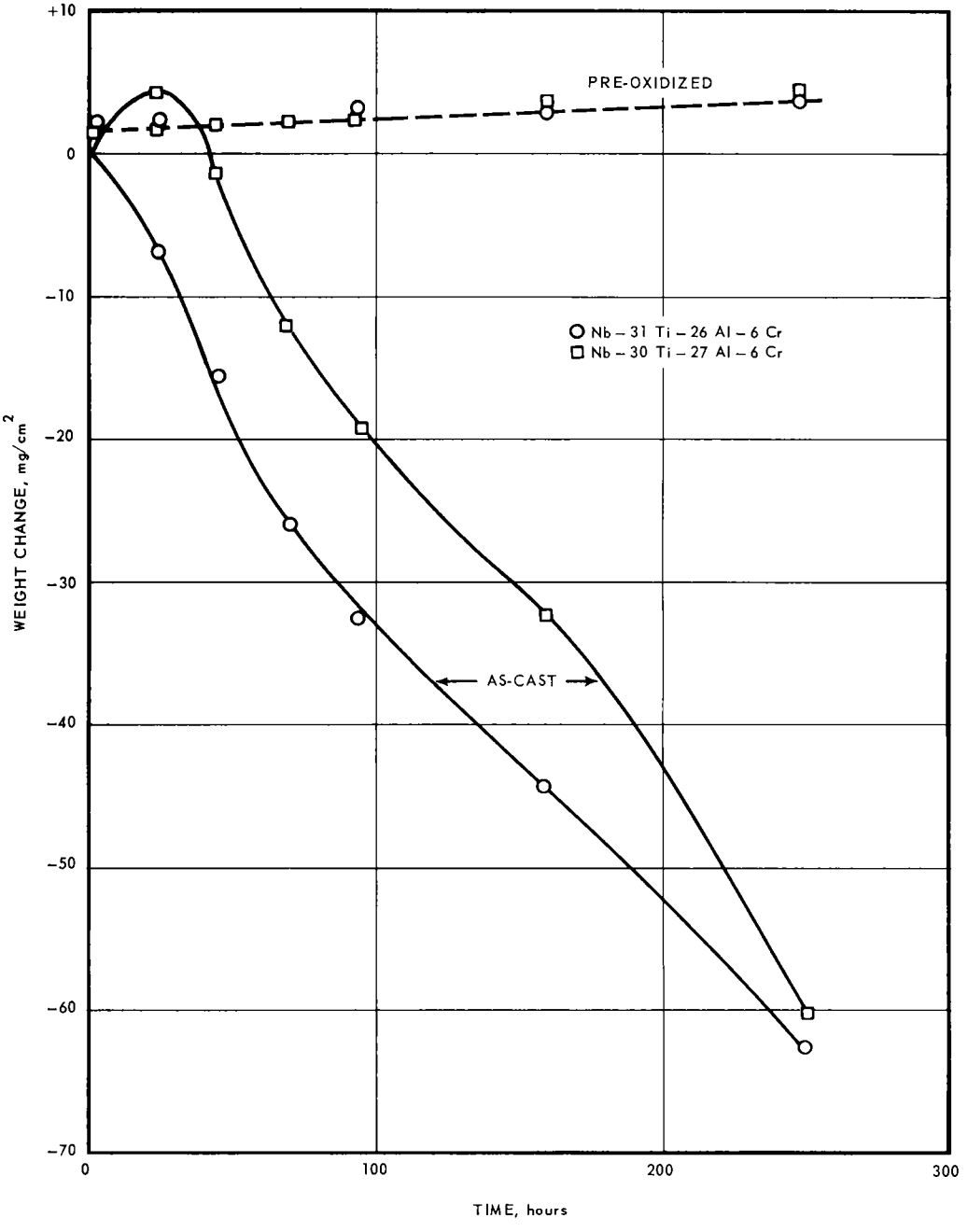

Fig. 1.2-3 – Oxidation rates of pre-oxidized and as-cast Nb-Al-Ti-Cr specimens tested at 1150°C

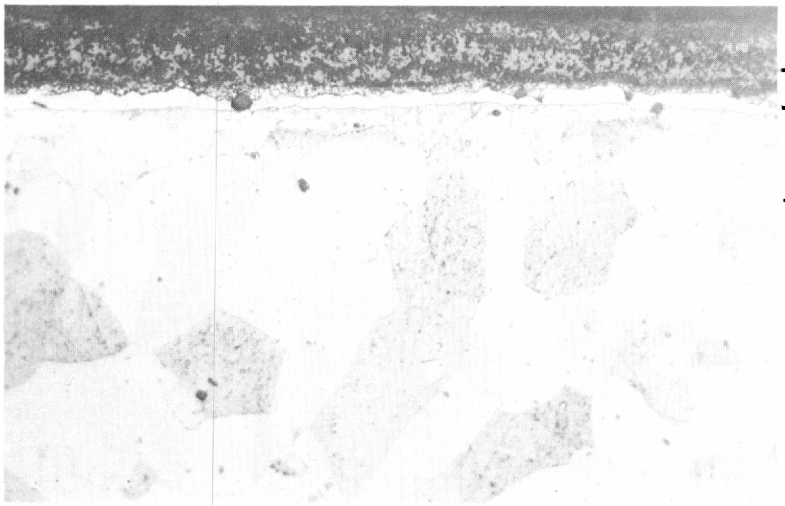

AFTER 110 HOURS AT 1200°C

Neg. No. 436, Etched 250 X

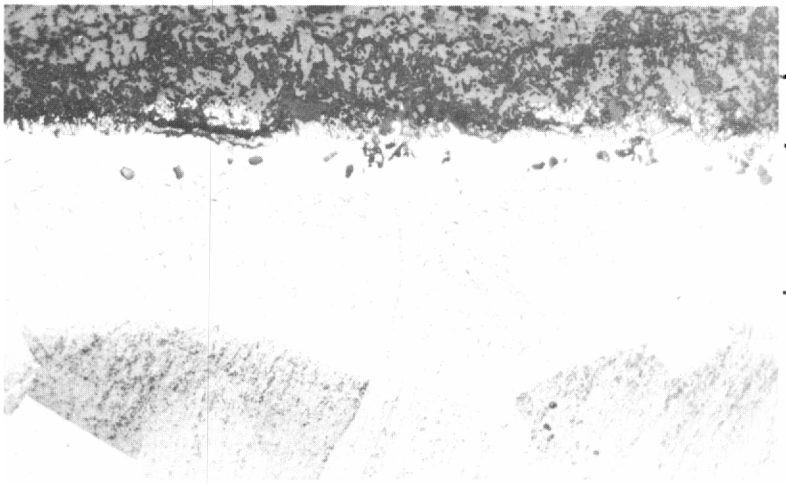

AFTER 110 HOURS AT 1315°C

Neg. No. 434, Etched 250 X

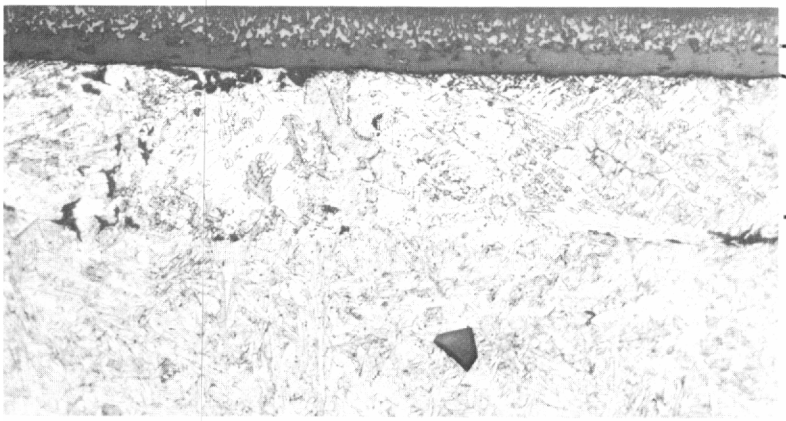

AFTER 20 HOURS AT 1425°C

Neg. No. 431, Etched 250 X

Fig. 1.2-4 – Microstructures of Nb-Al-Ti alloy oxidized in air at 1200°C, 1315°C, and 1425°C

TABLE 1.2-1

ELECTRON MICROPROBE RESULTS ON Nb-Al-Ti AND Nb-Al-Ti-Cr ALLOYS

	Analysis, weight percent			
	Ti	Al	Nb	Cr
Nb-Al-Ti Alloy				
Specimen 35F - 113 hours at 1200°C				
Matrix	34	30.8	35.2	
Light oxide	24.5	16	0	
Dark oxide	14	9.5	7	
Phase next to oxide	23.4	21.4	55.2	
Specimen 35C - 110 hours at 1315°C				
Matrix	31.7	31.7	36.6	
Light oxide	28	0	14.5	
Dark oxide	3	17	0	
Phase next to oxide	23	4	22	
Specimen 35B - 20 hours at 1425°C				
Matrix	35.8	23.8	40.4	
Light oxide	18	6	0	
Dark continuous oxide	0	20	0	
Nb-Al-Ti-Cr Alloy				
Specimen 39A - 108 hours at 1200°C				
Matrix	31	23.8	33.7	5
Oxide layers	0	40	0	0
Layer under oxide	16.5	13	55	15
Second phase in matrix	12.5	13.5	50	24
Specimen 40C - 110 hours at 1315°C				
Matrix	29.7	23	40.0	5
Oxide layer	0	39	0	0
Layer under oxide				15
Specimen 40A - 110 hours at 1425°C				
Matrix	30.2	23.7	39	5
Oxide layer	0	37	0	0
Layer under oxide				15

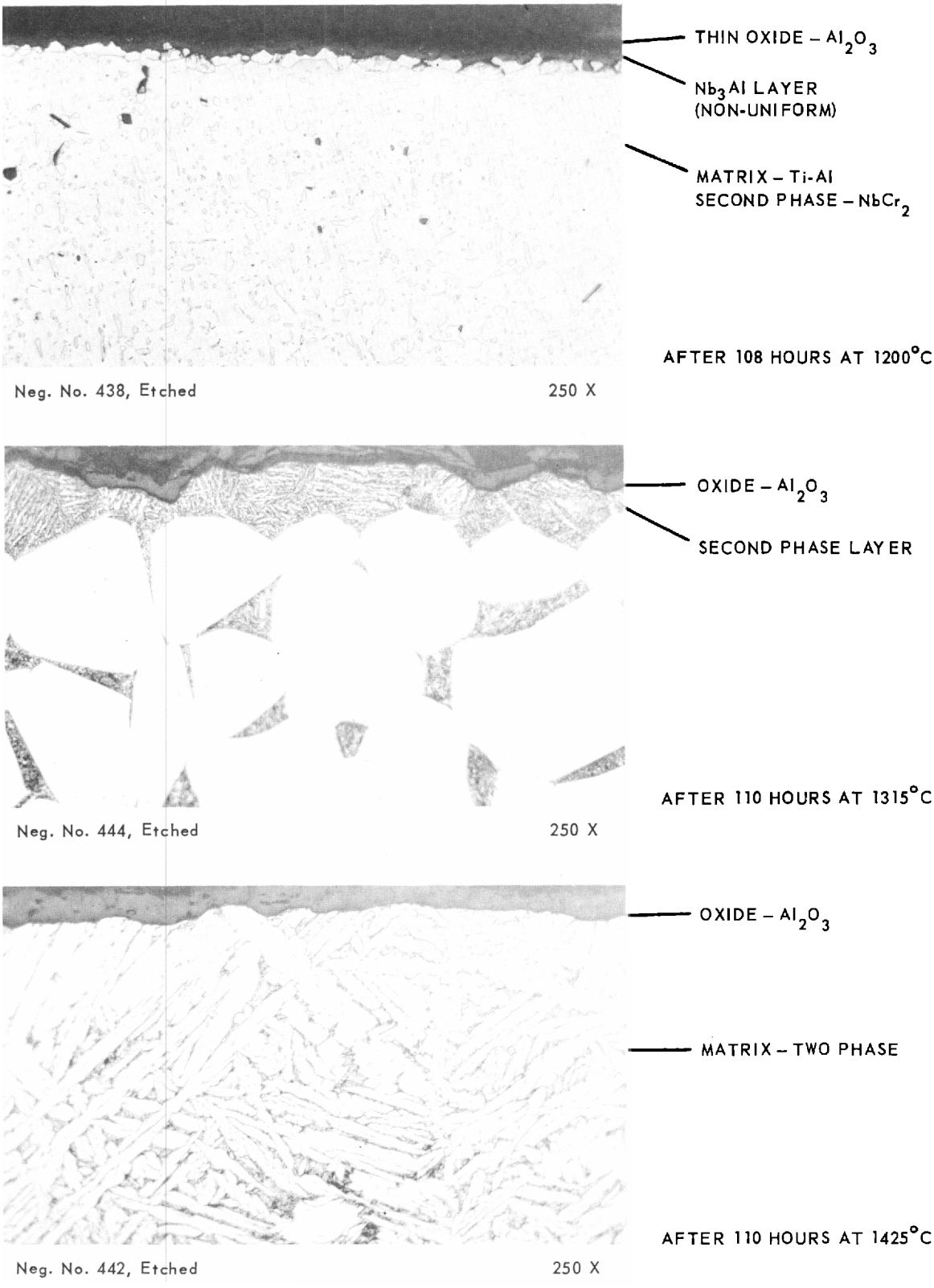

Fig. 1.2-5 – Microstructures of Nb-Al-Ti alloys with chromium additions oxidized in air at 1200°C, 1315°C, and 1425°C

$NbCr_2$ phase occurs. At 1425°C further changes in structure occur as a result of the depletion of aluminum and titanium from the matrix.

Considering this analysis of the oxidation behavior and of the structural changes that occur during oxidation, together with the brittleness and the relatively low melting points, the continuation of effort on the Nb-Al-Ti alloy does not seem to be warranted. A topical report will be issued summarizing the Nb-Al-Ti investigations.

1.3 NOBLE METALS

The high melting points and excellent oxidation resistance of the noble metals of the platinum group are of interest for high-temperature service in air. This group consists of platinum, palladium, rhodium, iridium, ruthenium, and osmium. Because ruthenium and osmium are extremely hard and brittle even at high temperatures, and cannot be worked satisfactorily, only palladium, platinum, rhodium, and iridium are presently of interest for high-temperature fuel elements. Some of the significant properties of these noble metals are shown in Table 1.3-1. Palladium is limited by its melting point to a maximum service temperature of 1400°C, but is promising as a long-life fuel element material at 1100° to 1200°C. Platinum may be operated as high as 1600°C, but because of its cost and high density has less potential except in the alloyed form. Rhodium has some temperature advantage over platinum but is considerably more costly. Iridium has the highest melting point and is of maximum interest as a high-temperature oxidation-resistant material. All of these noble metals are subject to varying degrees of instability at high temperatures due to an evaporation of the metal or a sublimation of the oxide. It is the purpose of this program to determine these rates of evaporation or sublimation at various temperatures up to their melting points and, having established their optimum stability in air, to evaluate the noble metals as fuel element materials in combination with UO_2.

The noble metals oxidize according the the general reaction

$$xM + \frac{y}{2} O_2 \rightarrow M_xO_y\uparrow$$

which describes the formation of a volatile oxide. The exact nature of the oxides formed is uncertain, and data contained in the literature are not always in agreement concerning the exact rates of oxidation and volatilization of oxides and metals in the platinum group. It is uncertain whether the oxidation proceeds by reaction with metal vapor or as a surface phenomenon with eventual sublimation of the oxide. Because of the low rates exhibited, the inherent oxidation characteristics are sensitive to impurities. Also, because of the

TABLE 1.3-1
CHARACTERISTICS OF NOBLE METALS HAVING POTENTIAL AS FUEL ELEMENT MATERIALS

Element	Melting Point, °C	Density, g/cc	Thermal Conductivity, Cgs	Coefficient Of Expansion x 10^{-6}	Tensile Strength,[a] tsi	Annealed Hardness, VHN	Cost, $/Troy Oz.
Palladium	1552	12.02	0.17	11.67	10	40	25
Platinum	1769	21.45	0.17	8.9	9	40	84
Rhodium	1960	12.44	0.36	8.5	30.6	110	140
Iridium	2410	22.4	0.35	6.5	16	220	75

[a] At room temperature.

volatile nature of the oxides, the oxidation rates are affected by the partial pressure of oxygen at the metal surface and by the velocity of the atmosphere over the metal surface.

Most of the noble metal work done to date has been to establish base-point - weight-change data for four reference metals. These data will provide comparative rates for eventual alloy studies. Specimens of platinum, rhodium, palladium, iridium, and platinum-30 rhodium were prepared from 0.020-inch-thick sheet stock in the form of 1 by 1/2-inch tabs. Sapphire rods supported the specimens for heating in muffle furnaces in which the air atmosphere was essentially static. Initially, tests at 1200°, 1400°, and 1600°C were conducted. Specimens were removed periodically (about every 50 hours) for visual examination and measurements of weight and thickness. Results of testing for 1000 hours at 1200°C and 1400°C, and 400 hours at 1600°C, are shown in Figure 1.3-1. Data are presented as equivalent thickness change per (tab) side, based on calculations derived from weight losses as a function of time. Palladium was omitted from the 1600°C test because its melting point is 1552°C.

The shape of the curves at 1200°C fits a pattern related to the sublimation temperatures of the commonly reported oxides:

1. IrO_2 - 1140°C
2. Rh_2O_3 - 1100°C
3. PdO - 870°C
4. PtO - 507°C

The curves for rhodium, palladium, and platinum reflect a differential rate of oxide formation and sublimation as a direct function of the difference between test temperature and oxide-sublimation temperature. The rapid loss of iridium is evidently due to a much greater rate of volatilization of the oxide since the oxide sublimation temperature is only slightly higher than that of Rh_2O_3. At 1400°C and 1600°C, the shape of the curves indicates a direct relationship between volatility and temperature.

Calculation of the thickness change for the two best materials, platinum and platinum-30 rhodium alloy, shows:

1. Loss of 0.001 inch after 10,000 hours at 1200°C
2. Loss of 0.001 inch after 1,300 hours at 1400°C
3. Loss of 0.001 inch after 233 hours at 1600°C

These rates appear as an approximately straight line when plotted in semilog fashion as a function of temperature. Rhodium exhibits loss rates somewhat greater than these values.

Since the stability of these noble metals at high temperatures is a function of a volatile oxidation product, it is expected that weight could vary with changes in velocity of the atmosphere at the specimen surface. In a truly static condition, saturation of the surrounding atmosphere could obtain equilibrium and result in no weight change.

A comparative study was made to determine the effects of flowing air on the stability of noble metals. Tests in flowing argon were also made for comparative purposes. Specimens of 0.020-inch-thick sheet of the metals described above were held in a ceramic boat in a tube furnace at 1400°C and 1600°C as preheated air was blown over the specimens. A flow rate of 0.2 scfm (3.85 in./sec) was initially used at both test temperatures; after 100 hours, the flow rate of the 1400°C test was increased to 0.4 scfm (7.70 in./sec). The results are shown in Figure 1.3-2. The loss of surface metal under the 0.2 scfm test condition was twice that found for static conditions. Increasing the air velocity directly increased the loss of metal. The iridium sample completely volatilized in 200 hours at 1400°C. That these values are not absolute is shown by the anomaly exhibited by rhodium.

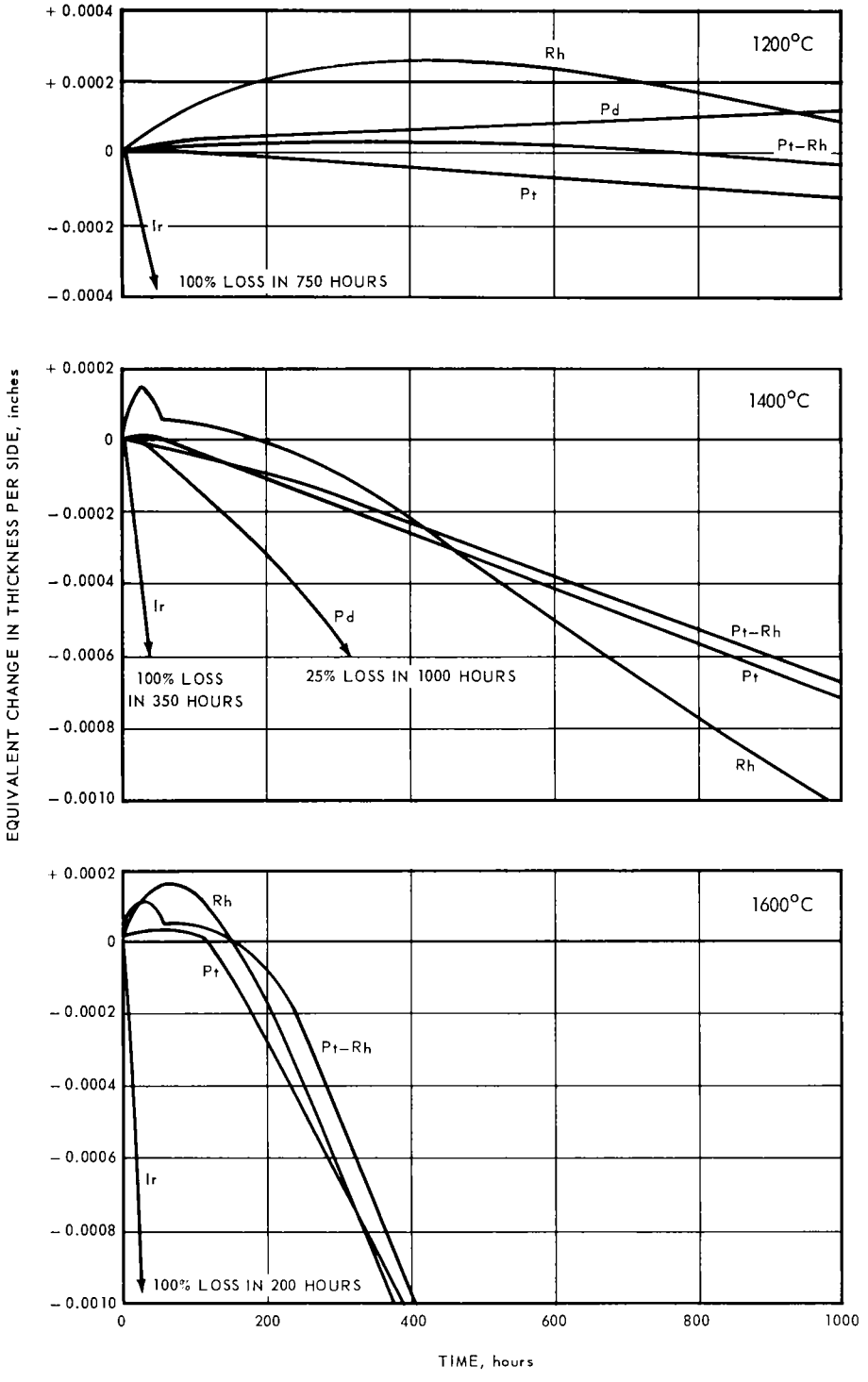

Fig. 1.3-1–Thickness change versus time for noble metals tested at 1200°, 1400°, and 1600°C in static air

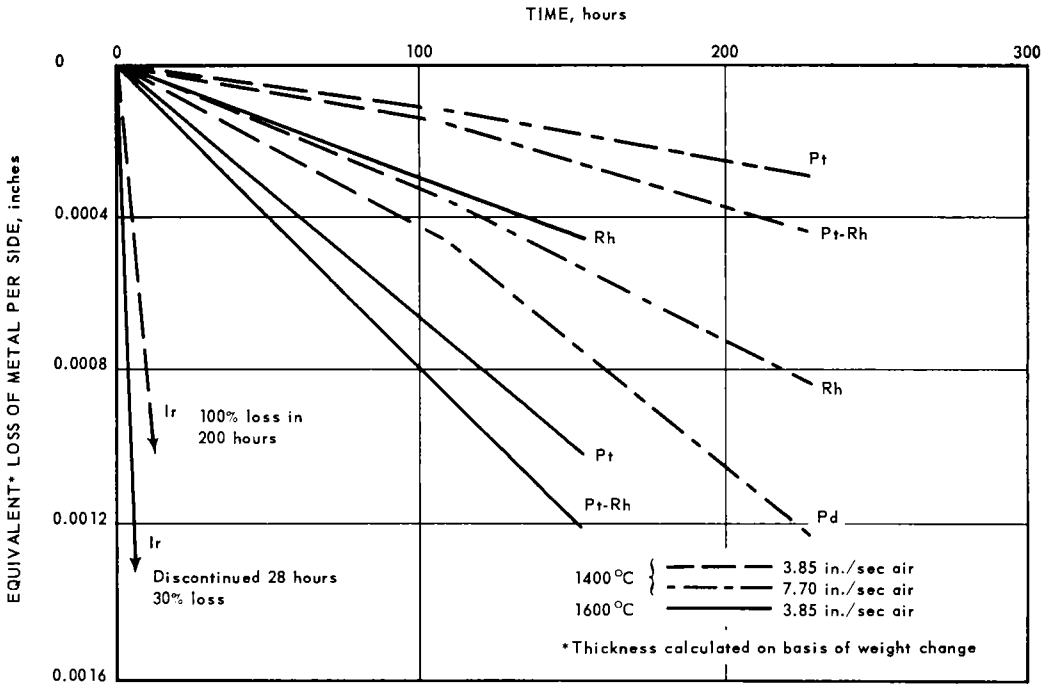

Fig. 1.3-2 - Thickness change versus time for noble metals heated at 1400°C and 1600°C in flowing air

For comparison, similar tests were conducted at 1400°C in both flowing and static argon gas. These results are shown in Figure 1.3-3. Particularly striking is the fact that iridium, platinum, and rhodium appear to be little affected by temperature or flow rate in the argon atmosphere, yet, palladium loses metal in argon almost as rapidly as in air and in direct relation to gas velocity. Under these test conditions, platinum, rhodium, and iridium lose metal as a result of sublimation of oxides, while palladium losses are a result of evaporation of metal. These conclusions are substantiated by the available vapor pressure data for the noble metals, indicating that the vapor pressure of palladium is greater by a factor of 10^4 than that of platinum, and the vapor pressure of iridium is drastically lower than that of the other metals of this group. Some of these noble metals have useful oxidation resistance at temperatures well above 1600°C. Program plans include testing such oxidation resistant metals and alloys to their melting points. Tests of rhodium and iridium in flowing air, and rhodium in argon, at 1800°C have been made for times up to 84 hours. The thickness-loss data obtained from these tests are shown in Figure 1.3-4. These data show that the volatility of rhodium in flowing air at 1800°C increases by a factor of 20 from the rate at 1600°C. By extrapolation, 100 percent loss of rhodium would occur in about 220 hours. After 34 hours testing in air at 1800°C, an atmosphere of flowing argon was introduced, sharply retarding the loss of rhodium. A similar effect was noted for the series of tests at 1400°C and 1600°C in argon. Considered together, these data support the conclusion that rhodium weight losses are due to oxide sublimation.

At 1800°C, iridium shows the previously observed rapid evaporation in flowing air, but the rate of evaporation is not appreciably greater than that observed at 1400°C and 1600°C. In 26 hours at 1800°C, iridium lost approximately half its original thickness; it is estimated that 100 percent loss would have occurred in about 60 hours. Iridium was not tested in flowing argon, but it is assumed that, like rhodium, the loss would have been sharply retarded.

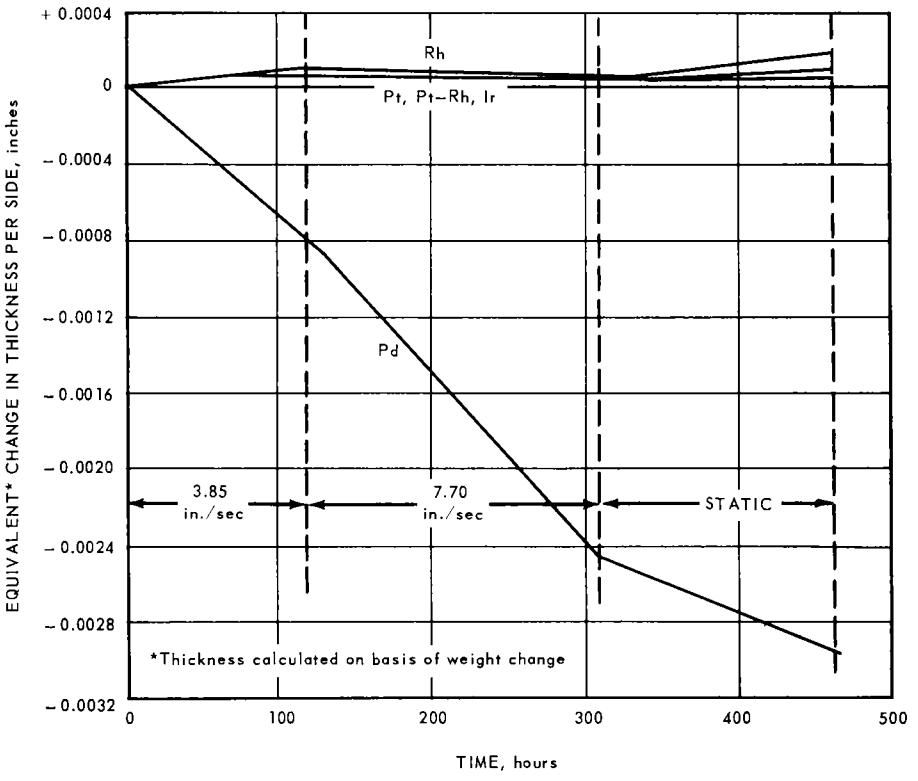

Fig. 1.3-3–Thickness change versus time for noble metals at 1400°C in flowing and static argon

Previous data has shown that palladium evaporates rapidly at 1400°C in flowing air, but only slightly at 1200°C. Palladium should be considered, then, only for fuel element applications under 1300°C where long-life considerations warrant the added cost of a noble metal fuel element, such as portable power reactors or marine power plants. The excellent stability of palladium at 1000°C was demonstrated when three standard sheet specimens, 0.020-inch thick, and weighing 1 gram each, were tested in flowing air for 262 hours. The specimens were periodically removed from the furnace and weighed. The weight gain data obtained are shown in Table 1.3-2 and indicate a negligible oxidation or evaporation of the palladium sheet.

The ability of palladium to contain UO_2 at temperatures exceeding 1200°C was demonstrated by the use of simple capsules made of palladium tubing and loaded with a blend of palladium powder containing 45 volume percent UO_2 (enriched). To insure a core of high density and good contact with the capsule wall, the sealed capsules were heated at 1115°C in argon for 1 hour to sinter the core material and then cold-swaged for a reduction of about 20 percent. This sintering and swaging treatment was repeated, leaving the capsule with a final diameter of 0.090 inch and a wall thickness of about 0.015 inch. Alpha count measurements of surface activity were made using a large chamber proportional counter. Duplicate capsules were tested at 1400°C in static air and removed periodically for alpha measurements. These alpha count data are shown in Table 1.3-3. After 750 hours of testing at 1400°C, these palladium-clad UO_2 specimens have lost less than 10 percent of their total weight, which is equivalent to about 0.0015 inch of cladding thickness. On the basis of this data, palladium appears compatible with UO_2 at 1400°C and indications are that it would be useful as a fuel element material for thousands of hours of service at temperatures from 1000° to 1200°C.

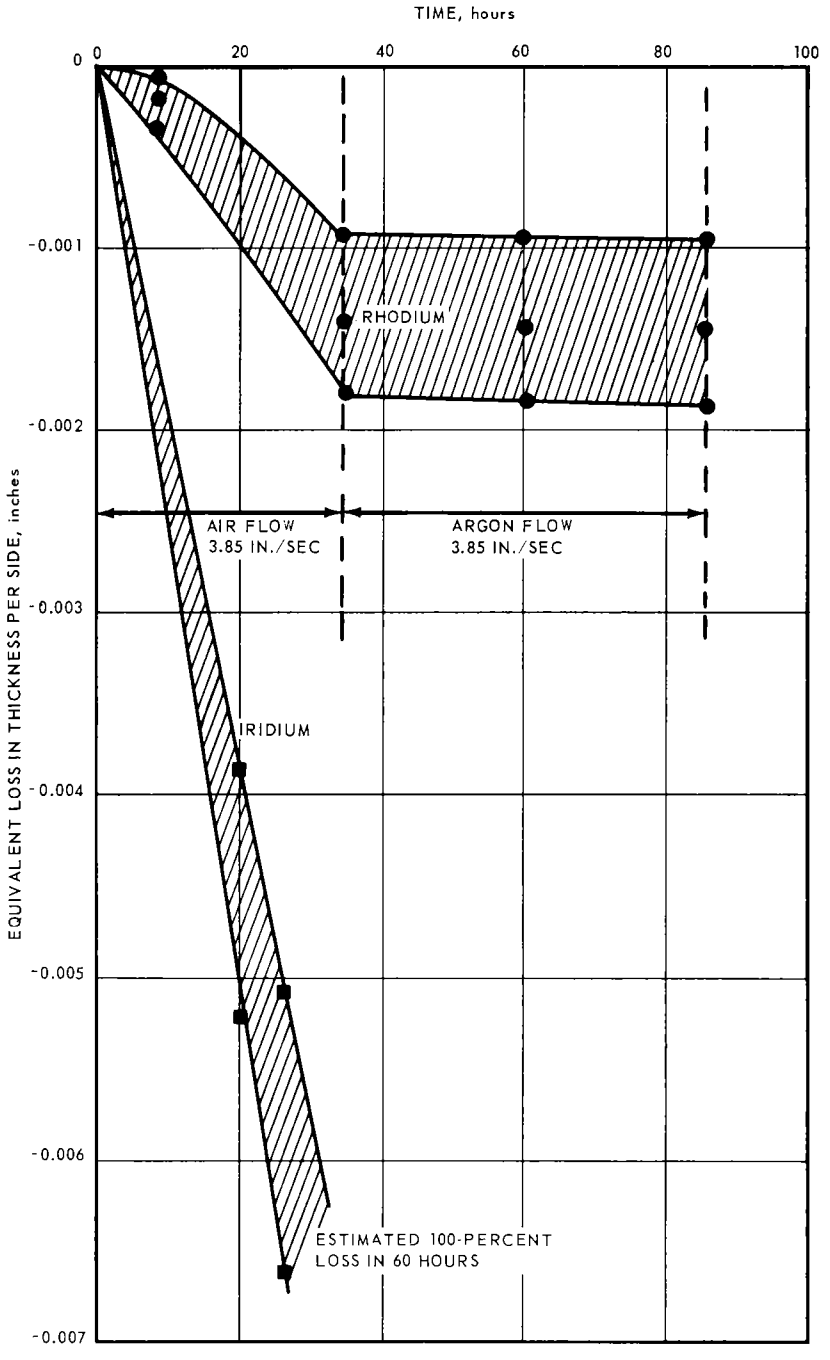

Fig. 1.3-4–Thickness loss versus time for rhodium and iridium sheet specimens at 1800°C in flowing air and argon

TABLE 1.3-2

STABILITY OF PALLADIUM AT 1000°C IN FLOWING AIR[a]

Specimen No.	Net Weight Gain, mg/in^2			
	23 Hours	94 Hours	145 Hours	262 Hours
1	0.6	0.2	0.3	0.6
2	-0.1	0.1	Nil	Nil
3	0.2	0.4	0.1	0.3
Average	0.23	0.23	0.13	0.30

[a]Airflow rate of 3.85 inches per second over specimens.

TABLE 1.3-3

COMPATIBILITY OF PALLADIUM WITH UO_2 AT 1400°C BASED ON ALPHA COUNT DATA

Test Time, hr	Alpha Count Per Minute From Core Area[a]	
	Pd-1	Pd-3
0	5	3
24	18	8
47	1	11
117	3	15
185	2	11
300	5	9
419	8	6
586	1	3
750	3	1

[a]Approximately 0.07 square inch exposed to counter.

1.4 SUMMARY AND CONCLUSIONS

Basic studies of the oxidation mechanism of the Fe - 25Cr - 4Al - 1Y alloy at temperatures up to 1425 °C are nearing completion. These studies have led to the conclusion that oxidation of the alloy proceeds by diffusion of oxygen ions through the surface scale to form the oxide at the metal-oxide interface. Grain-boundary oxides formed early in the tests appear to act as "anchors" for the surface oxide, thus preventing spalling of the oxide.

Fe-Cr-Al-Y-UO_2 compatibility tests at 1300 °C showed that an Al_2O_3 barrier is formed when Cr_2O_3 is added to the UO_2. This barrier prevents the reduction of UO_2 by aluminum. The utility of U_3O_8 in forming a barrier is questionable since it results in internal oxidation of the cladding rather than barrier formation.

The oxidation resistance of the Nb-Al-Ti alloy at temperatures up to 1425 °C is improved by the addition of 6 weight percent chromium which prevents spalling of the oxide coating. Chromium also causes precipitation of a second phase which increases the brittleness of the alloy. In view of the peculiar oxidation behavior and the structural changes that occur

in the Nb-Al-Ti alloy during oxidation, together with the brittleness problem and relatively low melting point, further evaluations of this alloy as a fuel element material do not seem to be warranted.

Basic studies of the high-temperature stability of four of the noble metals have resulted in the following conclusions.

1. Weight losses are a result either of metal evaporation or of oxide sublimation and are a function of the velocity of air flowing over the surfaces of the noble metal.
2. At temperatures up to 1600°C, platinum is the most stable of the group tested in both static and flowing air, followed closely by rhodium.
3. At 1800°C in flowing air, both rhodium and iridium lose weight rapidly as a result of oxide sublimation.
4. Palladium losses occur as a result of metal evaporation in the temperature range of 1300° to 1400°C, but excellent stability is exhibited from 1000° to 1200°C.
5. Palladium is also compatible with UO_2 at temperatures up to 1400°C and appears to be a useful fuel element material for long-time service at intermediate temperatures.

1.5 PLANS AND RECOMMENDATIONS

In view of the excellent oxidation resistance of the FE-Cr-Al-Y alloy and the expectation of its successful application as a cladding material, a continuation of the effort with a threefold objective is planned. (1) Achieve improvements of the high-temperature properties by eliminating the low melting phase YFe_9 and strengthening the material. Moderate improvements in strength might be obtained by dispersions of Y_2O_3, Y-AlO_3, or other stable oxides. (2) Determine the basic parameters by which oxide barriers are formed between the fueled cores and the alloy cladding and the stability of such barriers. (3) Establish the performance of the Fe-Cr-Al-Y alloy as a fuel element material under reactor conditions for long periods of time.

Although the Nb-Al-Ti alloy exhibits good oxidation resistance to 1425°C and has interesting nuclear properties, its low melting phases, structural peculiarities and inherent brittleness limit its application as a fuel element material. In view of this, no further efforts with the Nb-Al-Ti alloy system are planned except for the issuance of a topical report.

Data are available in current technical literature giving theoretical and idealized experimental oxidation losses for the noble metals. Work is planned to evaluate these metals more exactly under conditions approximating fuel element application. Additional plans include exploring the effectiveness of coatings in reducing the evaporation of iridium, a study of the benefits of alloying of the several noble metals, an investigation of the compatibility of the various noble metals and their alloys with UO_2 fuels, and, for those systems which appear most promising, fabrication of simple fuel element specimens for eventual irradiation testing at elevated temperatures.

2. HIGH-TEMPERATURE NONFUELED REACTOR CORE COMPONENTS

2.1 MODERATOR FABRICATION AND TESTING (57006)

The use of Y - 5Cr (weight percent) hydride as a high-temperature neutron moderator material had already been established by previous work.* A 0.003-inch coating of chromium was applied by flame spraying to this material which was then hydrided at 1050°C to an N_H value of 4.5 (1.75 weight percent hydrogen). These cores were then clad in cans of 0.020 to 0.035-inch-thick Fe - 25Cr - 5Al and autoclave-bonded at 1000°C and 10,000 psi.†

The only available data for this material was obtained by using a small (3-inch by 0.8-inch by 0.4-inch) rectangular assembly in an advanced reactor design concept. A thinner clad was used in that application; the optimum thickness was 0.010 inch and the maximum was 0.016 inch. Although this reactor component was designed to operate at 1000° to 1100°C for periods of 1000 hours, the only thermomechanical or irradiation stability data obtained for long exposures was at temperatures of 900°C or less, except for one thermocycling test.

The objective of this program, therefore, is to establish thermal stability data for clad hydrided yttrium alloy material for periods of 1000 hours at temperatures up to 1100°C. Included in this task is one reactor test, planned to attain a fast neutron dosage of 10^{20} nvt at 1100°C.

STUDIES OF YTTRIUM ADDITION FOR OXIDATION STABILITY

Initial oxidation stability tests on moderator pieces of this geometry clad with 0.010 inch of Fe - 27Cr - 3.5Al indicated that these specimens were subject to cladding rupture and catastrophic oxidation of the core after 300 hours at 1100°C in both static and Mach 0.2 air. Similar tests in static air at 1000°C showed no evidence of failure after 1500 hours at temperature. Metallographic examination of the ruptured specimens showed that grain boundaries in the Fe-Cr-Al extended across the entire clad thickness. This suggested that either a thicker clad or a grain-growth-inhibited clad was needed to increase the temperature capability of the assembly; both techniques were explored.

Because yttrium is a grain inhibitor in iron based alloys, several Fe-Cr alloys containing yttrium were evaluated for oxidation stability and over-all fabricability. Tests were performed on 0.010-inch-thick coupons of Fe - 30Cr - 1Y, Fe - 30Cr - 3Al - 1Y, and Fe - 27Cr - 3.5Al at 1000°, 1100°, and 1200°C. All materials tested were still sound after 1700 hours at 1000°C. But at 1100°C and 1200°C, only the Fe - 30Cr - 3Al - 1Y alloy was intact after 1000 hours. However, fabrication difficulties with the yttrium containing alloys were encountered during cold-rolling below 0.020 inch. After succeeding in rolling

*See references 1 through 5 at the end of section 2.1.
†See references 6 through 8 at the end of section 2.1.

a small amount of material to a thickness of 0.010 inch and fabricating it into cans, minute TIG and electron beam weld leaks were found. Because of these fabrication difficulties, an investigation was made of a thicker (0.016-inch-thick) clad of the Fe-Cr-Al alloy.

EVALUATION OF THICKER Fe-Cr-Al CLAD

A series of hydrided moderator cores were canned in 0.016-inch-thick Fe - 20Cr - 4.5Al from an available commercial heat and oxidation-tested in static air at 1000°, 1050°, and 1100°C. (The analysis of this material was originally reported as Fe - 27Cr - 3.5Al. Later, an analysis check indicated that it is Fe - 20Cr - 4.5Al.) These tests confirmed the previous tests in that failure occurred in less than 300 hours at 1100°C, but the cans tested at 1000°C and 1050°C were still intact after 1300 hours. Although no weld defects had been detected, failures all started in the area of the end cap welds, also suggesting that failure was associated with grain size.

From these results it appeared that a considerable effort might be required to develop a cladding suitable for 1100°C operation. Since the primary objective is the evaluation of the hydride as a moderator and not the development of a cladding alloy, the conclusion was reached that the goals of this program can be satisfied by in-pile tests in air at 1000° to 1050°C or in an inert atmosphere at 1100°C to eliminate the problem of cladding oxidation. After reaching this decision, the remainder of the program is being directed toward fabricating and testing a sufficient number of moderator specimens to satisfy in-pile test requirements.

CLAD MODERATOR EVALUATION

A total of 84 moderator specimens, clad in 0.016-inch-thick Fe - 20Cr - 4.5Al, were fabricated following the procedures shown in Figures 2.1-1 and 2.1-2. No unusual diffi-

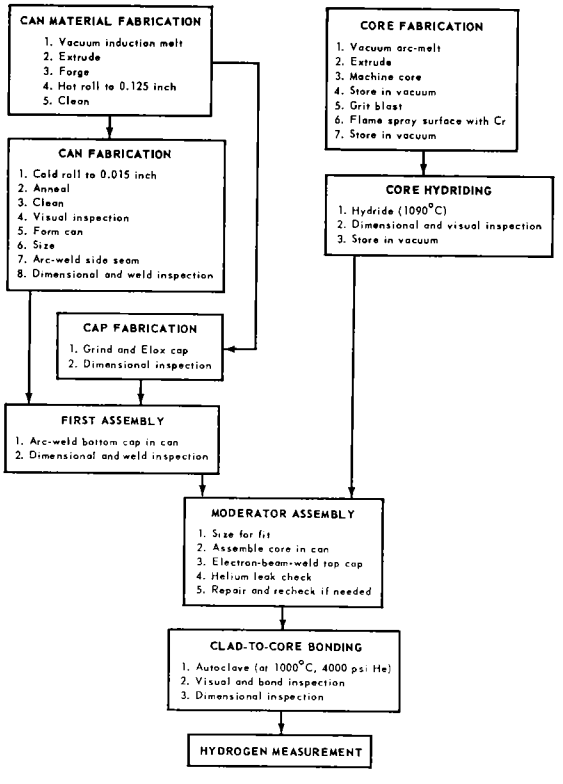

Fig. 2.1-1 – Flow sheet of moderator fabrication

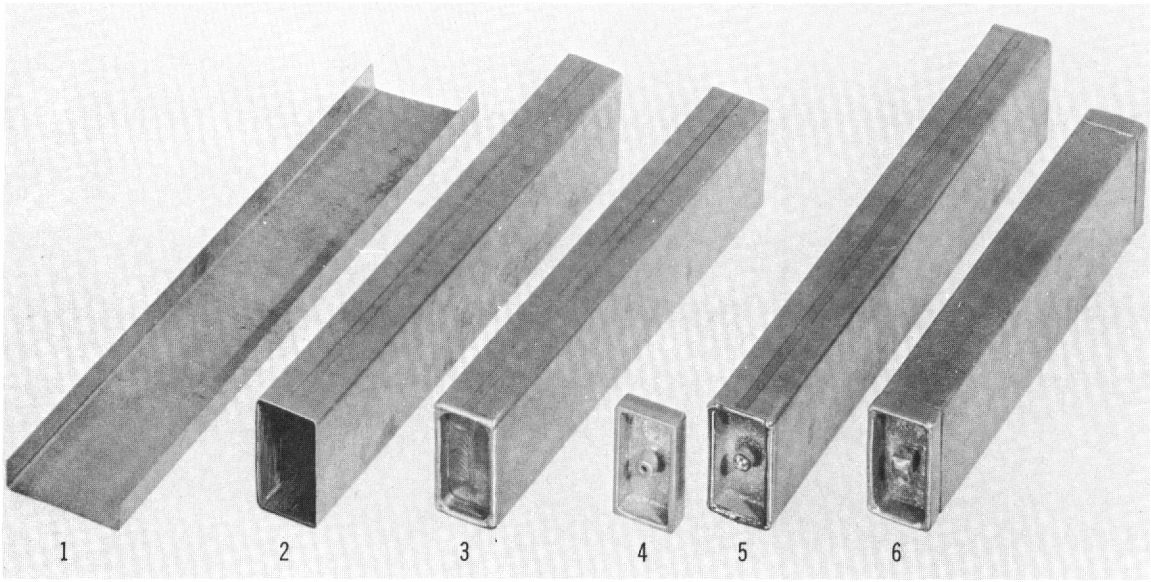

Fig. 2.1-2 – Illustration of steps in cladding of hydrided yttrium alloy. From left: (1) shaped half, (2) TIG welded sleeve, (3) welded sleeve with one end cap attached, (4) vented end cap, (5) sealed core with vented end cap sealed, and (6) clad moderator composite after autoclave bonding. (Neg. U-39240-B)

culties were encountered in the fabrication of these pieces. Some autoclaving studies were performed to reduce crimping of the clad at the core-cap interface. A maximum bonding pressure of 4800 psi at 1000°C was established.

Oxidation Resistance Evaluation

Oxidation stability tests were performed on these clad moderator samples under both dynamic and high-pressure static air conditions. The dynamic tests were performed on four samples at 1000°C, with an airflow of 2 lb/ft^2-second, corresponding to an exit air velocity of 114 feet per second. Static air tests were performed on three samples at 1000°C with an air pressure of 95 psia. Both series of tests were terminated after 1300 hours with no evidence of sample failure. Figures 2.1-3a and 2.1-3b illustrate the sample cross-section and interface bond condition at the conclusion of the tests.

A summary of oxidation stability tests to date is given in Table 2.1-1.

Hydrogen Retention

A method was devised for nondestructively measuring the hydrogen content of the samples after bench and in-pile testing. The moderator samples are placed in a collimated neutron beam, using Ra-Be in a sigma pile as the source. The amount of hydrogen in the sample influences the degree of neutron scattering; the scattered neutrons are measured by BF_3 ionization chambers. Analyzing identical samples by this method and then by vacuum fusion analysis has established that there was no measurable loss of hydrogen from the 95Y - 5Cr moderator samples after 1550 hours at 1000°C.

SUMMARY AND CONCLUSIONS

The results of these tests have established the capability of this moderator material, clad with Fe - 20Cr - 4.5Al, to withstand exposure to air at 1000°C for long periods while retaining hydrogen in a non-nuclear environment. Fabrication and major inspection procedures have been established.

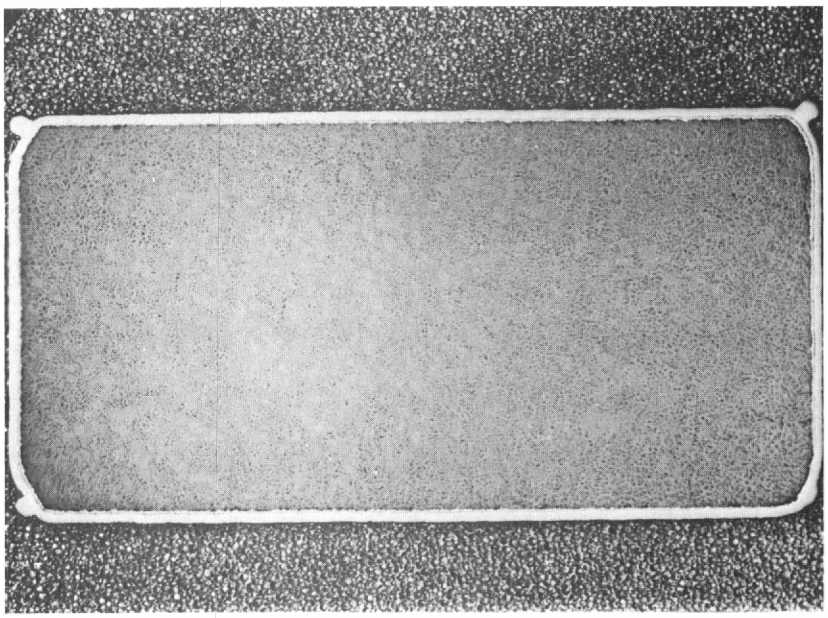

(Neg. No. 648) 5X

Fig. 2.1-3a – Cross section of Fe – 20Cr – 4.5Al-clad moderator sample tested at 980°C for 1550 hours

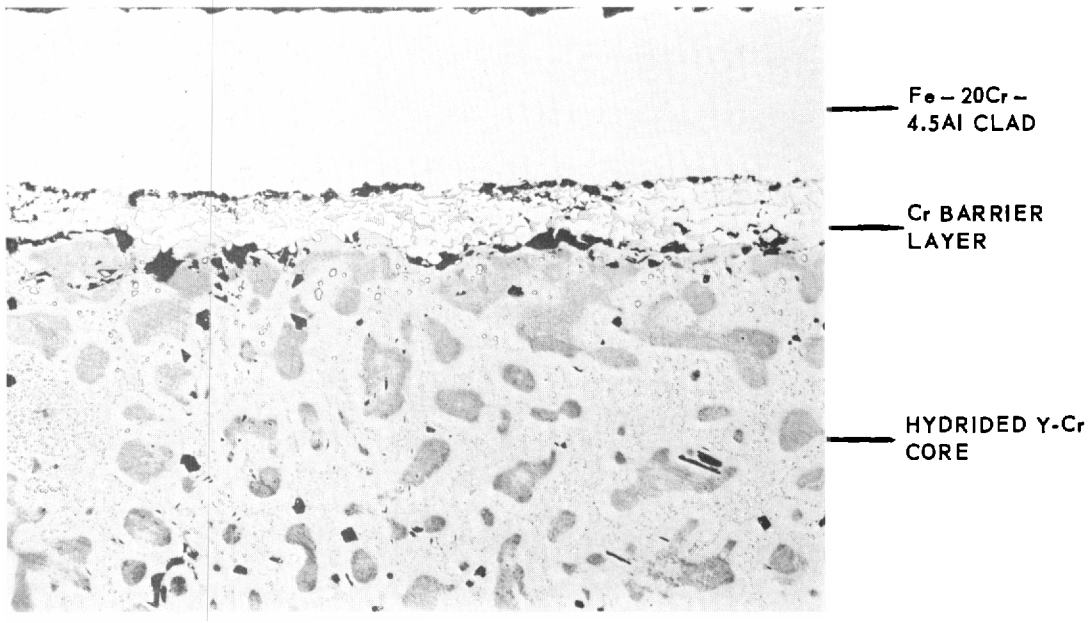

(Neg. No. 649) 100X

Fig. 2.1-3b – Microstructure of clad, barrier layer, and core interfaces showing bond condition and some yttrium diffusion after 1550 hours at 980°C

TABLE 2.1-1

SUMMARY OF OXIDATION STABILITY TESTS

Composition[a]	Number And Type	Clad Thickness, in.	Condition	Temperature, °C	Time, hr	Results
Fe - 27Cr - 3.5Al Fe - 30Cr - 1Y Fe - 30Cr - 3Al - 1Y	4 coupons	0.010	Low pressure static air	1000	1700	Samples intact
Fe - 27Cr - 3.5Al Fe - 30Cr - 1Y Fe - 30Cr - 3Al - 1Y	4 coupons	0.010	Low pressure static air	1100	1000	Fe - 30Cr - 3Al - 1Y intact, others badly oxidized
Fe - 27Cr - 3.5Al Fe - 30Cr - 1Y Fe - 30Cr - 3Al - 1Y	4 coupons	0.010	Low pressure static air	1200	1000	Fe - 30Cr - 3Al - 1Y intact, others badly oxidized
Fe - 27Cr - 3.5Al	2 Moderator pieces	0.010	Low pressure air	1000	1550	Sample intact - no hydrogen loss
Fe - 27Cr - 3.5Al	2 Moderator pieces	0.010	Low pressure air	1100	150-300	Failed at end cap
Fe - 27Cr - 3.5Al	2 Moderator pieces	0.010	Low pressure air	1200	7	Failed at end cap
Fe - 20Cr - 4.5Al	2 Moderator pieces	0.016	Low pressure air	1000	1800	Sample intact - H_2 analysis in progress
Fe - 20Cr - 4.5Al	2 Moderator pieces	0.016	Low pressure air	1050	1300	Sample intact - H_2 analysis in progress
Fe - 20Cr - 4.5Al	2 Moderator pieces	0.016	Low pressure air	1100	140	Samples failed at end cap
Fe - 20Cr - 4.5Al	3 Moderator pieces	0.016	High pressure air	1000	1300	Sample intact - H_2 analysis in progress
Fe - 20Cr - 4.5Al	4 Moderator pieces	0.016	Dynamic air (114 ft/sec)	1000	1300	Sample intact - H_2 analysis in progress

[a]Expressed as weight percent.

PLANS AND RECOMMENDATIONS

The effect of a radiation environment on 95Y - 5Cr is not established but preparations for such testing are complete. An in-pile test of four samples is planned, either in the ETR at 1000°C under dynamic air cooling or in the LITR in static helium-air mixtures at 1100°C.

REFERENCES

1. Simmons, C. R., Magee, C. B., Funston, E. S., McGurty, J. A., and Calkins, V. P., "Chemistry and Metallurgy of Yttrium," GE-ANPD, APEX-475, July 1959.
2. Calkins, V. P., Funston, E. S., McGurty, J. A., and Simmons, C. R., "The Technology of Hydrided Yttrium," GE-ANPD, APEX-545, March 1960.
3. Williams, J. M., and Huffine, C. L., "Properties of Hydrided Yttrium Alloys," GE-ANPD, APEX-551, October 1959.
4. "Alloying To Improve The High-Temperature Ductility of Yttrium Hydride," Battelle Memorial Institute, BMI-1412, February 1960.
5. McGurty, J. A., "Milestone I for Task 7474. Topical Report on Hydrided Yttrium and Clad Hydrided Yttrium Moderator Components," GE-ANPD, DC 57-11-71, November 1957.
6. McGurty, J. A., Funston, E. S., and Bohlander, K. M., "Fabrication and Properties of Hydriding Yttrium," GE-ANPD, APEX-529, April 1959.
7. "Cladding of Yttrium Hydride with Iron-Chromium-Aluminum By Gas-Pressure Bonding," Battelle Memorial Institute, BMI-1411, February 1960.
8. Young, R. S., "Bonded-Cladded Development for Moderator Alloy," GE-ANPD, APEX-570, August 1960.

2.2 HIGH-TEMPERATURE CONTROL MATERIALS (57002)

The objective of this task is to develop nuclear control materials capable of operating in high-performance reactors in the temperature range from 1100° to 1200°C or higher.

The primary emphasis during this program has been on europium sesqui-oxide* (Eu_2O_3 - melting point 2240° ± 20°C). This material is particularly attractive in long-life, high-temperature nuclear control applications due to its unusual decay products Eu^{152} (13-year half-life, $\sigma_a = 500b$) and Eu^{154} (16-year half-life, $\sigma_a = 1400b$).

Because Eu_2O_3 is ceramic in nature, it has the typical low conductivity, low strength, and porosity problems of ceramic materials. However, a Eu_2O_3-metal matrix combination, e.g., Eu_2O_3-Ni, combines the nuclear advantages of europium with the thermo mechanical properties of the metal.

Eu_2O_3 MATRIX STUDIES

Fe-Cr-Al and Fe-Cr-Y Compatibility Studies

Previous work had demonstrated that Eu_2O_3-Ni matrix materials clad with 80Ni - 20Cr (< 0.2% Si) are capable of operation in air at 1000°C for at least 1000 hours. However, the life of these Eu_2O_3-Ni nuclear control elements is limited by oxidation, low mechanical strength, and dimensional instabilities that occur during repeated thermal cycling.†

*R. S. Roth and S. J. Schneider, *Journal of Research of National Bureau of Standards*, Vol. 64-A, No. 4, July-August 1960.

†J. R. Miller and W. G. Baxter, "Thermal Cycling Induced Growth of Nickel-Europium Oxide Cermets," *Trans. Amer. Nuc. Soc.*, Vol. 4, No. 2, November 1961, p. 350.

Therefore, to increase the useful life of Eu_2O_3-metal matrix control elements, a new matrix material with higher oxidation resistance and lower cermet thermal-cycle growth rates is required.

The Fe-Cr-Al and Fe-Cr-Y alloy systems were evaluated as possible matrix materials to increase the temperature capability of the control material from 1000° to 1200°C. Individually, each of these metallic materials had demonstrated oxygen stability at temperatures above 1200°C in air. Thus, Eu_2O_3 dispersed in these metallic matrices and clad with a metallic oxidation-resistant material is potentially a superior nuclear control material, providing the materials are thermodynamically compatible and their growth rates are lower than Eu_2O_3-Ni. (Insufficient thermodynamic data is available to permit the accurate prediction of possible Eu_2O_3 chemical reactions and no theory for prediction of growth rates exists.)

Fabrication Studies

Hot extrusion of cold-pressed and sintered compacts was selected as the best fabrication technique to achieve increased densities and lowered growth rates, based on the results obtained with the Eu_2O_3-Ni system. Compacts of Fe - 30Cr - 1Y - 43Eu_2O_3 (weight percent), Fe - 30Cr - 3.5Al - 43Eu_2O_3, and Fe - 30Cr - 3.5Al - 1Y - 43Eu_2O_3 were fabricated by cold pressing at 15 tsi and sintering in vacuum for 4 hours at 1400°C.

The Fe-Cr-Al and Fe-Cr-Al-Y alloys were found to react with Eu_2O_3 after the 4-hour vacuum sinter at 1400°C to produce a low density body that could not be further worked. Chemical analysis revealed that most of the europium had been lost during sintering; an X-ray diffraction analysis disclosed an unidentified reaction product of complex structure. This reaction has been tentatively identified as reduction of Eu_2O_3 by Al to produce europium metal (boiling point - 1440°C)* which then vaporized out of the compact. Therefore, as previously reported† no further work on these systems was conducted.

The Fe - 30Cr - 1Y - 43Eu_2O_3 cold-pressed compacts sintered to 68 percent of theoretical density with no apparent chemical reaction. These sintered compacts were machined, inserted into an Fe - 30Cr - 1Y extrusion billet, (Figure 2.2-1), and extruded at 1100°C with a 14:1 reduction ratio, which further densified the core to 92 percent of theoretical. This extrusion produced a 1-inch-diameter rod with a core diameter of 0.5 to 0.6 inch. The cladding was metallurgically bonded to the core.

Thermal Expansion Studies

A thermal expansion specimen 0.25 inch in diameter and 2 inches long was machined from the extruded rod. This specimen was slowly heated and cooled in vacuum to determine the thermal-cycle-induced growth of Fe - 30Cr - 1Y - 43Eu_2O_3 compared to that of Eu_2O_3-Ni, and to measure its thermal expansion coefficient at the same time. After two thermal cycles to 980°C, the length of the sample was found to have increased by only 0.00015 inch per inch. By comparison, after two similar heat treatments, the length of Eu_2O_3-Ni cermets increased by 0.0009 to 0.0010 inch per inch. Thus, Eu_2O_3-Fe-Cr-Y compacts demonstrated a lower thermal-cycle induced growth rate than Eu_2O_3-Ni compacts.

Oxidation Testing

Oxidation tests on the extruded rod were conducted at 1000°, 1100°, and 1200°C. The results of these tests are shown in Figure 2.2-2. After an exposure of only 50 hours at 1000°C, the cladding was oxidized more than 30 mils deep. The 1200°C test was discontinued after only 100 hours because of the catastrophic rate of oxidation.

*F. H. Spedding and V. H. Daane, *The Rare Earth Alloys*, John Wiley and Sons, Inc., New York, 1961, p. 180.

†NMP-HTMP-1, "High Temperature Materials Program Progress Report No. 1." GE-NMPO, May 1, 1961 – June 30, 1961.

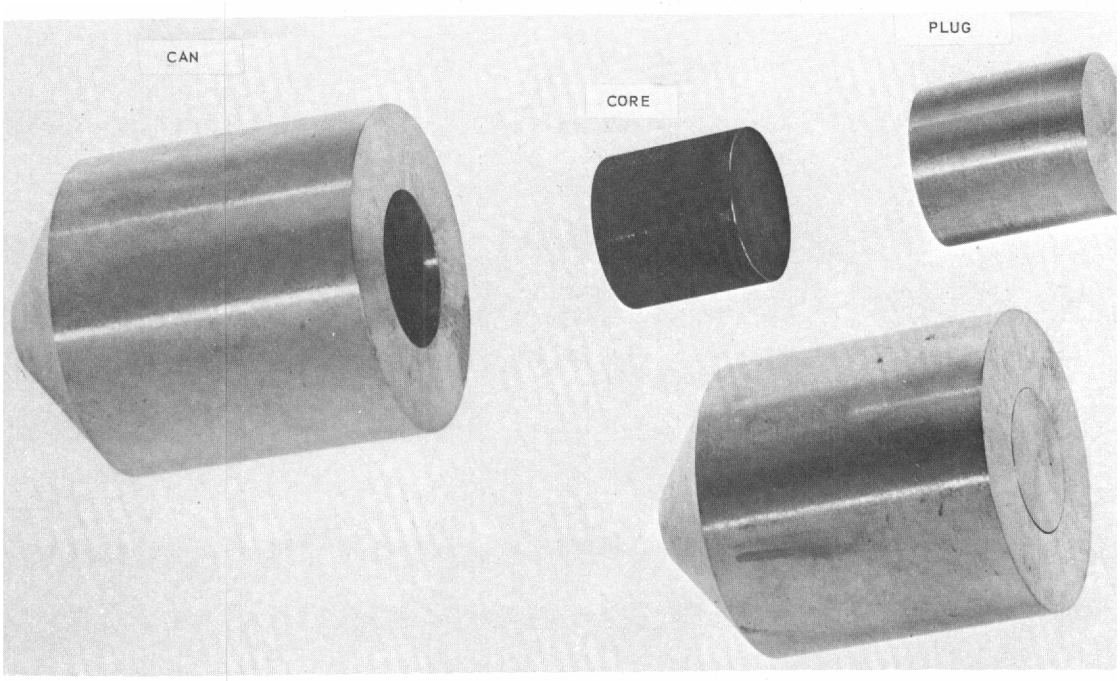

Fig. 2.2-1 – Exploded view of Fe – 30Cr – 1Y – 43 weight percent Eu_2O_3 core and Fe – 30Cr – 1Y extrusion can (Neg. P61-10-3)

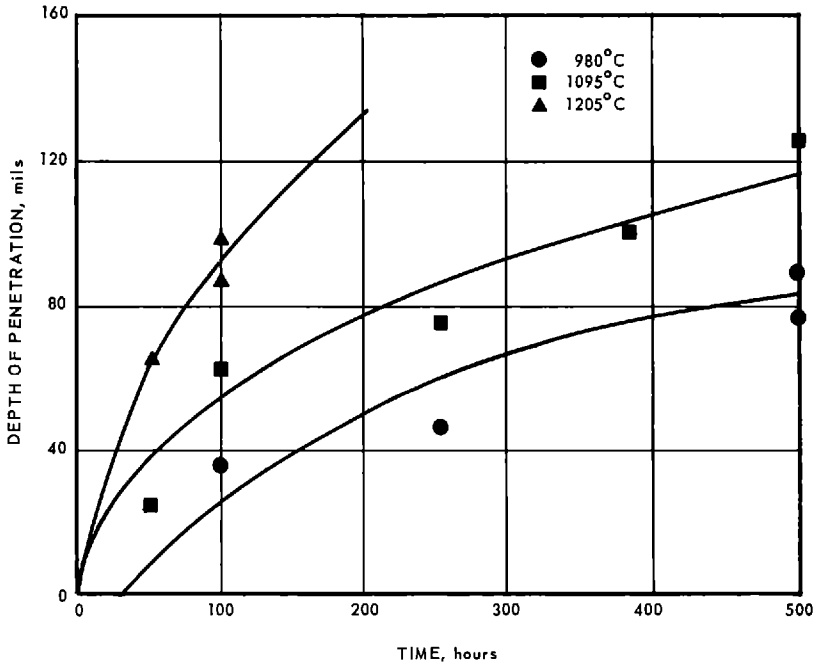

Fig. 2.2-2 – Oxidation penetration as a function of time for Fe – 30Cr – 1Y – 43 weight percent Eu_2O_3 reacted in air at various temperatures

The activation energy for this oxidation was calculated to be about 26 Kcal per mole assuming the parabolic oxidation law which Felten has shown* to be valid for Fe-Cr alloys. Felten has also reported that the activation energy for oxidation of Fe - 30Cr - 1Y is about 70 Kcal per mole and for Fe - 30Cr about 47 Kcal per mole. Thus, the oxidation resistance of Fe - 30Cr - 1Y - 43Eu_2O_3 is not only less than Fe-Cr-Y alone, but is also lower than the unimproved base alloy (Fe - 30Cr).

Metallographic and Electron Probe Analyses

To determine the cause of this unexpected lowering of the oxidation resistance, one sample of 43Eu_2O_3 - Fe - 30Cr - 1Y that had been heated for 100 hours in air at 980°C was examined metallographically and chemically using an electron-beam microprobe. The results of these examinations are shown in Figure 2.2-3. Where the yttrium content originally was present as a component of the metallic Fe-Cr-Y matrix, the electron-beam microprobe data show only iron and chromium in the metallic phases of the matrix. Even the cladding close to the core shows yttrium-free metallic phases. The yttrium content of the core is found in association with the europium oxide phases, presumably as a Y_2O_3 reaction product. Thus, a chemical mechanism involving the reduction of europium sesqui-oxide by elemental yttrium to produce yttrium sesqui-oxide and a lower oxide of curopium or elemental europium is indicated. Since the yttrium content of the Fe - 30Cr - 1Y alloys is essential for satisfactory oxidation resistance and a satisfactory level of this element cannot be maintained in the alloy in contact with Eu_2O_3, no further work is planned for these materials.

The use of diffusion barriers, coated particles, flame spraying or other techniques to protect the Eu_2O_3 might circumvent this problem. Additional effort with these materials may be warranted if such barrier materials and techniques are proven useful.

NOBLE AND REFRACTORY METALS

Although the Fe-Cr-Y alloys proved to be incompatible with Eu_2O_3 materials, the investigation of europium sesqui-oxide continued with the noble metals Pt, Pd, and Ir for applications in oxidizing atmosphere and with the refractory metals Mo, Nb, Re, Ta, and W in non-oxidizing environments.

Preliminary compatibility investigations were conducted to obtain material data on the combinations of Eu_2O_3 and the noble metals at temperatures up to 1300°C in air for periods of 10,000 hours. Cold-pressed compacts of Pt - 50Eu_2O_3 (weight percent), Pd - 50Eu_2O_3, and Ir - 50Eu_2O_3 were heated in air at 1370°C and 1430°C. Specimens of the Pt and Ir compositions were also heated to 1630°C. Exposure for two hours in air at these test temperatures revealed no evidence of reactivity or instability of the Eu_2O_3 with the metallic phases. Further long-time environmental tests at 1200°, 1300°, and 1400°C, fabrication studies, and mechanical property evaluation of noble metal - Eu_2O_3 bodies are in progress.

For high-temperature gas-cooled reactors that use nonoxidizing working fluids such as H_2, He, or Ne, the refractory metals W, Ta, Mo, Rh, and Nb were studied. Combinations of these metals with Eu_2O_3 in hydrogen at 1370°C showed evidence of reactivity.

Work was being conducted at the end of this reporting period to determine if the reduction of the Eu_2O_3 proceeds to a lower oxide or to europium metal. If the reduction is to the metal, the systems are of no interest. If the reduction proceeds to a lower oxide, this compound will be investigated in combination with the refractory metals for control element applications.

*E. J. Felten, "High Temperature Oxidation of Fe-Cr Base Alloys with Particular Reference to Fe-Cr-Y Alloys," GE Research Laboratory, Report No. 60-GC-85, March 1960.

SUMMARY AND CONCLUSIONS

The Fe-Cr-Al and Fe-Cr-Y alloys are unstable in the presence of Eu_2O_3 because both Al and Y reduce Eu_2O_3 to a lower oxidation state. Diffusion-barrier or coated-particle techniques will be required to protect Eu_2O_3 if it is to be considered for application with Fe-Cr-Al or Fe-Cr-Y alloys.

Europium sesqui-oxide combined with Pd indicates short-time thermal stability in air at 1400°C. Similarly, combinations of Pt and Ir with Eu_2O_3 are stable in air up to 1600°C. Long-time stability tests of Eu_2O_3 with the noble metals are in progress.

PLANS AND RECOMMENDATIONS

The noble metals Pt and Ir combined with Eu_2O_3 indicate a 1600°C potential as nuclear control materials, while Pd-Eu_2O_3 can be considered for 1400°C applications. A comprehensive metallurgical and thermomechanical evaluation of these materials is planned. This will include fabrication studies on powder mixtures of these materials and noble-metal-fiber-reinforced bodies. Isothermal, thermal cycling, and reactor testing on the most stable of these bodies are planned.

2.3 HIGH-TEMPERATURE THERMAL-INSULATION DEVELOPMENT (57010)

The objective of this program is to develop thermal insulation of reduced weight to reduce the operating temperature of control and structural components of high-performance reactors.

Refractory fiber insulation encased in thin metal sheets is satisfactory at temperatures up to 1000°C in high-velocity gas streams. Above 1000°C, the thin metal sheets do not have sufficient resistance to deformation, and the stronger refractory metals require additional coating or cladding for oxidation resistance. The use of honeycomb or sandwich combinations of metals, nonmetals, and/or foamed ceramics will be evaluated during this program. The present work is concerned with the development of techniques for preparing foamed BeO and the evaluation of the resulting structure for thermal conductivity and thermal and structural stability.

FOAMED BeO STUDIES

Foamed BeO (UOX Grade)

The procedure* for foaming BeO using -325-mesh beryllium metal and a 30 percent solution of H_3PO_4 has been proved to be reproducible. This procedure resulted in a foamed structure with a density of approximately 1.0† gram per cubic centimeter and an average pore size of 0.05 centimeter (0.02 inch) in diameter. The process consists of a 48-hour cure at 600°F, a 3-hour air sinter at 1400°C, and a 2-hour H_2 sinter at 1400°C. Ignition of the material in air does not bring about the complete elimination of the phosphate produced during foaming. However, sintering in a hydrogen atmosphere at 1400°C yields a pure UOX grade BeO foamed structure free of phosphorous.

A thermal gradient test was conducted on a 5/16-inch-thick sample of this foamed BeO and on a 1/4-inch-thick sample of ZrO_2 with a density of 4.27 grams per cubic centimeter. An oxyacetylene torch was used as a heat source. The thermal gradients measured during these tests are shown in Figure 2.3-1. These tests, although preliminary in nature, indi-

*GEMP-5A, "High Temperature Materials Program Progress Report No. 5, Part A," GE-NMPO, November 15, 1961, p. 54.

†Determined since being reported as 0.6 g/cm^3 in GEMP-7A, "High-Temperature Materials Program Progress Report, No. 7, Part A," GE-NMPO, January 15, 1962, p. 59.

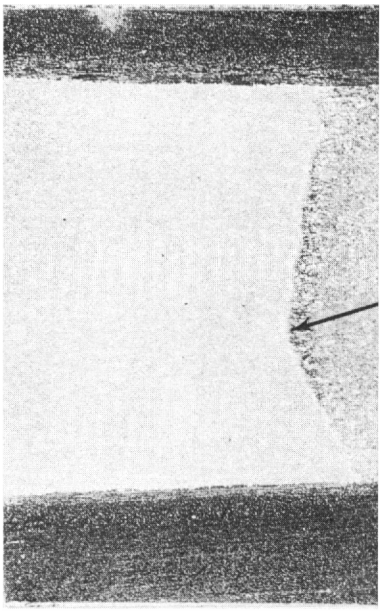

A. MACROSTRUCTURE

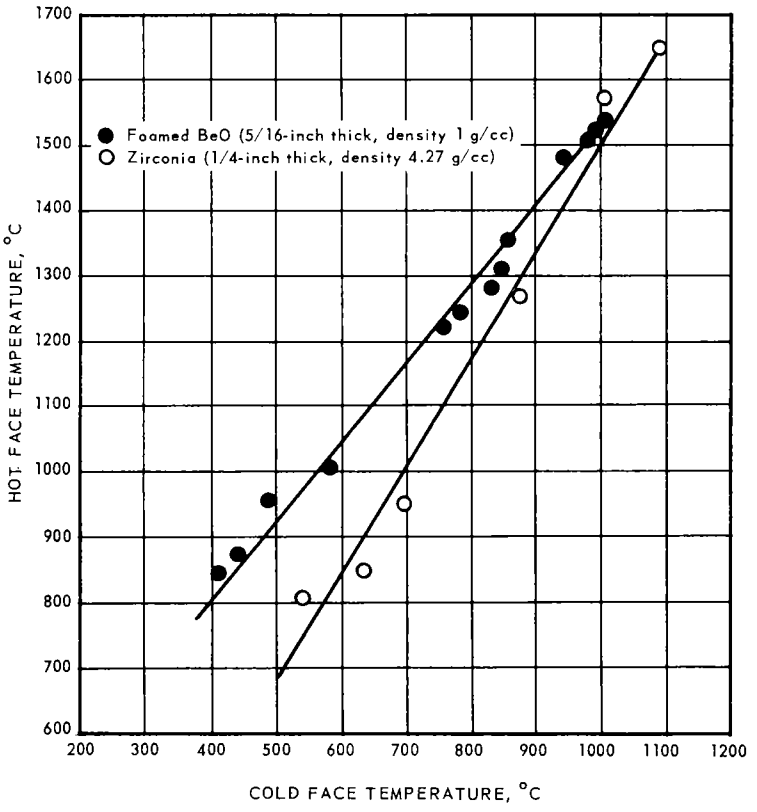

Fig. 2.3-1 – Comparison of thermal gradient of foamed BeO and zirconia

cate that weight-optimized insulations may be developed for service at higher temperatures than presently available.

Foamed BeO (Refractory Grade)

The fabrication of foamed BeO using -325-mesh refractory grade BeO was also investigated. Foamed bodies of refractory grade BeO were produced with difficulty due to the slower rate of chemical reaction between refractory grade BeO and H_3PO_4. The best product resulting from this study had a density of 1.5 grams per cubic centimeter and an average pore size of 0.025 centimeter. Because of the higher density and slow reaction rate with the H_3PO_4, the use of this material for the total body was discontinued. However, the smaller pore sizes and lower shrinkage attained during the firing of refractory grade BeO indicated that this material does have certain advantages.

As a result of this observation, foamed BeO structures using mixtures of refractory grade and UOX grade BeO were produced. A tabulation of the compositions that were investigated is shown in Table 2.3-1. The composition that contained the highest proportion of refractory grade BeO shrank the least during processing. Over the range of compositions studied, the compositions containing the most UOX grade BeO did not have the lowest densities. The 60-percent refractory grade - 40 percent UOX grade BeO was found to have the finest pore size and most uniform structure. These bodies are shown in Figure 2.3-2.

SUMMARY AND CONCLUSIONS

Small (2 inches by 4 inches by 1/2 inch) foamed UOX grade and refractory grade BeO bodies have been reproducibly fabricated with a resulting density of 1.0 gram per cubic centimeter.

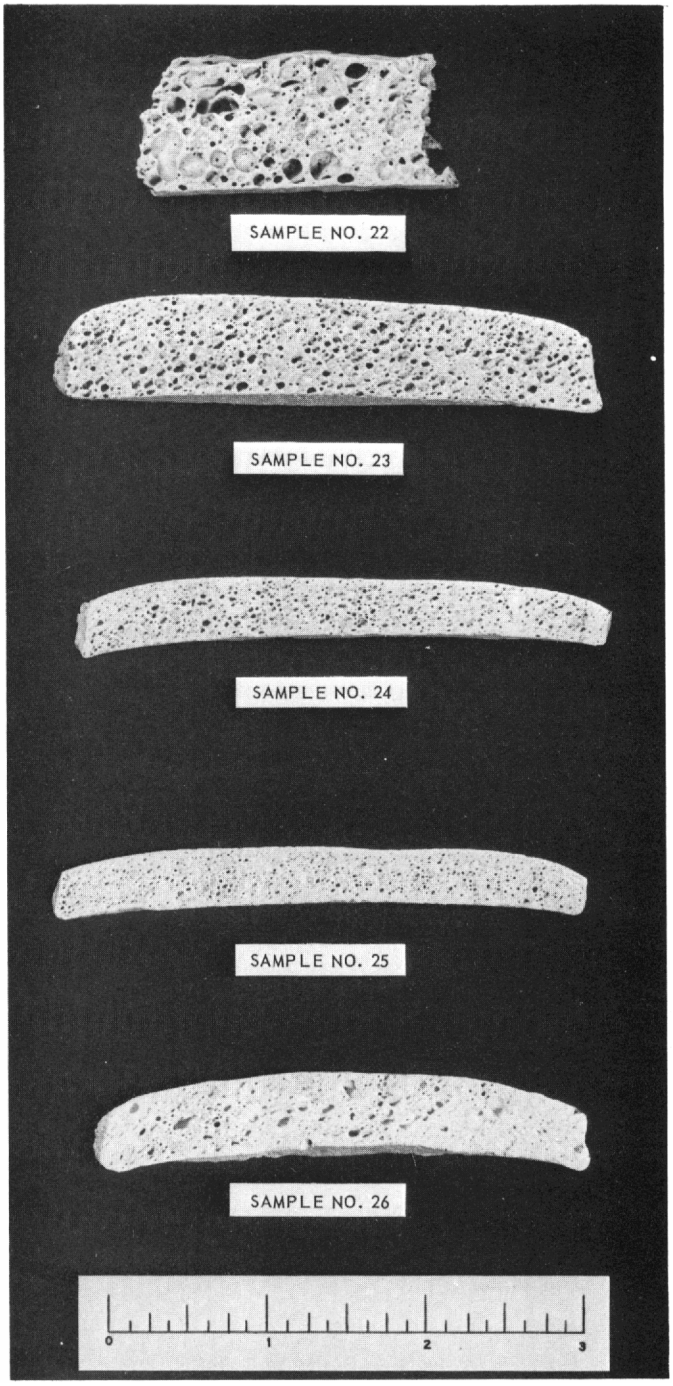

Fig. 2.3-2 – Variation in pore size of foamed BeO of various UOX-refractory grade mixtures (Neg. P61-12-30)

TABLE 2.3-1

PROPERTIES OF FOAMED BeO CONTAINING VARIOUS PROPORTIONS OF REFRACTORY GRADE AND UOX GRADE BeO

Sample No.	Percent RG	Percent UOX	Amount Of Powders, g	Volume Of Acid,[a] ml	Area Shrinkage,[b] %	Density, g/cc	Pore Size, cm
22	90	10	200	100	2.5	0.87	0.02-0.5
23	80	20	177	100	12	0.81	0.01-0.25
24	70	30	147	100	20	1.0	0.01-0.2
25	60	40	112	100	20	0.99	0.01-0.15
26	50	50	104	100	27	0.98	0.02-0.3

[a]30% solution of H_3PO_4.
[b]After sintering at 1540°C for 1 hour in air.

PLANS AND RECOMMENDATIONS

An extensive ceramic processing study and thermomechanical evaluation program is planned for foamed BeO. This will include investigating other methods of foaming and the fabrication of larger rectangular bodies. Thermal conductivity, density, dimensional stability, strength, and erosion resistance evaluations are planned, as well as the fabrication and evaluation of composite refractory metal honeycomb structures and foamed ceramics such as BeO composites.

2.4 STRUCTURAL MATERIALS (57003)

The objective of this program is to provide process specifications for the fabrication of reliable reactor supporting structures capable of operating in excess of 850°C for periods of 1,000 to 10,000 hours. This work includes a fundamental investigation on the wetting and flow characteristics of braze alloys of interest; braze-alloy - base-metal compatibility studies; remelt characteristics; and thermomechanical evaluation of brazed sections of a selected high-temperature alloy and a refractory-metal joining-study. The present program has concentrated on one representative high-temperature precipitation hardening alloy, Rene' 41. Prior work* had demonstrated that Rene' 41 could be successfully brazed with M-61, a new brazing alloy. However, when structural assemblies containing a large number of braze joints were brazed in industrial furnaces, inconsistent results were obtained with laboratory procedures that had previously produced high-quality braze joints on small assemblies.

The program on vacuum brazing of Rene' 41 has been directed toward determining optimum conditions for flow for braze-alloys (M-61 and GE-81) on Rene' 41 as a function of (1) surface finish, (2) brazing temperature, (3) magnitude of vacuum, and (4) joint clearance. To date substantial data on surface finish only has been otained.

VACUUM BRAZING EQUIPMENT

A vacuum-muffle resistance-heated furnace was designed and constructed for the initial phase of the vacuum brazing program. The furnace is instrumented to permit meas-

*J. C. Marshall, "Rene' 41 – M-61 Vacuum Brazing Investigation," GE-ANPD, DC 61-7-7, July 1961.

urement of the vacuum in both the hot and cold zones. The temperatures are measured by thermocouples attached directly to the specimens and/or by sighting on them with a radiation pyrometer. A steady state pressure of 3 x 10^{-5} mm of Hg can be attained on the entire system at 1135°C. The specimens are placed on the work basket in the cold zone, the cold zone is evacuated, and the work basket is transferred to the hot zone by means of a push rod. A typical time - temperature - vacuum plot of a brazing cycle in this furnace is shown in Figure 2.4.1.

A second high-vacuum brazing furnace utilizing a molybdenum wire heating element is also being used for this work. The furnace is a three-chamber semicontinuous-type furnace with an entrance chamber, working chamber, and exit chamber. The size of this equipment will permit the brazing of parts 11 by 11 by 42 inches up to 1650°C in a vacuum (5 x 10^{-5} mm Hg). The furnace can also be operated in argon or hydrogen. Figure 2.4-2 illustrates the working chamber of this furnace.

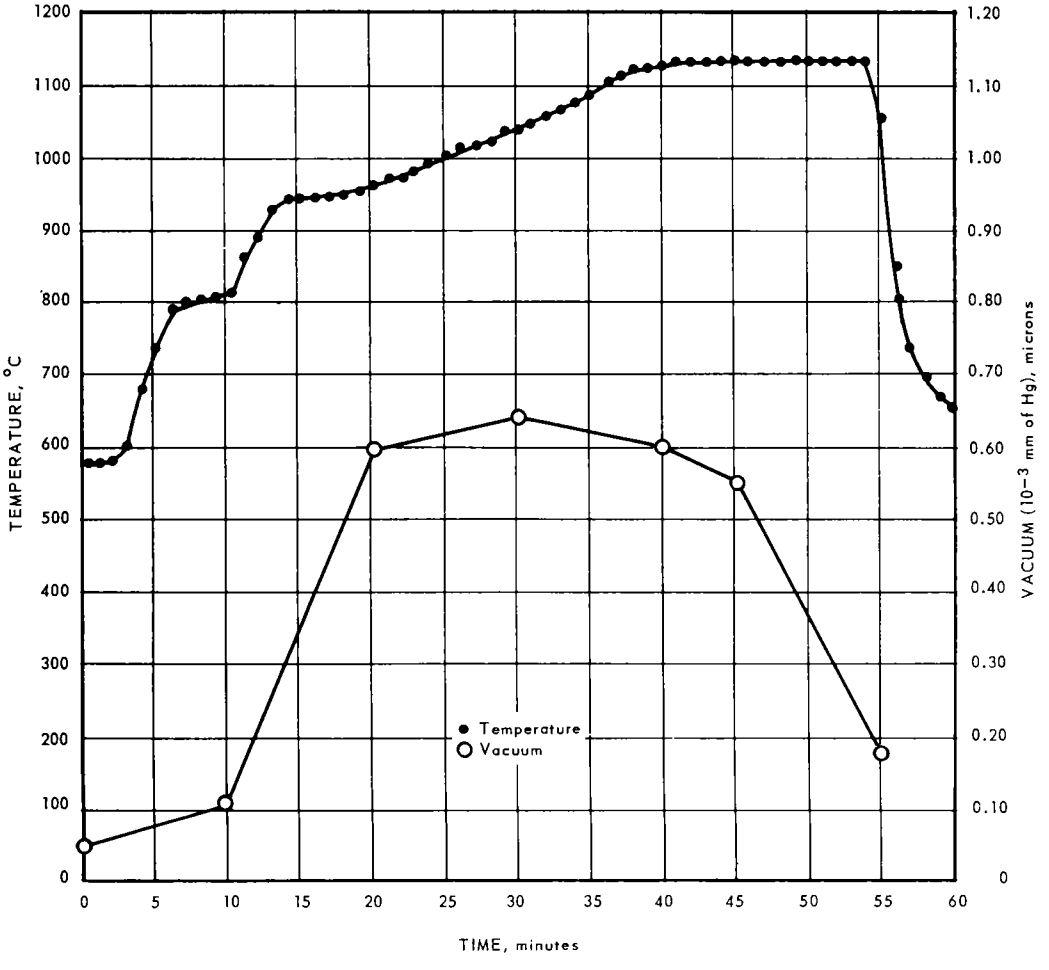

Fig. 2.4-1 – Typical brazing cycle for GE-81 and M-61 brazing alloys

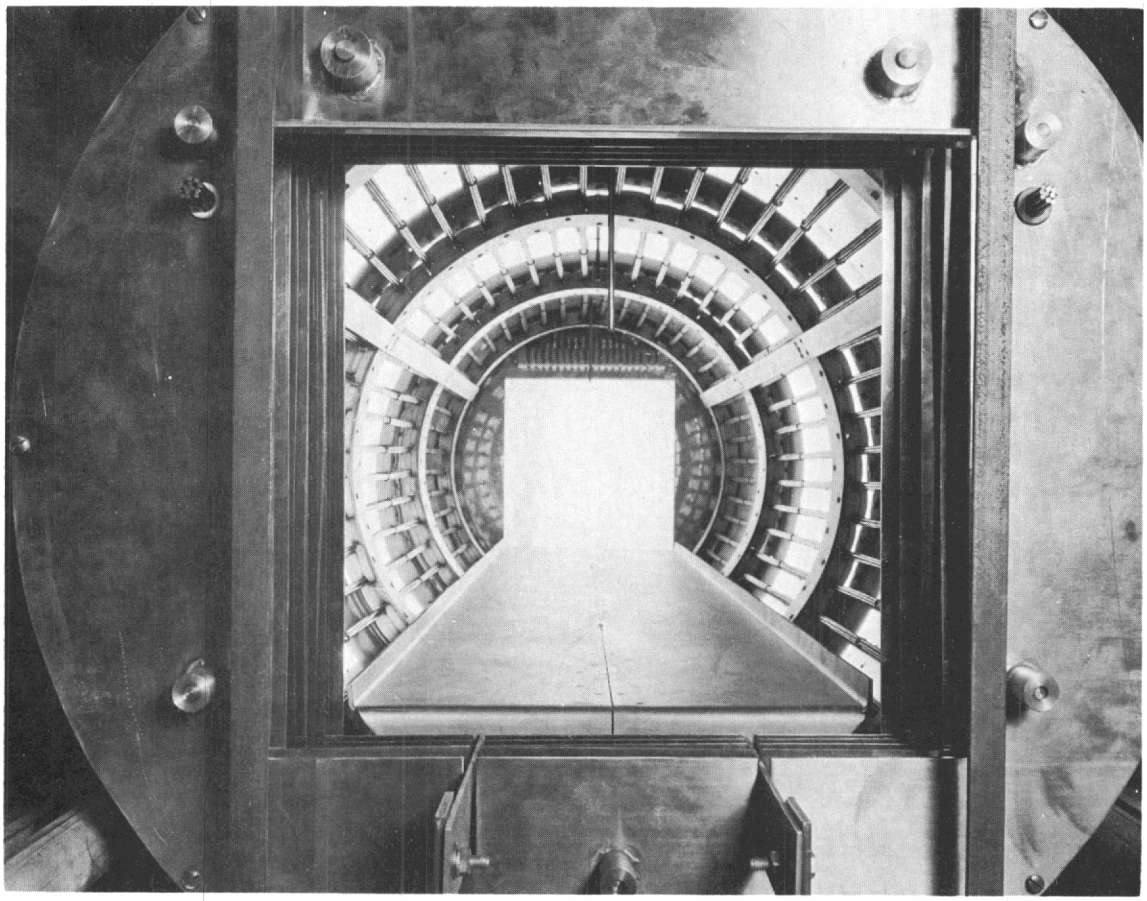

Fig. 2.4-2 – Vacuum-brazing furnace with molybdenum wire elements

VACUUM BRAZING STUDY ON RENE' 41

Some of the effects of the surface condition of Rene' 41 on the flow characteristics of GE-81 and M-61 braze alloys have been established through the evaluation of wetting indexes.*

A T section and four Rene' 41 base plates (1 by 1 by 1/16 inch) of varying surface finish were simultaneously subjected to the brazing cycle described in Figure 2.4-1. The T section was used as a control to insure that the wetting and spreading tests were being conducted under conditions that would produce a satisfactory braze joint. Each base plate had a different surface finish: (1) as received, 25 microinches (RMS), (2) 20 to 25 microinches (RMS), (3) 65 to 75 microinches (RMS), and (4) 120 to 140 microinches (RMS). The variation in surface finish was attained by grit blasting with alumina. Preliminary electron microprobe analyses have established that the Rene' 41 surface as received is depleted of Al and Ti by the mill-pickling process.†

In the melting and flow test, a 0.06-gram cold-pressed pellet of braze alloy was placed on each Rene' 41 base plate. Possible errors, caused by variables other than surface finish, were minimized by maintaining constant brazing cycles, vacuum conditions, and sample preparation techniques.

*W. Feduska, "High Temperature Brazing Alloys – Base Metal Wetting Reactions," *Welding Journal, Vol. 38,* March 1959.

†NAOH 2 to 5 percent NAH, 750° to 800°F, 30 minutes; rinse, $KMNO_4$ 2 to 6 percent solution with 1 to 3 percent NAOH, 130° to 140°F, 30 minutes; rinse; Nitric – hydrofluoric acid, 140° to 150°F, 30 minutes; rinse; scrub.

Although it is normally recommended that GE-81 and M-61 be used at 1175°C, satisfactory T sections were obtained at 1135°C, and this temperature was maintained throughout all of the described tests.

From the data obtained to date, it is apparent the braze-alloy flow is affected by three surface conditions: roughness, chemistry, and directionality. Additional tests will be required to establish the order of magnitude to which these three surface conditions affect braze-alloy flow and to establish the degree of statistical confidence in all of the data. The results to date on the surface condition of Rene' 41 with M-61 and GE-81 flow are presented in Figure 2.4-3. Under the brazing conditions described, it can be demonstrated that: (1) the alumina grit embedded in the Rene' 41 surface during the grit-blasting process causes a decrease in the wetting index for GE-81 and M-61 braze alloys and (2) the removal of the alumina grit and the depletion of the surface during the mill-pickling process causes the wetting index for GE-81 to increase on the grit-blasted and mill-pickled Rene' 41 surface. Thus, the wetting index for GE-81 on a grit-blasted and mill-pickled Rene' 41 surface increases as the surface roughness increases. It can also be demonstrated that (3) greater variations in flow as a function of surface condition occurred with GE-81 on Rene' 41 than with M-61 on Rene' 41 under the specific brazing conditions used.

Additional studies at higher temperature (1175°C) are planned to study the effect of surface condition on the flow of these braze alloys with Rene' 41.

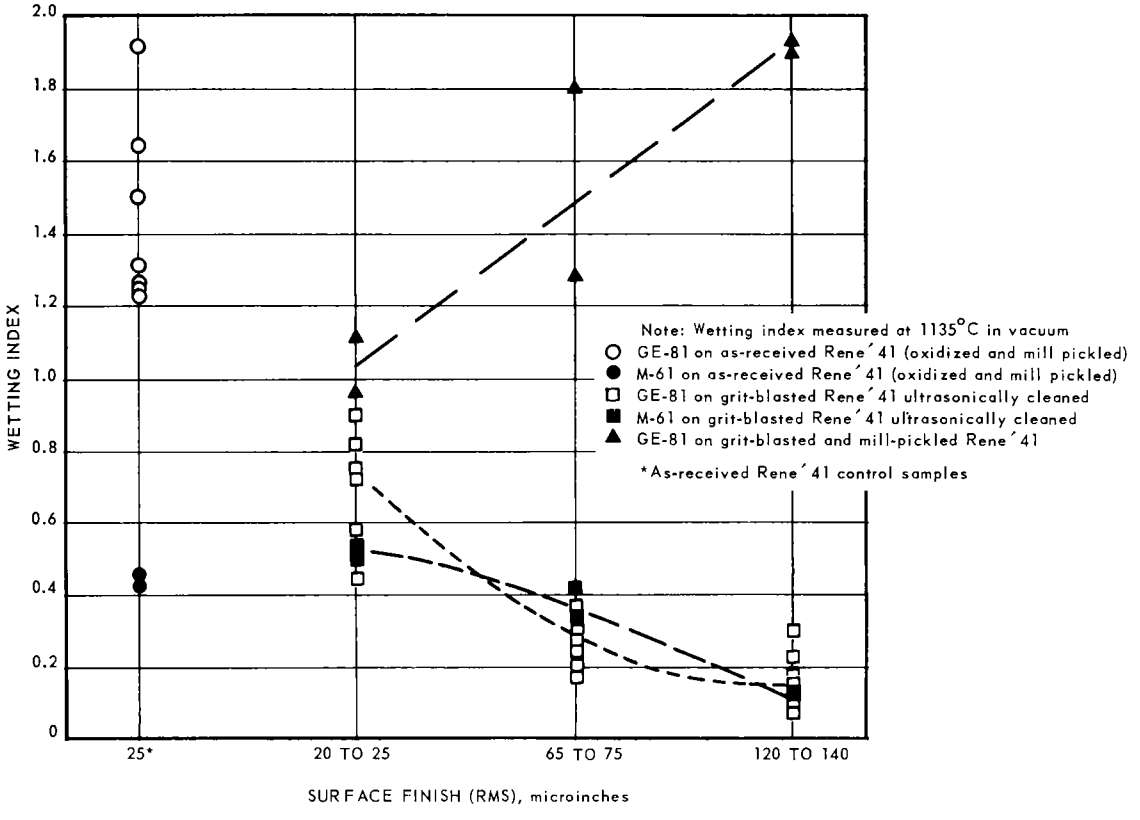

Fig. 2.4-3 – Wetting index for GE-81 and M-61 braze alloys as a function of surface finish

SUMMARY AND CONCLUSIONS

The effects of surface finish on the flow of the braze alloys M-61, GE-81, and Rene' 41 at 1135°C and 3 x 10^{-5} mm Hg has been established. The GE-81 alloy exhibits greater variation in flow than the M-61 alloy on Rene' 41 at 1135°C.

PLANS AND RECOMMENDATIONS

An increase in the refractory-metal joining effort is planned to include electron-beam welding and electron-beam brazing as well as diffusion-bonding investigations. Evaluating all these joining methods for application to refractory fuel-element structures and refractory-metal reactor-structure components by determining mechanical strength of typical joints as a function of temperature, time, and stress level will be initiated. The brazing investigation on Rene' 41 and GE-81, M-61 braze alloys to determine effects of higher temperature and joint clearance will be continued, and the relation of these parameters to stress rupture properties of brazed joints will be determined.

3. RADIATION EFFECTS

3.1 HIGH-TEMPERATURE ALLOYS (57004)

The objective of this work is to determine the effect of radiation on the time-, temperature-, and stress-dependent properties of selected high-temperature alloys; to identify the causes of any observed reductions in these properties; and attempt to develop remedial measures.

The preliminary investigations that have been made of the effects of irradiation on the stress-rupture properties of A-286 and Inconel X, two important structural materials, revealed an incipient problem area in the design of high performance reactor systems. These studies of the long time properties of these alloys indicated that substantial reductions in their 650°C and, to a lesser extent, 540°C stress-rupture strengths occurred after neutron irradiation at pile ambient and also at elevated temperatures. The losses in strength were accompanied by significant reductions in rupture ductility. These effects were observed for dosages ranging from 10^{17} to 10^{20} nvt ($E_n \geq 1$ Mev). In addition, indications were that the damage was not mitigated by complete re-solution treatment and subsequent aging.

As a result of these studies an experimental program was established to continue these investigations in broader scope using test specimens made from alloys of A-286, Hastelloy X, and Rene' 41.

The A-286 alloy is an intermediate-temperature (650°C) precipitation-hardening high-strength commercial material. Hastelloy X is a high-temperature solution-strengthened oxidation-resistant commercial alloy possessing useful strength levels and suitable for high temperature applications up to about 1200°C. Rene' 41 is one of the strongest high-temperature precipitation-hardening commercial alloys currently available for high stress applications up to temperatures of about 920°C.

The basic program consists of eleven experiments supported by structural studies and complemented by investigations of related binary or ternary alloys. The major portion of the data to be generated under the program will be obtained by the end of this fiscal year and preliminary evaluations will be completed. The concluding experiments, final results and analysis, and the conclusions will be completed before the end of the following year. The program is based on the following three phases of work.

PHASE I - EXPERIMENTAL PROGRAM

The tensile, stress-rupture, fatigue and relaxation properties of A-286, Hastelloy X and Rene' 41 will be measured using specimens that have been exposed in a neutron environment at temperatures from ambient to about 870°C and dosages to about 10^{19} nvt ($E_n \geq 1$ Mev). The 11 experiments comprising this phase are described in Table 3.1-1, and in addition, a preliminary summary of the results on stress-rupture testing is listed. The postirradiation testing of all specimens will be performed at temperatures ranging from room temperature to 870°C. Unirradiated specimens from the same heats and re-

ceiving the same identical heat treatments will also be tested to give the required control data for comparative purposes. With a few exceptions all of the control specimens will receive a temperature-time treatment intended to simulate the in-pile thermal-time conditions.

The specimens used in these tests and their determinations are shown in Figure 3.1-1.

The mechanical-thermodynamic capsule design, stress rupture equipment, pneumatic fatigue equipment, and testing procedures are given in the Addendum to this section.

PHASE II - STRUCTURAL STUDIES

The objective of this phase is to develop an understanding of the damage mechanism(s). The nature of any structural changes produced in these alloys by irradiation will be investigated using selected specimens from Phases I and III. Several irradiated and control specimens of this program have already been studied with the electron microscope. The techniques and some of the results on these test specimens are discussed later in this report.

PHASE III - STUDIES OF THE Ni-Al SYSTEM

This phase of the program is a fundamental study of the effects of irradiation on the aging characteristics and other properties of a relatively simple, metallic alloy. The alloy system currently under investigation is 92 weight percent Ni - 8 weight percent Al.

This alloy is a face-centered cubic precipitation-hardening and the precipitant phase is Ni_3Al which is the pure form of γ' (the primary hardener in A-286 and Rene' 41). This alloy was selected because of the substantial knowledge available on Ni_3Al and similar intermetallic compounds.

EXPERIMENTAL PROGRAM

Irradiated Specimen Status

Approximately 370 specimens have been or are being irradiated, for the most part at Idaho in the ETR 99 facility. The specimens were exposed in special capsules designated MT-27, MT-38, MT-43, and MT-51. The first three capsules each contained 81 test specimens and the last contained 120 specimens. Other capsules designated MT-35A, MT-35B, MT-36, and MT-44A, MT-44B, MT-44C, and MT-44D were fabricated for experiment No. 5 and experiment No. 7, respectively. Irradiation of specimens from experiment No. 5 has been completed in the C-48 facility of the LITR at Oak Ridge; the preliminary results of post-testing are reported later in this document. The capsules containing specimens for experiment No. 7 is now at Oak Ridge scheduled for irradiation sometime in February. Approximately four additional irradiations remain to be made.

Postirradiation physical property testing has started on the specimens from MT-27 at Evendale and at the Idaho Test Station. Several test stands are to be used in this work at BMI under a subcontract with GE-NMPO. The Battelle Memorial Institute (BMI) post-irradiation physical property tests were scheduled to start in January.

Control Specimen Status

During this period 71 rupture tests were completed. Of these, 54 specimens had been given a simulated reactor-cycle-temperature treatment. To determine any difference in resulting properties, 17 specimens were tested in the original heat treated condition.

This group of tests included A-286, Hastelloy X and Rene' 41 specimens in support of experiments No. 1, 2, 4, and 5. These data are listed in Tables 3.1-2, 3.1-3, and 3.1-4.

TABLE 3.1-1

SUMMARY OF EXPERIMENTAL PROGRAM

Experiment No.	Objective	Alloys	Number[a] and Type[b] of Specimens	Irradiation Data: Capsule[c]	Irradiation Data: Average Dosage nvt ($E_n \geq 1$ Mev)	Irradiation Data: Average Temperature,[d] °C	Rupture Strength,[e] psi: 100 Hours Control	100 Hours Irradiated	1000 Hours Control	1000 Hours Irradiated
1	To investigate the effects of neutron irradiation on the tensile and stress-rupture properties of high temperature alloys receiving the standard heat treatment[f] for these experiments. To generate the background data needed on these alloys for comparison with other experiments.	A-286	26 S,C,T,NT	MT-27	7×10^{19}	540	100,000		82,000	
			16 S,C,T,NT	MT-38	7×10^{19}	650	54,000		41,000	
			22 S,C,T,NT	MT-43	7×10^{19}	650				
		HASTELLOY X	16 S,C,T,NT	MT-27	7×10^{19}	540	66,000		54,000	
			16 S,C,T,NT	MT-38	7×10^{19}	650	43,000		26,000	
			5 S,C	MT-43	7×10^{19}	650				
			28 S,C,T,NT	MT-51	4×10^{19}	870				
		RENE' 41	6 S,C	MT-27	7×10^{19}	540				
			16 S,C,T,NT	MT-38	7×10^{19}	650	117,000		87,000	
			14 S,NT	MT-43	7×10^{19}	650				
			20 S,C,T,NT	MT-51	4×10^{19}	870				
2	To investigate the effect on the stress-rupture properties of a standard heat treatment[f] following neutron irradiation.	A-286	16 S,C,T	MT-27	7×10^{19}	540	98,000		76,000	
			7 S,C,T	MT-38	7×10^{19}	650	54,000		40,000	
		HASTELLOY X	11 S,C,T	MT-27	7×10^{19}	540	61,000		52,000	
			7 S,C,T	MT-38	7×10^{19}	650	39,000		25,000	
			10 S,C,T	MT-51	4×10^{19}	870				
		RENE' 41	7 S,C,T	MT-38	7×10^{19}	650	101,000		81,000	
			10 S,C,T	MT-51	4×10^{19}	870				
3	To investigate the role of grain size and other related structural characteristics in the possible mechanisms of neutron induced stress-rupture property changes.	A-286	20 S,C,T	MT-43	7×10^{19}	650				
		RENE' 41	10 S,C,T	MT-43	7×10^{19}	650				
			10 S,C,T	MT-51	4×10^{19}	870				
4	To investigate the effect of the degree of pre-irradiation aging on the stress-rupture properties of irradiated alloys.	A-286	6 S	MT-27	7×10^{19}	540	96,000	80,000	74,000	70,000
			6 S	MT-38	7×10^{19}	650				
		RENE' 41	6 S	MT-38	7×10^{19}	650				
			6 S	MT-51	4×10^{19}	870				
5	To determine whether some parameter that is a function of thermal neutrons has an effect on stress-rupture properties.	A-286	2(shielded) S,C	MT-35A	3.5×10^{16} 2.4×10^{16}g	36	57,000	~51,000	38,000	~33,000
			2(shielded) S,C	MT-35B	2.6×10^{16} 1.6×10^{16}g	36				
			5(unshielded) S,C	MT-36	3.0×10^{16} 1.2×10^{16}g	36				
6	To investigate the effect of neutron reactions with trace quantities of boron generally present in alloys on their stress-rupture properties.	A-286	4 (Heat 1) S	To be assigned	~7×10^{20}	650				
			4 (Heat 2) S	To be assigned	~7×10^{20}	650				
			4 (Heat 3) S	To be assigned	~7×10^{20}	650				
			4 (Heat 4) S	To be assigned	~7×10^{20}	650				
7	To determine whether neutron irradiation at reactor ambient temperatures induces strain rate embrittlement.	A-286	5 NT	MT-44B	~3×10^{19}	Reactor ambient				
			3 S,NT	MT-44D	~3×10^{19}					
		HASTELLOY X	5 NT	MT-44A	~3×10^{19}					
			1 NT	MT-44D	~3×10^{19}					
		RENE' 41	5 NT	MT-44C	~3×10^{19}					
			1 NT	MT-44D	~3×10^{19}					
8	To determine the fast neutron threshold of radiation induced changes for stress-rupture properties of high temperature alloys.	A-286	6 S	To be assigned	~10^{17}	650				
			6 S	To be assigned	~10^{15}	650				
		HASTELLOY X	6 S	To be assigned	~10^{17}	650				
			6 S	To be assigned	~10^{15}	650				
		RENE' 41	6 S	To be assigned	~10^{17}	650				
			6 S	To be assigned	~10^{15}	650				

TABLE 3.1-1 (Cont.)

SUMMARY OF EXPERIMENTAL PROGRAM

Experiment No.	Objective	Alloys	Number[a] and Type[b] of Specimens		Irradiation Data: Capsule[c]	Irradiation Data: Average Dosage nvt($E_n \geq 1$ Mev)	Irradiation Data: Average Temperature,[d] °C	Rupture Strength,[e] psi: 100 Hours Control	Rupture Strength,[e] psi: 100 Hours Irradiated	Rupture Strength,[e] psi: 1000 Hours Control	Rupture Strength,[e] psi: 1000 Hours Irradiated
9	To investigate the effect of neutron irradiation on the relaxation properties of high temperature alloys.	A-286	4	R	To be assigned	$\sim 10^{19}$	650				
		RENE' 41	4	R	To be assigned	$\sim 10^{19}$	730				
10	To investigate the effect of neutron irradiation on the high temperature fatigue properties of high temperature alloys.	A-286	10	F	MT-51	4×10^{19}	540	68,000(10^7)[h]		56,000(10^8)	
			10	F	MT-51	4×10^{19}	650				
		RENE' 41	10	F	MT-51	4×10^{19}	650				
			10	F	To be assigned	$\sim 4 \times 10^{19}$	870				
11	To investigate the effect of neutron irradiation on the stress-rupture properties of welded joints of high temperature alloys.	HASTELLOY X	6	S	MT-51	4×10^{19}	870				
			5	S	To be assigned	$\sim 10^{19}$	650				
		RENE' 41	6	S	MT-51	4×10^{19}	870				
			5	S	To be assigned	$\sim 10^{19}$	650				

[a]Not including unirradiated control specimens

[b]See Figure 3.1-1 for description of specimens
- S = Smooth bar - stress rupture
- C = Combination notched and smooth bar - stress rupture
- T = Smooth bar - tensile
- NT = Notched bar - tensile
- R = Special bar - relaxation
- F = Smooth bar - fatigue

[c]Capsules MT-27, -38, -43, and -51 irradiated in ETR-99 Facility
Capsules for Experiment 5 irradiated in LITR C48 Facility at ORNL
Capsules for Experiment 7 to be irradiated at ORNL
Capsules for remaining experiments will be irradiated either at ORNL or ITS

[d]The same temperature applies to the data tabulated for rupture strength in this table (Specimens will also be tested at temperatures other than those received during irradiation)

[e]Since most of the irradiated specimens are now undergoing post-irradiation testing this tabulation will not be complete at this time. Other physical properties, such as tensile data, will be reported as they are generated.

[f]The standard heat treatment for these experiments are given as footnotes in Tables 3.1-2, 3.1-3, and 3.1-4 for A-286, Hastelloy X, and Rene' 41, respectively.

[g]Slow neutron flux (almost thermal)

[h]The 10^7 in parentheses refers to the number of cycles at the given stress.

UNCLASSIFIED

TABLE 3.1-2

A-286 CONTROL STRESS-RUPTURE TEST DATA

Specimen No.	Test Temperature, °C	Stress, psi	Rupture Life, hr	Specimen Type[a]	Heat No.	Elongation,[b] %	Reduction Of Area, %	Failure Distance From Fillet, in.	Applicable Exp. No.	Pre-Mfg. Treatment[d]	Pre-Test Treatment
31AS	540	110,000	32.8	S	2527	3.6	5.5	1/8	2	Standard	100 hours at 540°C, solution and age in argon
34AS	540	100,000	37.1	S	2527	5.2	10.8	1/8	2	Standard	100 hours at 540°C, solution and age in argon
43AS	540	100,000	88.0	S	2527	2.9	4.7	3/16	2	Standard	100 hours at 540°C, solution and age in argon
33AS	540	95,000	223.5	S	2527	1.6	1.8	1/2	2	Standard	100 hours at 540°C, solution and age in argon
42AS	540	95,000	116.3	S	2527	2.8	3.1	1/2	2	Standard	100 hours at 540°C, solution and age in argon
11J	540	90,000	242.0	C	2527	3.6	5.5	1/4	2	Standard	500 hours at 540°C, solution and age in argon
12J	540	100,000	71.0	C	2527	8.0	7.8	1/8	2	Standard	500 hours at 540°C, solution and age in argon
13J	540	88,000	87.6	C	2527	-	ruptured in notch	N[c]	2	Standard	500 hours at 540°C, solution and age in argon
50AS	650	50,000	136.9	S	2527	13.0	1.	1/2	2	Standard	100 hours at 650°C, solution and age in argon
17AA	540	100,000	94.0	S	7611	8.3	12.5	1/8	4	900°C, OQ and over-age	500 hours at 540°C
19AA	650	57,500	22.6	S	7611	8.3	21.3	1/8	4	900°C, OQ and over-age	500 hours at 650°C
20AA	650	58,250	22.0	S	7611	10.2	22.5	1/8	4	900°C, OQ and over-age	500 hours at 650°C
7AA	540	75,000	1066.0	S	7611	13.1	11.0	3/8	4	900°C, OQ	500 hours at 540°C
8AA	540	90,000	142.0	S	7611	27.3	29.7	1/8	4	900°C, OQ	500 hours at 540°C
9AA	650	57,500	86.5	S	7611	14.8	19.9	3/16	4	900°C, OQ	500 hours at 540°C
10AA	650	50,000	137.0	S	7611	13.1	31.6	1/8	4	900°C, OQ	500 hours at 540°C
37AS	540	110,000	43.5	S	2527	5.6	4.7	1/2	1	Standard	As-machined
38AS	540	100,000	126.8	S	2527	3.6	6.2	1/2	1	Standard	As-machined
39AS	540	105,000	38.7	S	2527	3.3	6.3	1/2	1	Standard	As-machined
47AS	540	100,000	132.6	S	2527	1.9	0.8	1/2	1	Standard	100 hours at 540°C
48AS	540	110,000	22.8	S	2527	8.3	8.6	3/8	1	Standard	100 hours at 540°C
49AS	540	110,000	32.2	S	2527	4.6	4.7	1/2	1	Standard	100 hours at 540°C
45AS	540	100,000	77.6	S	2527	1.6	4.7	1/2	1	Standard	100 hours at 540°C
17J	540	95,000	132.0	C	2527	-	notch	N[c]	1	Standard	500 hours at 540°C
19J	540	100,000	105.6	C	2527	-	notch	N[c]	1	Standard	500 hours at 540°C
27J	650	50,000	272.7	C	2527	11.4	9.4	1/8	1	Standard	As-machined
56AS	650	50,000	228.3	S	2527	14.0	16.0	1/2	1	Standard	100 hours at 650°C
57AS	650	53,000	177.8	S	2527	12.6	10.8	1/8	1	Standard	100 hours at 650°C
58AS	650	57,500	68.7	S	2527	10.5	13.2	1/2	1	Standard	100 hours at 650°C
59AS	650	65,000	10.7	S	2527	4.9	7.8	1/8	1	Standard	100 hours at 650°C
22AC	650	57,500	84.5	C	2527	16.2	13.2	1/8	1	Standard	100 hours at 650°C
23AC	650	50,000	17.8	C	2527	24.4	18.3	1/8	1	Standard	100 hours at 650°C
1AS	649	70,000	14.2	S	2527	4.1	4.7	1/4	1	Standard	As-machined
2AS	649	60,000	37.0	S	2527	7.5	12.0	1/4	1	Standard	As-machined
33J	649	65,000	16.0	C	2527	6.6	7.1	3/16	1	Standard	500 hr at 650°C
20J	649	57,500	85.5	C	2527	6.8	6.7	3/16	1	Standard	As-machined
16J	538	80,000	350	C	2527	-	-	N[c]	1	Standard	500 hr at 540°C
1J	538	90,000	424	S	2527	1.5	10.2	3/8	1	Standard	500 hr at 540°C
35J	538	100,000	143	C	2527	-	4.7	N[c]	1	Standard	As-machined
3AC	538	75,000	457	C	2527	-	-	N[c]	1	Standard	As-machined
14J	538	90,000	255	C	2527	-	-	N[c]	1	Standard	500 hr at 540°C
18AA	538	90,000	157	S	7611	7.4	11.0	3/16	6	900°C, OQ[e]	500 hr at 540°C
28J	649	53,000	190	C	2527	11.4	11.7	3/16	1	Standard	As-machined
29AS	538	110,000	84	S	2527	2.5	5.5	1/8	1	Standard	As-machined
30J	538	95,000	234	C	2527	2.6	3.2	1/8	1	Standard	As-machined

[a] "S" indicates smooth bar and "C" combination bar with smooth and notched section.

[b] Over appropriate gage length; i.e., 0.5 inch for combination bars, and 1.5 inches for smooth bars.

[c] "N" indicates that failure occurred in the notch.

[d] Standard heat treat: 900°C for 2 hours, then OQ; 720°C for 16 hours, then AC; 650°C for 16 hours, then AC.

[e] "OQ" indicates oil quench.

UNCLASSIFIED

TABLE 3.1-3

HASTELLOY X CONTROL STRESS-RUPTURE TEST DATA

Specimen No.	Test Temperature, °C	Stress, psi	Rupture Life, hr	Specimen Type[a]	Heat No.	Elongation,[b] %	Reduction Of Area, %	Failure Distance From Fillet, in.	Applicable Exp. No.	Pre-Mfg. Treatment[c]	Pre-Test Treatment
19HS	540	75,000	80.8	S	9500	46.5	28.7	1/4	2	Standard	100 hours at 540°C, solution in argon
9HC	540	70,000	12.9	C	9500	55.4	33.0	1/8	2	Standard	100 hours at 540°C, solution in argon
10HC	540	60,000	96.8	C	9500	35.4	30.5	1/8	2	Standard	100 hours at 540°C, solution in argon
11HC	540	65,000	21.1	C	9500	43.0	no rupture in test	1/8	2	Standard	100 hours at 540°C, solution in argon
6HS	650	55,000	9.0	S	9500	27.4	24.5	1/4	2	Standard	100 hours at 650°C, solution in argon
7HS	650	45,000	41.0	S	9500	18.6	18.5	1/4	2	Standard	100 hours at 650°C, solution in argon
8HS	650	35,000	151.0	S	9500	29.0	20.1	3/4	2	Standard	100 hours at 650°C, solution in argon
70H	650	45,000	29.4	C	9500	24.2	18.9	1/8	2	Standard	100 hours at 650°C, solution in argon
71H	650	35,000	233.4	C	9500	23.4	22.4	1/8	2	Standard	100 hours at 650°C, solution in argon
12HS	540	60,000	800.0	S	9500	19.0	17.6	1/8	1	Standard	As-machined
13HS	540	70,000	44.9	S	9500	24.9	21.7	1/4	1	Standard	As-machined
22HC	540	60,000	218.3	C	9500	31.0	20.6	1/8	1	Standard	As-machined
23HC	540	75,000	21.0	C	9500	39.6	23.3	3/16	1	Standard	As-machined
24HC	540	70,000	61.7	C	9500	34.4	19.4	1/8	1	Standard	As-machined
21HC	540	55,600	76.2	C	9500	24.2	16.3	1/8	1	Standard	As-machined
14HS	540	70,000	62.5	S	9500	27.7	18.2	3/4	1	Standard	100 hours at 540°C
15HS	540	65,000	149.4	S	9500	23.8	14.8	1/2	1	Standard	100 hours at 540°C
57H	540	75,000	14.0	C	9500	57.0	36.1	1/4	1	Standard	100 hours at 540°C
58H	540	70,000	31.6	C	9500	42.0	25.4	1/8	1	Standard	100 hours at 540°C
59H	540	60,000	278.4	C	9500	27.8	20.6	1/4	1	Standard	100 hours at 540°C
19HC	650	35,000	330.0	C	9500	34.6	33.5	1/8	1	Standard	As-machined
20HC	650	45,000	57.6	C	9500	31.6	27.3	1/8	1	Standard	As-machined
61H	650	45,000	62.3	C	9500	52.6	41.5	1/4	1	Standard	500 hours at 650°C
6HC	650	55,000	23.1	C	9500	52.6	36.2	1/8	1	Standard	500 hours at 650°C
7HC	650	45,000	53.1	C	9500	57.2	47.2	1/8	1	Standard	500 hours at 650°C
8HC	650	35,000	360.0	C	9500	70.8	31.9	1/8	1	Standard	500 hours at 650°C
16HS	538	90,000	0.6	S	9500	42.0	43.5	1/8	1	Standard	As-machined
17HS	538	75,000	28	S	9500	30.5	25.1	3/16	1	Standard	As-machined
24HS	649	45,000	44	S	9500	27.0	34.5	3/16	1	Standard	As-machined
25HS	649	55,000	9	S	9500	19.5	18.9	3/16	1	Standard	As-machined

[a] "S" indicates smooth bar, and "C" combination bar with smooth and notched section.

[b] Over appropriate gage length; i.e., 0.5 inch for combination bars, and 1.5 inches for smooth bars.

[c] Standard heat treat: 1175°C for 1 hour followed by rapid air cool.

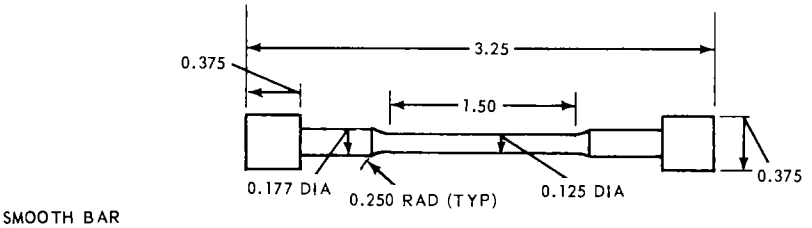

SMOOTH BAR

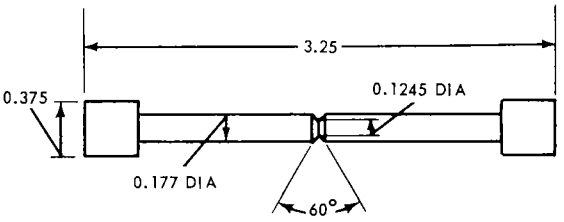

NOTCHED BAR

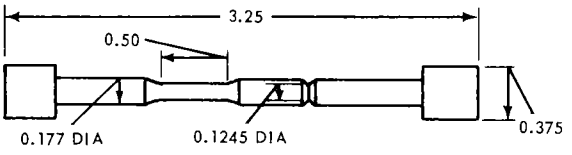

COMBINATION BAR

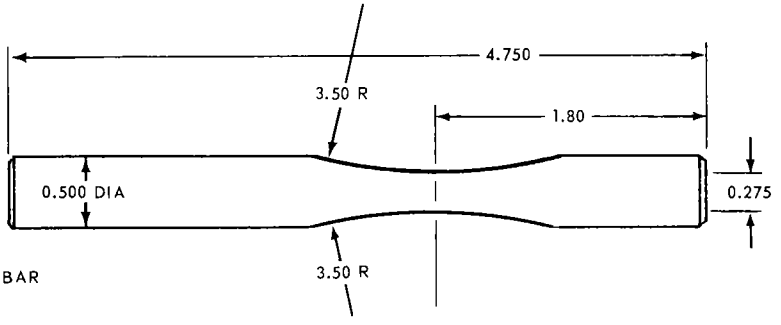

FATIGUE BAR

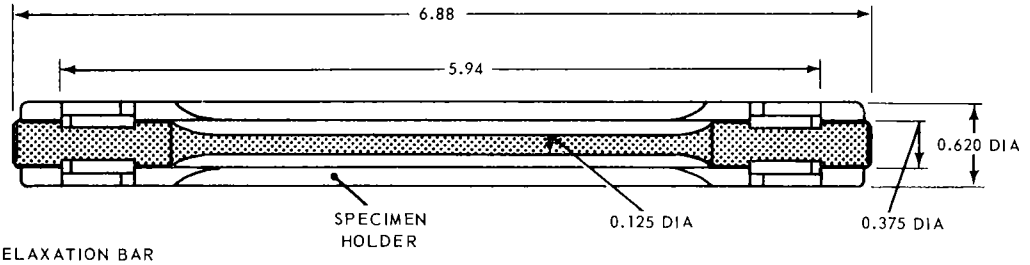

RELAXATION BAR

DIMENSIONS IN INCHES

Fig. 3.1-1 – Description of specimens

TABLE 3.1-4

RENE' 41 CONTROL STRESS-RUPTURE TEST DATA

Specimen No.	Test Temperature, °C	Stress, psi	Rupture Life, hr	Specimen Type[a]	Heat No.	Elongation,[b] %	Reduction Of Area, %	Failure Distance From Fillet, in.	Applicable Exp. No.	Pre-Mfg. Treatment[c]	Pre-Test Treatment
39RS	650	110,000	33.8	S	TV746	7.4	7.8	1/8	2	Standard	100 hours at 650°C, solution and age in argon
40RS	650	115,000	12.0	S	TV746	10.6	10.1	3/16	2	Standard	100 hours at 650°C, solution and age in argon
42RS	650	100,000	77.2	S	TV746	4.8	5.5	3/8	2	Standard	100 hours at 650°C, solution and age in argon
31RC	650	100,000	263.4	C	TV746	3.4	4.0	1/8	2	Standard	100 hours at 650°C, solution and age in argon
43RS	650	100,000	148.8	S	TV746	4.8	1.6	1/2	1	Standard	As-machined
44RS	650	115,000	21.6	S	TV746	4.8	3.9	1/2	1	Standard	As-machined
45RS	650	110,000	46.2	S	TV746	4.4	4.7	1/2	1	Standard	As-machined
29RC	650	100,000	425.6	C	TV746	3.0	2.4	1/8	1	Standard	As-machined
46RS	650	110,000	79.6	S	TV746	1.6	1.6	3/8	1	Standard	100 hours at 650°C
47RS	650	115,000	41.3	S	TV746	2.6	2.4	1/2	1	Standard	100 hours at 650°C
48RS	650	100,000	140.3	S	TV746	1.2	1.6	3/16	1	Standard	100 hours at 650°C

[a]"S" indicates smooth bar, and "C" combination bar with smooth and notched section.

[b]Over appropriate gage length; i.e., 0.5 inch for combination bars, and 1.5 inches for smooth bars.

[c]Standard heat treat: 1065°C for 2 hours then WQ; 1175°C for 1/2 hour then AC; 900°C for 4 hours then AC.

When all control data is complete, curves will be prepared for each experiment using the method of least squares to establish the curves of best fit. Control data in support of experiment No. 5, however, have been analyzed and are presented later in this report.

Dosimetry Studies

In order to determine the neutron environment in which the specimens were irradiated, special neutron dosimeters of a Ni-Co alloy were inserted in each capsule at different locations. Approximately ten dosimeters are used in the large capsules. These dosimeters are fabricated by NSEC* and the radiochemical analysis and analytical prediction of the fast and slow neutron dosage are furnished as part of the services. The method of analysis and cross sections used are given in section 3.2. In addition to the standard dosimeters, a number of the specimens are gamma scanned to determine the neutron dosage profile across the specimens. Radiochemical analysis is also performed on sections removed from representative specimens for absolute flux determination for normalizing the scan data. Plans are to theoretically predict the neutron spectrum at the specimen positions and compare calculated activities of the isotopes with the measured values. This differential neutron flux ($n/cm^2/sec$ /Mev) will then be used along with the other parameters, such as temperature and stress, in the interpretation of the resulting data on the effects of irradiation on metals.

The preliminary analysis of the gamma scan data of some specimens from capsule MT-27 indicates that the capsule was exposed to a total neutron dosage of about 10^{20} nvt ($E_n \geq 1$ Mev) rather than the scheduled value of about 3×10^{19} nvt. The gamma scan data, which is obtained by the use of a 256 channel analyser and a collimated crystal detector, measures the gamma spectrum and intensity from the specimen positioned in a fixed geometry. Specifically, the activities from the isotopes of Co^{58}, Mn^{54}, Cr^{51}, Co^{60}, and Fe^{59} are measured in this study. The initial data obtained from some of the fast neutron reactions in the specimens indicates that the fast neutron dosage will vary by about a factor of two from the one end of the capsule to the position where the flux is highest. The distribution of the fast neutron dosage across the specimens in capsule MT-27 is shown in Figure 3.1-2. These data include the gamma scan information normalized to the radiochemical analysis of sections from specimens used as monitors. The data to be obtained from NSEC on the standard Ni-Co dosimeters will be included at a later date. Since the specimens in the 30 rows cover a distance of about 28 inches, it is expected that the neutron dosage distribution reflect the axial power distribution across the ETR core. The temperature profile is also included in Figure 3.1-2 to show the change in temperature, as well as the neutron dosage, across the specimens for the capsule exposure. Similar correlations are being made for capsules MT-38, MT-43 and MT-51.

Capsule MT-27 Specimen Tests

The specimens to be used in a number of the experiments will be irradiated in several different capsules as indicated in Table 3.1-1. Therefore, when reference is made to a capsule number the temperature and neutron dosage are implicitly given since plans are to have curves showing this detailed information plotted as a function of axial position in each capsule. The specimen location within each capsule will also be given.

Testing of specimens (A-286) relating to experiment No. 4 and irradiated in capsule MT-27 at a temperature of 540 °C has been completed. Testing was conducted at the temperature of irradiation. These specimens were in the underaged† and/or overaged‡ con-

*Nuclear Science and Engineering Corporation, Pittsburgh, Pennsylvania.

†Underage: 900°C, 2 hours (inert atmosphere), oil quench

‡Overage: 925°C, 2 hours, water quench
815°C, 200 hours, air cooled
650°C, 100 hours, air cooled

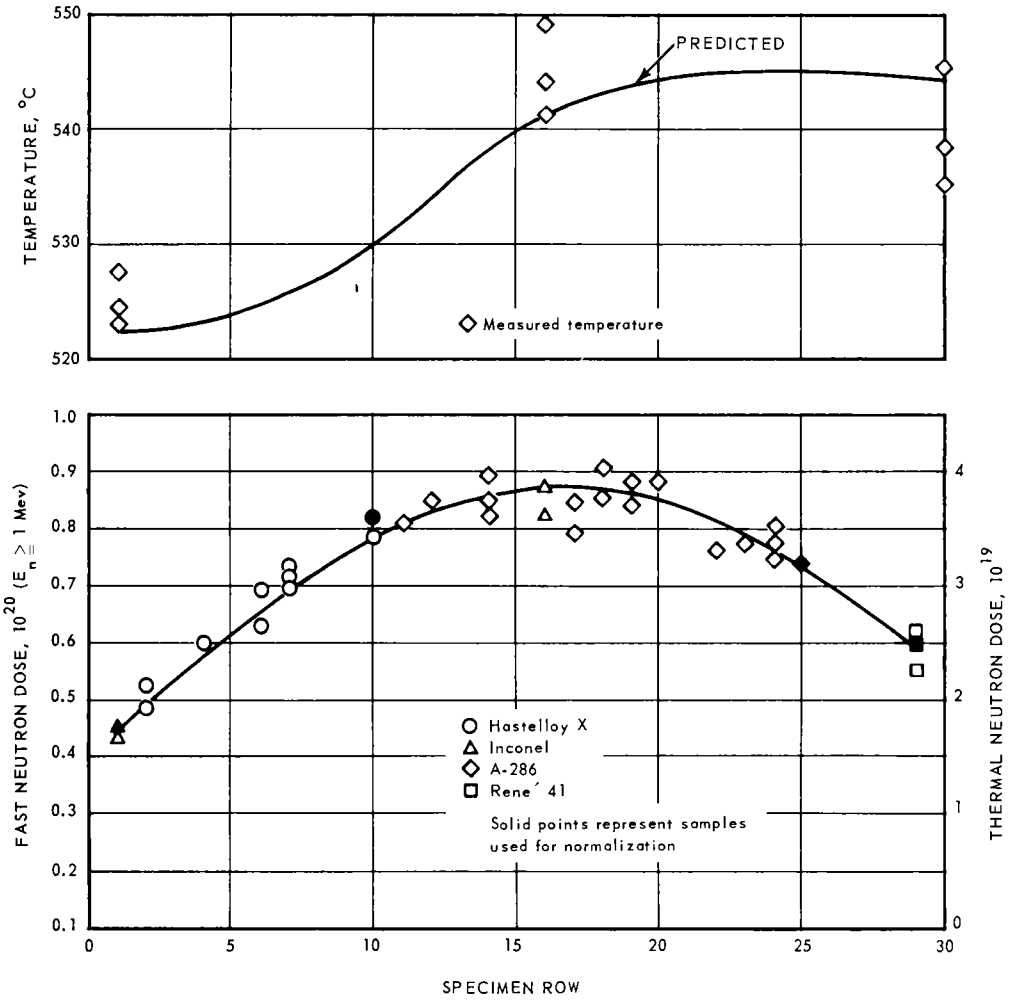

Fig. 3.1-2 – Neutron dose and temperature distribution across specimens in capsule MT-27

dition prior to irradiation. Analysis of the data showed no difference in rupture strengths between the overaged and underaged specimens. More testing in each category is necessary to firmly establish this result.

The preliminary results show that the 100-hour rupture strength decreased from 96,000 psi to 80,000 psi, whereas the 1000-hour rupture strength decreased from 74,000 psi to 70,000 psi. On this basis the stress versus rupture life curve of the irradiated and unirradiated specimens converged at the lower stress level. This trend indicates that the effects of irradiation on stress rupture life are less at the lower stress levels. This may be explained by a tendency for the damage to anneal out during relatively long times at testing temperatures.

Capsule MT-35A, MT-35B, MT-36 Specimen Tests (Experiment No. 5)

The rupture testing and preliminary analysis of the test data was completed for experiment No. 5. The purpose of this experiment was to determine if reactions dependent on thermal neutron dosage would effect rupture properties. Nine specimens of A-286 were simultaneously irradiated at a reactor ambient water temperature of 36 °C. The capsule containing the specimens was designed so that four specimens (2 smooth and 2 combination) would be exposed to a higher thermal neutron dosage than the other five (3 smooth and 2 combination).

The material for these tests was taken from a single bar (Heat C2527), 5/8 inch in diameter, mill annealed, and centerless ground. The chemical analysis of the A-286 alloy used in these tests are listed in Table 3.1-5.

The heat treatment given both pre-irradiated and unirradiated specimen was as follows:

900 °C - 2 hours - oil quench
720 °C - 16 hours - air cool
650 °C - 16 hours - air cool

TABLE 3.1-5

CHEMICAL ANALYSIS OF A-286, HEAT C2527

Element	Weight Percent
Carbon	0.047
Manganese	1.55
Silicon	0.52
Nickel	24.34
Chromium	15.03
Molybdenum	1.29
Iron	54.05
Sulphur	0.011
Vanadium	0.035
Aluminum	0.18
Titanium	2.16
Cobalt	0.25
Boron	0.0051

Two capsules using 1 percent B_{10} Type 304 stainless steel sheet and one capsule of similar design but without the B_{10} addition were fabricated. The loaded capsules were irradiated in the LITR, C-48 facility. After exposure to a fast flux of approximately 2.6 to 3.5 x 10^{16} nvt ($E_n \geq 1$ Mev), the specimens were stress rupture tested at 650 °C. The resulting data are presented in Table 3.1-6. Also shown in this table, for purposes of comparison, is a series of unirradiated specimens (smooth and combination bars) of the same heat and with the same heat treatment.

The data obtained from the unirradiated tests are presented graphically in Figure 3.1-3. These data were statistically analyzed using the method of least squares to calculate the curve of best fit. The nominal three standard deviation band (lower side of the band) was calculated from deviations of the test data; this band is represented by the lower dotted line. The combination bar data were not used in any of the statistical calculations and were not shown in the curve.

The data on the neutron dosimetry for these tests are given in Table 3.1-7.

The preliminary evaluation of the data for this experiment are indicated by the following:

1. The number of tests involved and the program of testing precluded statistical analysis to determine if any significant difference could be detected in rupture properties between the shielded and unshielded specimens. However, the arithmetical averages tend to indicate, for both the smooth and the combination bars, some parameter that is a function of the thermal neutrons has an effect on rupture life.
2. Based on the unshielded data, irradiation at 3 x 10^{16} nvt ($E_n \geq 1$ Mev) and at ambient reactor temperature lowered the 650°C stress-rupture strength by about 20 percent.

TABLE 3.1-6

RESULTS OF STRESS-RUPTURE TEST[a] OF IRRADIATED AND UNIRRADIATED A-286 SPECIMENS AT 650°C

Specimen No.	Specimen Type	Test Condition	Stress, psi	Rupture Time, hr	Fracture Location
Irradiated					
75L	Smooth	Unshielded	50,000	58	Reduced Section
24K	Smooth	Unshielded	45,000[b]	146	Reduced Section
20K	Smooth	Unshielded	45,000	99	Reduced Section
25J	Combination	Unshielded	50,000	3.7	Notch
26J	Combination	Unshielded	40,000	13.4	Notch
76L	Smooth	Shielded	50,000	131	Reduced Section
15J	Combination	Shielded	50,000	5.4	Notch
77L	Smooth	Shielded	50,000	174	Reduced Section
31J	Combination	Shielded	40,000	208	Notch
Unirradiated					
1	Combination	Controls	65,000	65.7	Reduced Section
2	Combination	Controls	65,000	36.8	Reduced Section
64L	Smooth	Controls	65,000	62.0	Reduced Section
1AS	Smooth	Controls	70,000	14.2	Reduced Section
2AS	Smooth	Controls	60,000	37.0	Reduced Section
20J	Combination	Controls	57,500	86.0	Reduced Section
28J	Combination	Controls	53,000	190.0	Reduced Section
27AC	Combination	Controls	50,000	272.7	Reduced Section

[a]The test data is for experiment No. 5
[b]Previously reported as 50,000 psi in GEMP-7A, Table 8, Page 35.

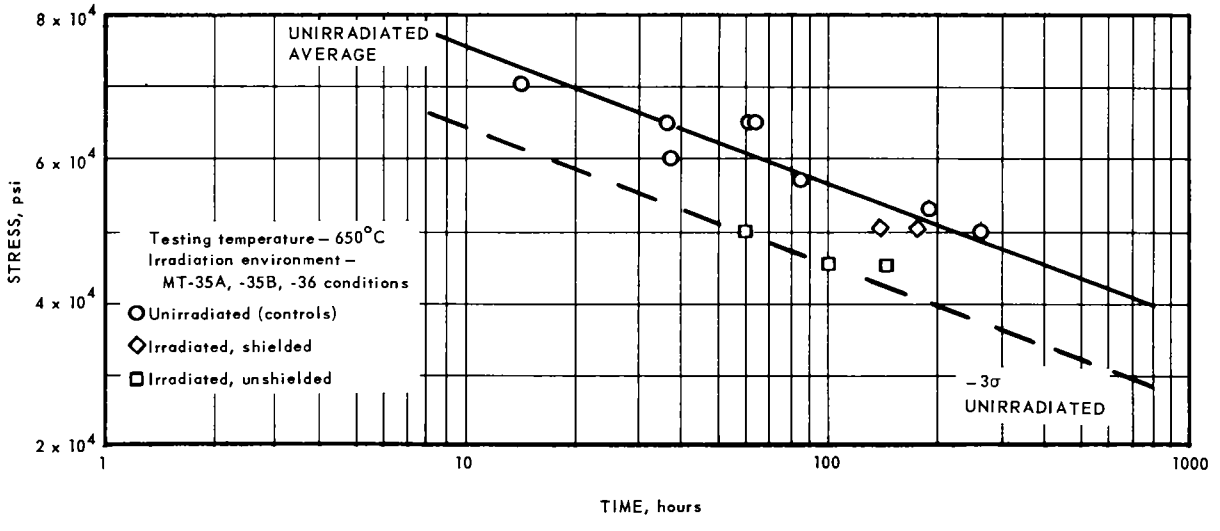

Fig. 3.1-3 – Stress-rupture properties of irradiated and unirradiated A-286 alloy (Heat C2527), experiment No. 5

TABLE 3.1-7

NEUTRON DOSIMETRY OF A-286 SPECIMENS (EXPERIMENT NO. 5)

Specimen No.	Specimen Type	Test Condition	Capsule	Dosage,[a] nvt	
				$E_n \geq 1$ Mev	Thermal
75L	Smooth	Unshielded	MT-36	3.0×10^{16}	1.2×10^{17}
24K	Smooth	Unshielded	MT-36	3.0×10^{16}	1.2×10^{17}
20K	Smooth	Unshielded	MT-36	3.0×10^{16}	1.2×10^{17}
25V	Combination	Unshielded	MT-36	3.0×10^{16}	1.2×10^{17}
26V	Combination	Unshielded	MT-36	3.0×10^{16}	1.2×10^{17}
76L	Smooth	Shielded	MT-35A	3.5×10^{16}	2.4×10^{16}
15V	Combination	Shielded	MT-35A	3.5×10^{16}	2.4×10^{16}
77L	Smooth	Shielded	MT-35B	2.6×10^{16}	1.6×10^{16}
31J	Combination	Shielded	MT-35B	2.6×10^{16}	1.6×10^{16}

[a]Irradiation Facility - LITR, C-48 position, pile ambient temperature (36°C).

This corresponds to a reduction in 100-hour rupture strength from 57,000 psi to 46,000 psi.

3. Irradiation caused notch weakening as evidenced by the results shown in Table 3.1-6, of the combination bars, whereas test results of unirradiated combination bars showed notch strengthening in all cases.
4. Test data indicates that the threshold of irradiation damage caused by neutron exposure at reactor ambient water temperature is somewhat less than 3×10^{16} nvt ($E_n \geq 1$ Mev), assuming that the fast neutrons were primarily responsible for the measured damage.

STRUCTURAL STUDIES

The initial selection of specimens to be used for the structure studies has been completed. Several replication techniques have been evaluated and an optimum method adopted for preparing the irradiated specimens for electron microscopy.

Two A-286 specimens from the shielded - unshielded irradiation (experiment No. 5), as well as an unirradiated control specimen, have been metallographically prepared and examined by optical and electron microscopy. The irradiation and the stress-rupture histories of the specimens No. 75L (unshielded), 76L (shielded) and 2AS (control) are listed in Table 3.1-6. The specimens were irradiated in the LITR at Oak Ridge at pile ambient temperatures and stress-rupture tested at 650°C. All three specimens were from Heat C2527 A-286 alloy.

Thin, direct-stripped nitrocellulose replicas for electron microscopy were obtained from polished and etched sections of the button heads of the three specimens. By avoiding the more highly stressed areas of the reduced sections of the broken specimens, it was felt that any microstructural changes which might be observed could be ascribed only to the neutron irradiation. Due to the relatively low neutron dosages involved in the shielded-unshielded experiment, the irradiated specimens displayed a low enough induced activity level to allow replication out of the hot cell along with the unirradiated control specimen.

Figure 3.1-4 is a photomicrograph, obtained from the unshielded specimen (75L) showing structure typical of normally heat-treated A-286. Although portions of the grain boundaries appear to be broadened, the higher magnifications and better resolutions available with the electron microscope are necessary to resolve the complete microstructure. Op-

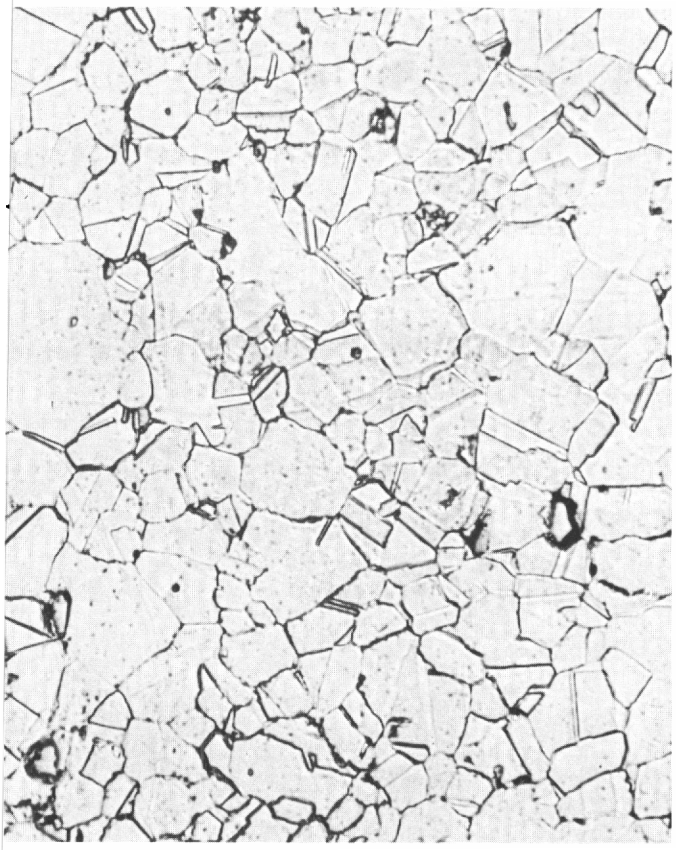

(Neg. R-21) 500 X

Fig. 3.1-4 – Optical micrograph of unshielded A-286

tical microstructures of the shielded and unirradiated specimens appeared similar to that of the unshielded specimen.

Figure 3.1-5 shows representative electron micrographs of the three specimens of interest. The microstructures of the unshielded and shielded irradiated bars are shown in Figures 3.1-5a and 3.1-5b, respectively, while Figure 3.1-5c shows the microstructure of the unirradiated control bar. As illustrated by these photographs, the microstructures of all three samples are very similar, with no apparent structural changes caused by irradiation. The microstructures exhibited by all three specimens are quite typical of A-286 alloy after normal heat treatment.* The phases appearing in the micrographs consist of rather large inclusions of (Ti, Mo)C both within grains and at grain boundaries, lamellae of η hexagonal Ni_3Ti phase and γ' cubic Ni_3 (Al, Ti) phase along grain boundaries, and a very fine dispersion of γ' evenly throughout the matrix. In addition to these phases, some evidence is seen of a very fine grain boundary precipitate presumed to be "G" phase, a complex cubic phase whose chemical formula is given as $Ti_6Si_7Ni_{16}$.† This "G" phase is quite often a constituent in the microstructure of normally heat-treated A-286.

*H. J. Beattie, Jr., "Structural Study of Relations Between Solution Treatment and Aging Response in Alloy A-286," General Electric Co., Large Steam Turbine Generator Department, DF61SL322, May 11, 1961.

†H. J. Beattie, Jr. and W. C. Hagel, "Intermetallic Compounds in Titanium Hardened Alloys," *Trans. AIME*, Vol. 211, 1957, p. 911.

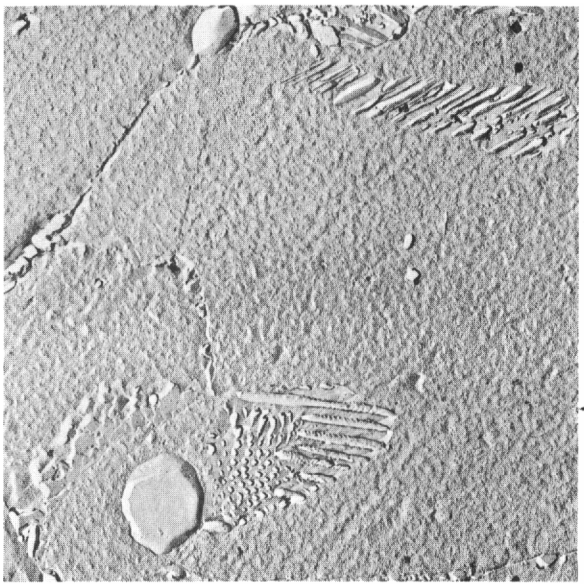

(Neg. 503E) 7500 X

← Fig. 3.1-5a – Electron microstructure of unshielded irradiated A-286

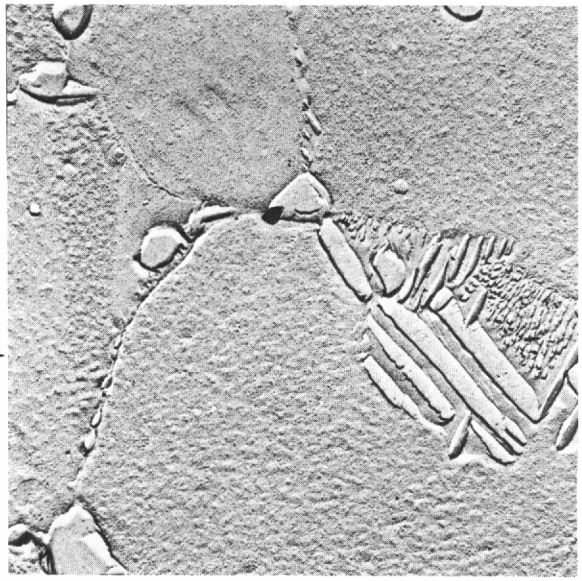

(Neg. 505D) 7500 X

Fig. 3.1-5b – Electron microstructure of shielded irradiated A-286 →

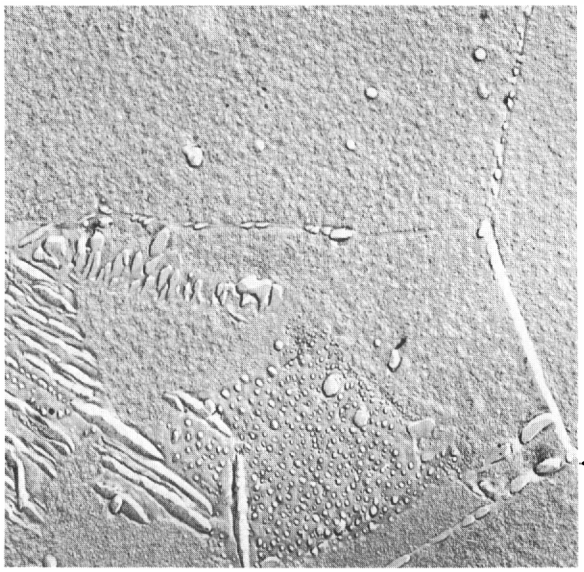

(Neg. MM528-1A) 7500 X

← Fig. 3.1-5c – Electron microstructure of unirradiated A-286

STUDIES OF Ni-Al SYSTEM

Initial work on this phase of the program was spent on the preparation and calibration of the Evendale Van de Graaff equipment for specimen irradiation in an argon atmosphere and in aging studies of the 92Ni - 8Al alloy.

Ingots of nominal composition 94Ni - 6Al, 92Ni - 8Al, and 90Ni - 10Al were vacuum-melted and cast in 4-inch-square ingots, each weighing about 45 pounds. Chemical analysis verified that the ingots were within 0.5 weight percent of the desired composition. Major impurities were found to be Fe (300 ppm) and C (85 ppm); other impurities were less than 30 ppm each.

Some preliminary aging studies on the 92Ni - 8Al alloy have been completed. The changes in hardness with aging time after solutioning at 1205°C and 1315°C were measured. The procedure followed in this study was use of a solutioning treatment at the given temperatures for one hour, followed by a water quench. At least three hardness measurements are made. The specimens were then aged, followed by water quenching, and then hardness was determined. The last procedure was repeated many times to obtain the data on hardness versus aging time. Based on these aging studies, the following observations can be made:

1. Adequate solutioning occurs in one hour at either 1205°C or 1315°C; as-solutioned hardness ranges from 160 to 180 DPH.
2. Maximum hardness after aging occurs in about 300 hours; 540°C aging produces a hardness of ~ 240 DPH; 650°C aging yields ~ 250 DPH.

Preliminary irradiation work on 92Ni - 8Al is in progress. The alloy sheet (0.030 inch thickness) from material solutioned at 1205°C is being exposed to electron beams in an argon atmosphere at 650°C.

Three lengths of 1-inch-diameter rods have been extruded from 3-inch billets at 1260°C. These will be centerless ground prior to swaging to 0.5-inch-diameter rods for machining into stress-rupture samples for subsequent neutron irradiation.

SUMMARY AND CONCLUSIONS

The major effort on this program up to this time was applied to specimen manufacture, design and fabrication of capsules for the reactor irradiation, to the calibration of equipment, and to the establishment of techniques and procedures for the postirradiation portion of the program. Including the specimens in capsule MT-51, approximately 80 percent of the specimens scheduled for irradiation are irradiated or are now at the ETR ready for reactor insertion. Over 50 percent of the control specimens have been tested. Postirradiation testing of specimens from capsule MT-27 has been started and testing of control and irradiated specimens for experiment 5 is now complete.

Only a few of the irradiated specimens have been tested for several of the experiments and one experiment (experiment No. 5) was completed. The preliminary conclusions based on results from experiment No. 5 are:

1. Irradiation to a dosage of about 3×10^{16} nvt ($E_n > 1$ Mev) and at pile ambient reactor temperature decreased the 100-hour stress-rupture strength for A-286 from 57,000 psi to 51,000 psi. This indicates that the apparent threshold of irradiation damage caused by neutron exposure at reactor ambient temperature is less than 3×10^{16} nvt, assuming that the fast neutrons were primarily responsible for the measured property changes.
2. Irradiation caused notch weakening in contradiction to the results on the unirradiated combination bars which showed notch strengthening in all cases.

PLANS AND RECOMMENDATIONS FOR FUTURE WORK

Work initiated this year on A-286, Hastelloy X, and Rene' 41 will be continued. The major portion of the testing program on these alloys will be completed, and a detailed evaluation will be made of the effect of neutron irradiation on their mechanical properties, particularly stress-rupture. Some additional testing is expected to be required in order to substantiate trends observed. Emphasis will be placed on the continuing study of the effect of neutron irradiation on their microstructural characteristics as the primary basis for understanding damage mechanisms. In addition, other properties such as hot hardness will be determined on sections of rupture tested specimens, and attempts made to correlate such information with the rupture data obtained.

A study of the influence of irradiation on the stress-rupture properties of refractory metals will be initiated. Tantalum, tungsten, and a liquid-metal containment alloy, Cb - 1Zr, are of particular interest.

A study of the influence of neutron spectrum on irradiation effects in A-286, Hastelloy X, and Rene' 41 will be undertaken. Efforts will be made to establish, tentatively at least, the energy threshold at which significant effects are observed. Careful experimental dosimetry will be an important phase of this effort and comparisons will be made between measured and predicted spectra.

Studies of neutron irradiation effects in Ni-Al and other relatively simple binary or elemental face-centered cubic and body-centered cubic systems will be continued and expanded based on the information obtained in Fiscal Year 1962.

The need for and feasibility of conducting in-pile stress-rupture or creep tests will be investigated, including selection of a technique by which such tests can be accomplished.

ADDENDUM TO SECTION 3.1, "HIGH-TEMPERATURE ALLOYS"

CAPSULE DESIGNS FOR IRRADIATION TESTS

The ETR irradiation test specimen capsules were designed for insertion in either the 66 or 99 facility. The capsules may be adapted to the larger 99 facility tube diameter by means of a double-wall can surrounding the capsule hardware designed for the 66 facility. In the case of capsule MT-27, shown in Figure 3.1-6 as installed in the 99 facility, there were essentially three flow passages: an outer annulus cooling the facility liner and outer can wall, an inner annulus cooling the inner can wall and specimen support, and an inner region cooling the specimens and specimen support. Airflow was balanced by means of orifice plates. Some of the parameters used for obtaining the aerothermal design of capsule MT-27 are listed in Table 3.1-8. The thermal design was based on a maximum gamma-heat generation rate of 10 watts per gram, or 1.24 Btu's per cubic inch of steel, and the following standard heat-transfer correlations:

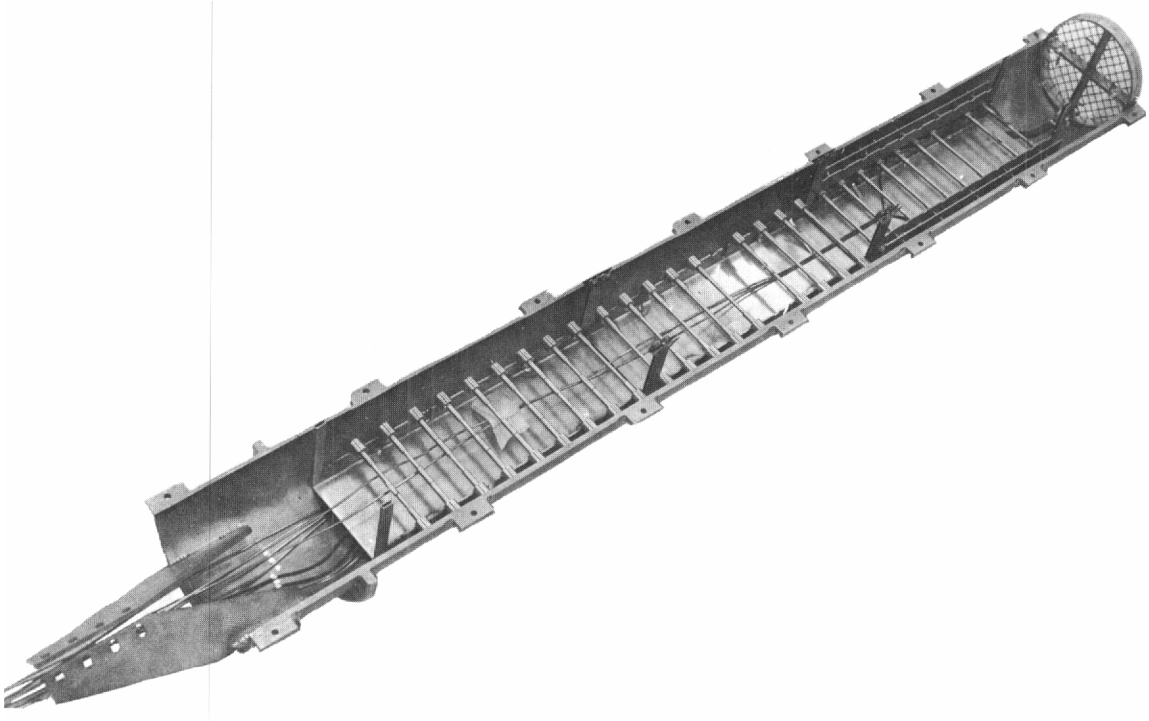

Fig. 3.1-6 – Capsule MT-27 during initial assembly (Neg. U39200-E)

TABLE 3.1-8

THERMODYNAMIC PARAMETERS FOR CAPSULE MT-27

Region	Maximum Heat Flux,[a] Btu/ft^2-hr	Heat Transfer Coefficient, Btu/ft^2-hr-^{o}F	Coolant Flow, lb/sec
Specimen			
0.125-inch diameter	20,100	435[b]	
0.177-inch diameter	28,300	415[b]	6.7
0.325-inch diameter	60,600	276[b]	
Can Wall	20,600		
Liner	27,600		
Inner Annulus		96	1.3
Outer Annulus		136	4.0
		Total	12.0

[a] Total heat generation - 167 Btu/sec.

[b] For 6.7 pounds per second flow rate, an inlet air temperature of 505^{o}C, and an empirical factor F = 1.5.

Inside tubes and annuli,

$$Nu_f = 0.021\ Re_f^{0.8}\ Pr_f^{6.4}$$

Tubes and rods in cross-flow,

$$Nu_f = 0.24\ F\ Re_f^{0.6}\ Pr_f^{6.33}$$

The first correlation utilizes the hydraulic diameter; the second, the rod or tube diameter. F is an empirical factor depending on the number of rows of tubes.

Capsule weights for MT-24, MT-38, and MT-43 are given in Table 3.1-9. The predicted temperature across the specimens of capsule MT-27 are shown in Figure 3.1-7. This figure also shows the predicted temperature profile for MT-38, MT-43, and MT-51.

TABLE 3.1-9

CAPSULE WEIGHTS FOR MT-27, MT-38, MT-43, AND MT-51

Material	Weights, lbs MT-27	MT-38, -43	MT-51
Specimens	3.3	3.3	10.8
Specimen support (and associated equipment)	31.2	31.6	38.1
Facility Liner (over capsule length)	11.0	8.7	8.7
Miscellaneous hardware	3.0	3.0	3.8
Totals	48.5	46.6	61.4

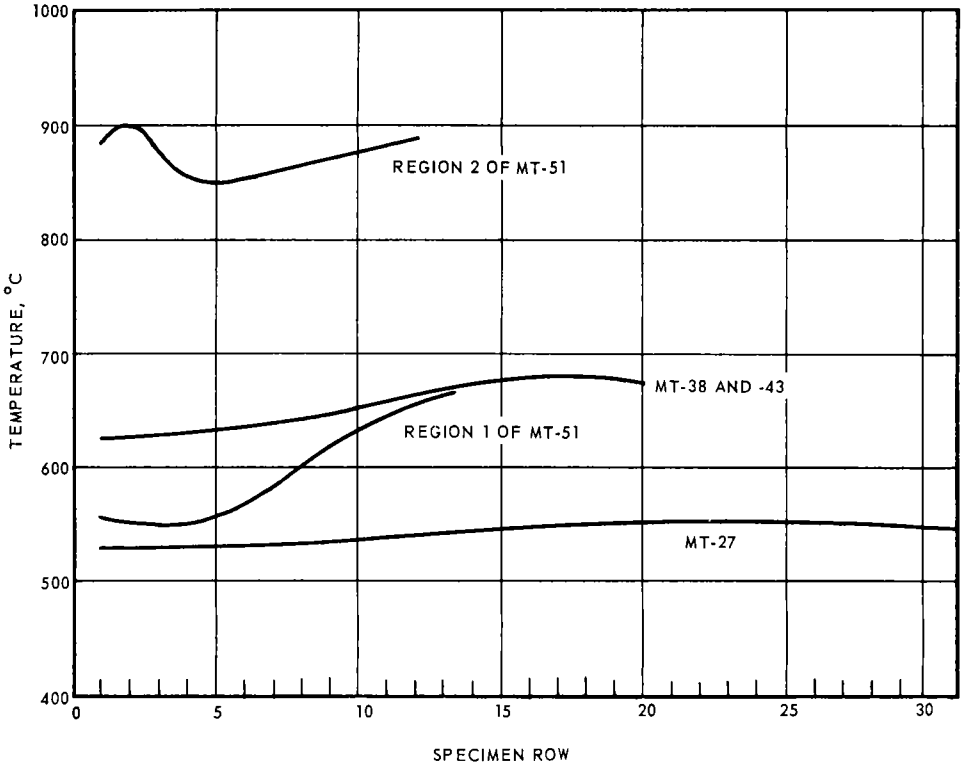

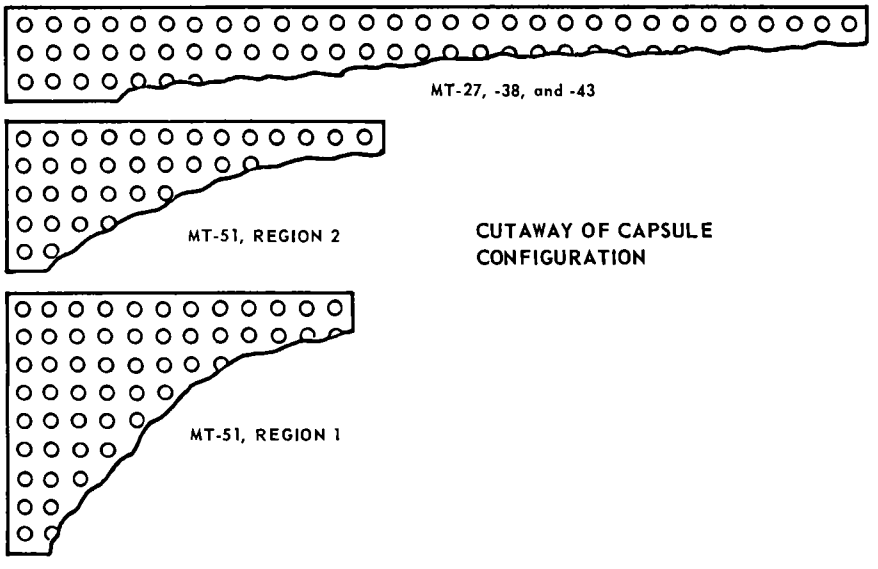

Fig. 3.1-7 – Predicted specimen temperatures for capsules MT-27, MT-38, MT-43, and MT-51

Capsules MT-27, MT-38, and MT-43 are generally similar in design, each containing 90 specimens for irradiation. Nine rejected specimens are used for mounting thermocouples and post-test dosimetry correlation; 81 specimens are available for post-test property measurements.

Capsule MT-51 illustrated in Figure 3.1-8 is designed for simultaneous irradiations at three different temperatures. It contains 120 specimens to be used for fatigue, tensile and stress-rupture testing. The irradiation test conditions require air coolant flow of about 10 pounds per second through the 99 facility of the ETR. The inlet air temperature is about 425°C with an inlet pressure of 200 psia.

The cartridge is constructed of two test sections; an upstream section that contains 10 A-286 fatigue specimens for 540°C irradiation, 10 A-286 fatigue specimens and 10 Rene' 41 fatigue specimens for 650°C irradiation, and a downstream section containing 38 Hastelloy X and 52 Rene' 41 tensile specimens to be irradiated at 870°C. The specimens are contained in rectangular shaped Type 310 stainless steel cans; the temperature of each section is controlled by a suitable orifice. Temperature measurements are obtained from seven thermocouples attached to specimens in the upstream section and eight thermocouples attached to specimens in the downstream section. In addition, each section contains thermocouples for measuring inlet and exit air temperatures. Both cans are contained in a Type 304 stainless steel circular-structural shell with the drawbar assembly attached to it. Temperatures of structural components are monitored by five thermocouples located in the test assembly. Static pressure taps are provided in the downstream test section for pressure measurements.

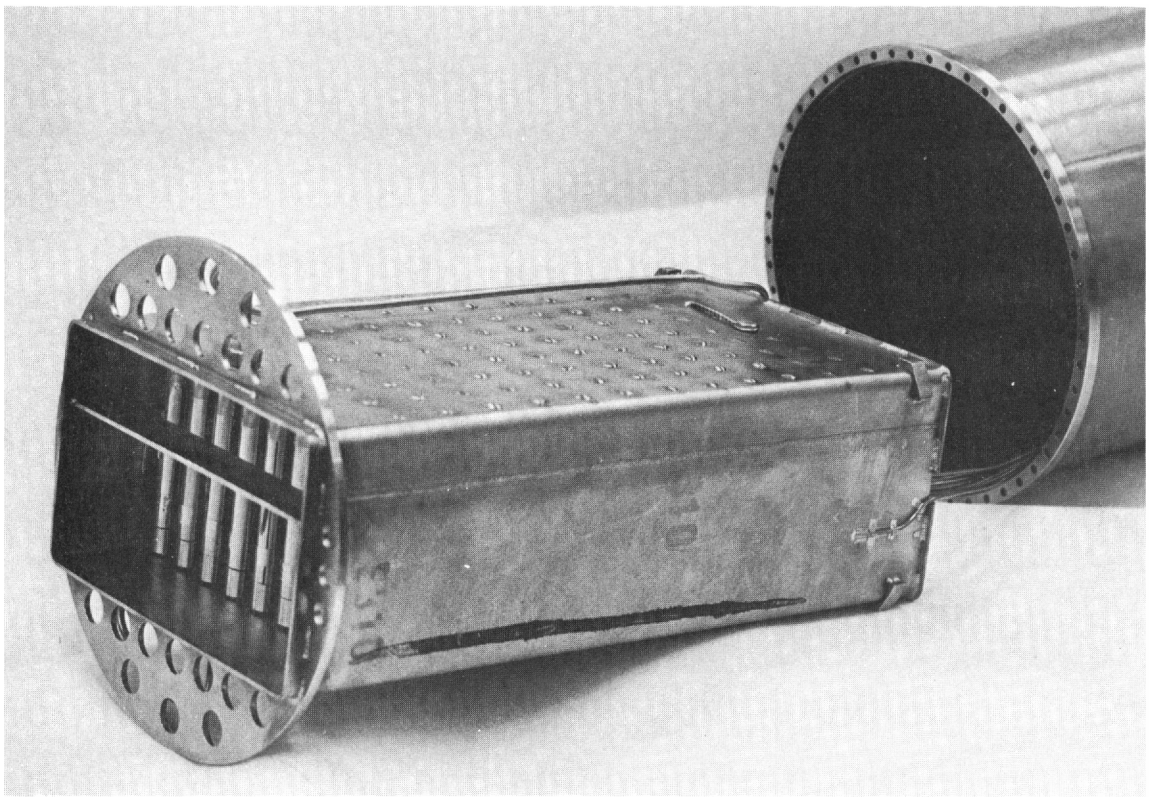

Fig. 3.1-8 – Photograph of capsule MT-51 showing box containing tensile specimens (Neg. P61-11-22a)

Capsules MT-35A, MT-35B, and MT-36 were relatively simple and much smaller. They were designed to accommodate 2, 2, and 5 specimens, respectively, for irradiation at LITR reactor ambient temperatures in water. MT-35A and MT-35B were shielded with boron-containing stainless steel to reduce the thermal neutron level. MT-36 was of similar design but unshielded. These capsules were used for experiment 5.

Capsules MT-44A, MT-44B, MT-44C, and MT-44D to be used in experiment No. 7, are small tubular capsules each containing six specimens. They will be irradiated in the LITR at reactor ambient temperatures.

STRESS-RUPTURE EQUIPMENT AND ALIGNMENT STUDIES

The six stress-rupture test stands used at the Idaho and Evendale sites for the irradiated specimens are lever loaded vertical stands. Four stands at BMI are being modified and alignment measurements evaluated for use in this program under a subcontract agreement.

Because of a loss in ductility of the specimen after irradiation, studies were performed to determine the degree of alignment required to minimize the effect of bending stress on rupture data. The stands in use at the beginning of the studies had end-pinned joints providing a one-plane alignment. The bending strain values of this equipment ranged from 65 to 215 microinches per inch with an average of 113 microinches per inch at a 600 pound load. The equipment was modified to improve the degree of alignment. The modified equipment utilizes four ball and socket joints, two above and two below the furnace; this arrangement provides a two-plane alignment. With this setup, the maximum strain values ranged from 8 to 66 microinches per inch with an average of 45 microinches per inch at a 600 pound load.

FATIGUE TEST EQUIPMENT

The pneumatic fatigue machines of the type shown in Figure 3.1-9 are now on hand for testing irradiated and unirradiated A-286 and Rene' 41 samples at temperatures up to 870°C.

The pneumatic fatigue machines operate on a "tuned" air column principle and the sample is vibrated at its natural frequency. One end of the sample is clamped in a vise to provide cantilever-type support. The collet assembly and piston are attached to the free end of the specimen with the pistons positioned between the opposed air nozzles to provide the driving mechanism. Air is supplied through a long Y-shaped pipe to the two nozzles. Since the effective length of the Y-shaped pipe can be varied, the system can be "tuned" for maximum sample amplitude. The sample amplitude is measured during test by means of a calibrated telescope. Sample frequency is measured by an acceleration transducer fixed to the base of the machine and fed to an Electronics Vibration Meter. The output from this meter is recorded and when sample frequency falls below a set point, i.e., sample failure occurs, a control switch automatically de-energizes the air supply, furnace power and time meter. A split furnace is installed around the sample and vise to provide for elevated temperature operation.

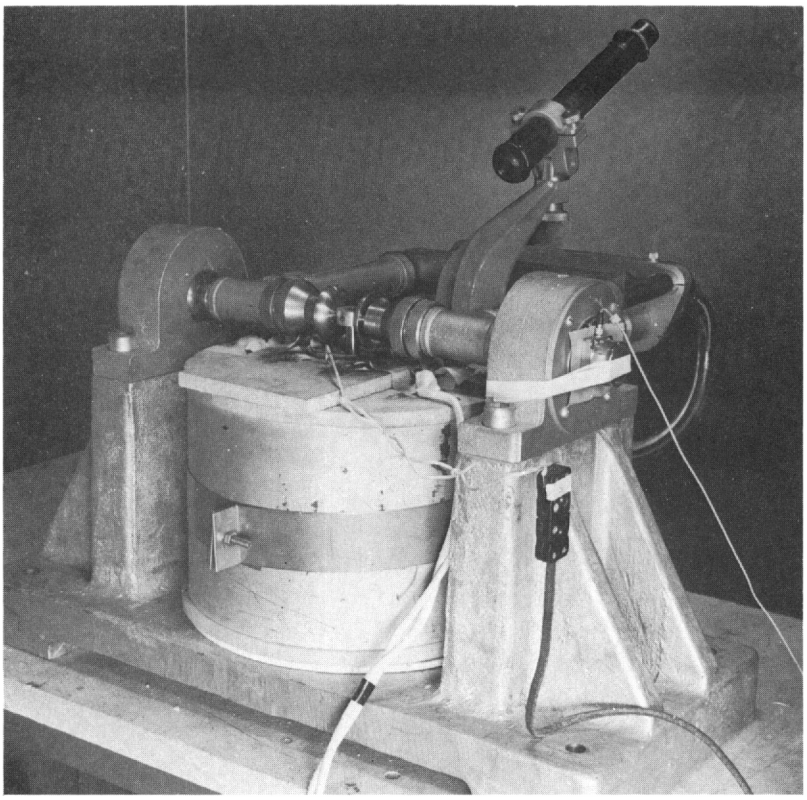

Fig. 3.1-9 – Fatigue test equipment showing furnace arrangement (Neg. P61-12-20B)

3.2 RADIATION EFFECTS ON BeO (57063)

The objective of this study is to define the physical and mechanical properties of irradiated BeO as they are influenced by purity, additives, grain size, density, and porosity at various irradiation temperatures and dosages.

Although the desirable properties of BeO for reactor applications such as moderators, reflectors, and fuel elements are well established, use of the material in many such applications is dependent on its ability to withstand extended irradiation. The future development of BeO for these applications requires more knowledge than currently exists on the factors that influence radiation behavior and on the definition of the property changes over a range of radiation dosages and temperatures.

The program is divided into three categories to be studied over a 2-year period: a composition series, a grain-size and density series, and special or supplementary studies. The properties to be determined in the first two of these series include density, linear dimensions, elastic constants, modulus of rupture, thermal expansion, and thermal conductivity. Specimens are also characterized in terms of grain size, pore size, shape, and distribution, and other microstructural features such as crystal orientation.

The objective of the composition series study is to determine the influence of variations in purity or composition on radiation stability. The series involves specimens of six compositions prepared from three commercially available grades of beryllium oxide or hydroxide; three of the compositions contain MgO or ZrO_2 as an additive. Irradiations in this series include exposures at 100°C over the range 5×10^{19} to 5×10^{20} n/cm^2 ($\geq$ 1 Mev) and exposures at 300°, 600°, 800°, and 1000°C at 3×10^{20} n/cm^2.

The objective of the grain size and density series is the determination of the influence of variation of these parameters on the property changes from irradiation. This series involves irradiation of specimens of three compositions and several grain sizes in each of three density ranges. Irradiations of these specimens will be made at elevated temperatures and high dosages.

The supplementary studies include measurements of helium and tritium gas accumulation and diffusion, single-crystal irradiations, statistical computer studies of atomic displacements, and measurements of the influence of stress during irradiation.

Studies so far conducted have been concerned primarily with the composition series of irradiations. The data reported include property measurements on specimens of this series prior to irradiation and the initial postirradiation measurements. The experimental procedures used in specimen preparation are also described.

EXPERIMENTAL PROGRAM AND RESULTS

Experimental results obtained to date were a part of the composition series of irradiations. In this series of tests, grain size and density are held constant and composition is varied by the use of three grades of BeO of varying purity and by the addition of MgO or ZrO_2. A total of six compositions are being investigated. The program, outlined in Figure 3.2-1, includes low-temperature irradiations over a range of dosages, and comparisons of thermal annealing with elevated-temperature irradiations. A summary of the irradiation test status and schedule is presented in Table 3.2-1.

All specimens of this series are of a nominal 20-micron grain size, 96 to 98 percent of theoretical density, and are solid, right-cylinders 3.5 inches long by 0.238 inch in diameter. They are prepared from the AOX, UOX, and HPA grades of BeO.*

*See Figure 3.2-1 for detailed compositions. Throughout this section, the expression UOX+MgO should be interpreted as UOX + 0.5 weight percent MgO.

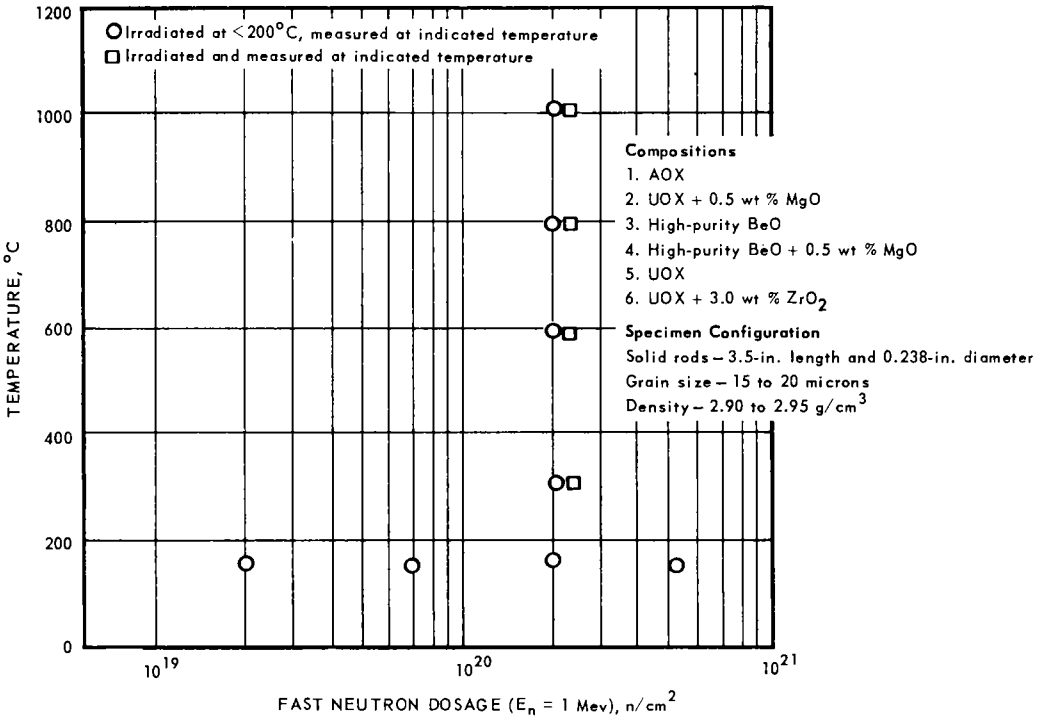

Fig. 3.2-1 – Outline of composition series of irradiation tests of BeO

1. The AOX-grade BeO is supplied by Brush Beryllium Company. It is a relatively low-purity material averaging about 1500 to 2000 ppm total impurities. The principal impurity elements, present in concentrations of 100 ppm or higher, are fluorine, sodium, silicon, carbon, and manganese. The size of the crystallites is about 400Å by X-ray analysis.
2. The UOX-grade BeO is also supplied by the Brush Beryllium Company. Although the production process has not been described by the manufacturer, UOX is generally considered to be derived from the sulfate. The principal impurity elements are sulfur (400 to 1000 ppm), calcium (~ 100 ppm), and carbon (~ 100 ppm); the total impurity concentration ranges from 800 to 1500 ppm. The crystallite size ranges from 600 to 1000Å.
3. The HPA-grade of BeO is a GE-NMPO designation for high-purity BeO derived from the basic acetate process. The material used in this program is obtained from the Mineral Concentrates and Chemical Company as beryllium hydroxide. After being calcined to BeO at 950°C, the material contains a total of 100 to 150 ppm of impurities and is comprised of crystallites of about 1000Å diameter. Specimens are fabricated by extrusion, sintering, and machining as described later in this section under Experimental Procedures.

In addition to the pre- and postirradiation measurements of the composition series summarized in the following sections, a few data obtained on specimens to be used in the grain size - density series are included in the data on unirradiated specimens.

Property Data of Unirradiated BeO

Microstructure - Microstructural features examined include grain size, orientation, and the size, shape, and distribution of pores.

TABLE 3. 2-1

IRRADIATION TEST SCHEDULE AND STATUS FOR BeO SPECIMENS OF COMPOSITION SERIES

Test Number	Type Of BeO[a]	Number Of Specimens	Temperature, °C	Estimated Dosage, n/cm^2 (≧ 1 Mev)	Irradiation ETR Cycle Dates Start	Irradiation ETR Cycle Dates End	Facility[b]	Number Of Cartridges	Status
33MT42	AOX	60	100	1×10^{20} to 2×10^{20}	9/14/61	10/2/61	J-13	1-2/3	Completed
	UOX+MgO	36	100	1×10^{20} to 2×10^{20}	9/14/61	10/2/61		1	10/2/61
33MT52	HPA	36	100	$\sim 3 \times 10^{20}$	10/2/61	11/13/61	I-13	1	Completed
	UOX	36	100	$\sim 3 \times 10^{20}$	10/2/61	11/13/61		1	11/13/61
33MT65	UOX+ZrO_2	36	100	$\sim 3 \times 10^{20}$	10/2/61	11/13/61		1	11/13/61
33MT57	Six compositions	6 each	100	$\sim 6 \times 10^{20}$	10/2/61	11/13/61	I-13	1	Completed
			100	in 2 cycles	11/13/61	12/24/61			12/24/61
33MT47	Six compositions	6 each	100	$\sim 2 \times 10^{19}$	11/13/61	12/24/61	Reflector	1	Completed
33MT48	Six compositions	6 each	100	$\sim 7 \times 10^{19}$	11/13/61	12/24/61	Positions	1	12/24/61
33MT45	Six compositions	6 each	600	$\sim 3 \times 10^{20}$	11/13/61	12/24/61		2	Completed
33MT52b	AOX	18	100	$\sim 3 \times 10^{20}$	11/13/61	12/24/61	I-13	1/2	12/24/61
	UOX+MgO	18	100	$\sim 3 \times 10^{20}$	11/13/61	12/24/61		1/2	
33MT67	HPA+MgO	36	100	$\sim 3 \times 10^{20}$	1/2/62	2/5/62		1	At ETR
33MT46	Six compositions	6 each	1000	$\sim 3 \times 10^{20}$	1/2/62	2/5/62	I-13	2	for
33MT58	Three compositions	6 each	800	$\sim 3 \times 10^{20}$	1/2/62	2/5/62		1	insertion
33MT69	Three compositions	6 each	800	$\sim 3 \times 10^{20}$	2/5/62	3/19/62		1	In preparation
33MT60	Six compositions	6 each	300	$\sim 3 \times 10^{20}$	2/5/62	3/19/62	I-13	2	1/1/62
99MT71	Six compositions	30 each[c]	800 and 1000	$\sim 3 \times 10^{20}$	2/5/62	3/19/62	99	1	In preparation 1/1/62

[a]Specimen description and compositions are shown in Figure 3. 2-1.

[b]Facility description is given in the irradiations section.

[c]Includes two specimens of each composition, 0. 995 inch in diameter and 3. 5 inches long, for thermal conductivity measurements.

With one exception, specimens of the composition series are single-phase material. A typical example of the single-phase structure is shown in Figure 3.2-2a. The exception is the UOX + 3 weight percent ZrO_2 in which some of the ZrO_2 exists as small grains, as shown in Figure 3.2-2b. Both photos contain small white spots from subsurface reflections; however, the ZrO_2 second phase is distinguished by a black-line particle boundary.

The grain size of the specimens in the composition series, nominally 20 microns, ranges from 15 to 22 microns for the different compositions. Specific grain-size data are included in subsequent data tables. Grain size is calculated by lineal analysis of polished sections as described in ASTM Method E 112. The average intercept is determined by measuring the total length of about 100 grains in several random parts of the cross section. Grain diameter in the plane of the section is then calculated to be 1.273, or $4/\pi$, times the average intercept. (This section diameter is smaller than the diameter of the three dimensional grain; in spheres, for example, it is 85 percent of the solid diameter. The section diameter is reported here, however, to conform to convention in ceramic literature.)

The total porosity of the composition series specimens ranges from 2.0 to 3.7 percent because all the specimens of the series are within the range 96.3 to 98 percent of theoretical density. The percentages of intergranular and intragranular pores show the same relationship to percent theoretical density as that reported for UO_2 by Belle and Lustman.* In the density range of these specimens, 90 percent of the porosity is intragranular and 1 to 2 microns in diameter.

Pores within the grains are believed to occur principally as negative crystals whose axes coincide with the crystal axes of the grain. In electron micrographs of the as-polished condition, the pores usually appear circular or elliptical, although an occasional crystal shape is found, as shown in Figure 3.2-3a. On removal of the polishing debris by etching or ultrasonic cleaning, however, all of the intragranular pores exhibit the structure of negative crystals. This structure is apparent in Figure 3.2-3b, which illustrates pores 2 microns and 9 microns in diameter in the same grain. The two pores exhibit the same "crystal" orientation, and the basal, prismatic, and pyramidal planes can be identified. Pores located at the grain boundaries appear primarily as spherical or ellipsoidal shapes. Distortion in the direction of the grain boundaries is common.

Orientation measurements have been made on a limited number of specimens using X-ray diffraction measurements and the uniaxial-interference figure. Both of these methods yield information on orientation of the crystal axes rather than of grains; it is not yet known whether the two are related. Qualitatively, the results indicated that orientation in the HPA compositions is random. The AOX specimens appeared random by uniaxial interference but by X-ray diffraction there was evidence of a small amount of radial orientation, i.e., excess c-axis orientation normal to the longitudinal axis of the specimen. In the UOX compositions, there was definite orientation of the crystals with the c-axis parallel to the longitudinal axis of the specimen. The additional measurements necessary for a quantitative description of orientation were in progress at the time of this report.

Lattice Constants - Lattice Constants were determined from X-ray powder photograms of the trimmed ends remaining from the machining operation; the results are summarized in Table 3.2-2. The magnitude of the standard deviations, which include both material and method variability, is such that the small differences in lattice parameters between the various compositions are not considered significant.

*J. Belle and B. Lustman, "Properties of Uranium Dioxide," U.S. Atomic Energy Commission, Fuel Elements Conference, Paris, November 18–23, 1957, Book 2.

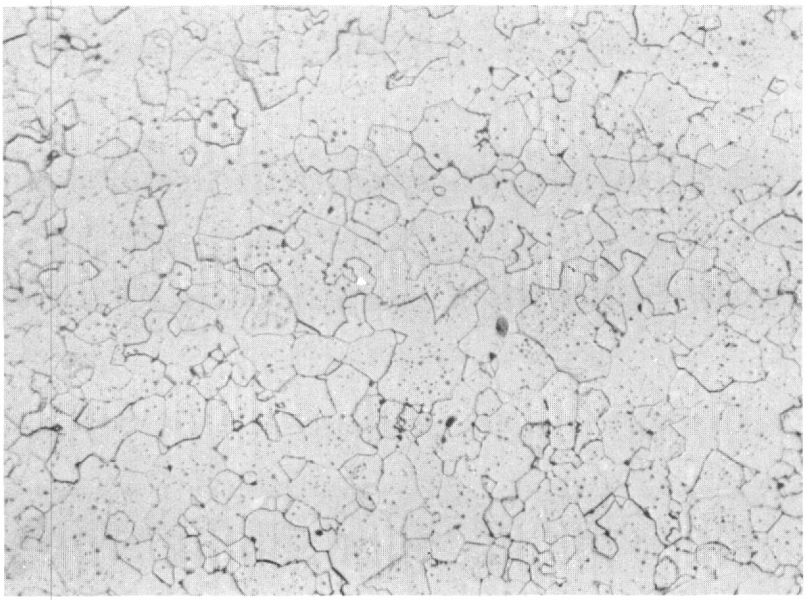

(a)

(Neg. 699) 250 X

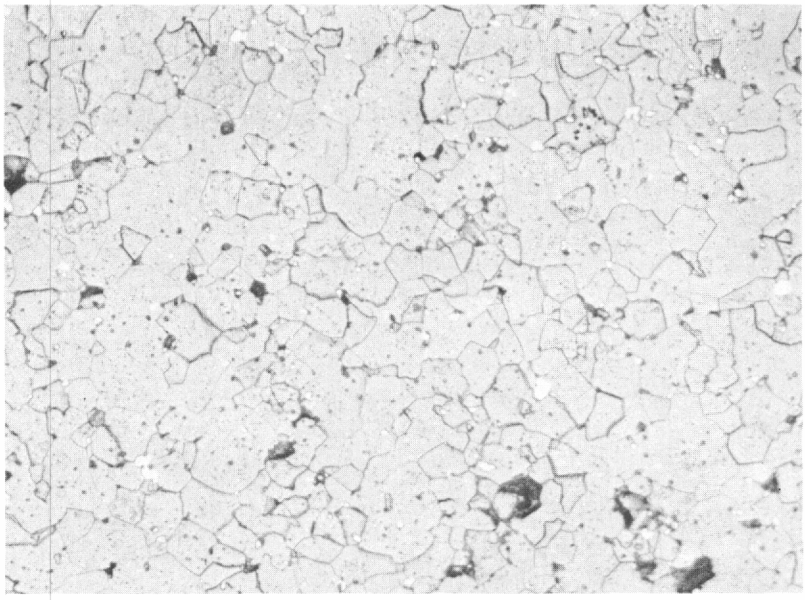

(b)

(Neg. 702) 250 X

Fig. 3.2-2 – Microstructure of sintered BeO. (a) Single-phase structure typical of specimens of composition series (except UOX + 3.0 ZrO_2), (b) Two-phase structure of UOX + 3.0 ZrO_2.

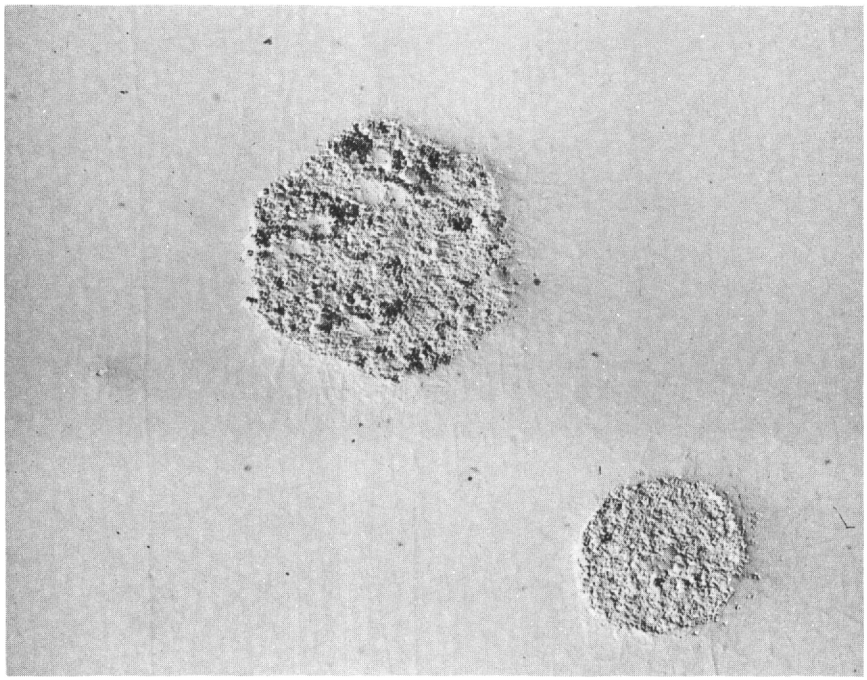

(Neg. 432C) (a) 13,500 X

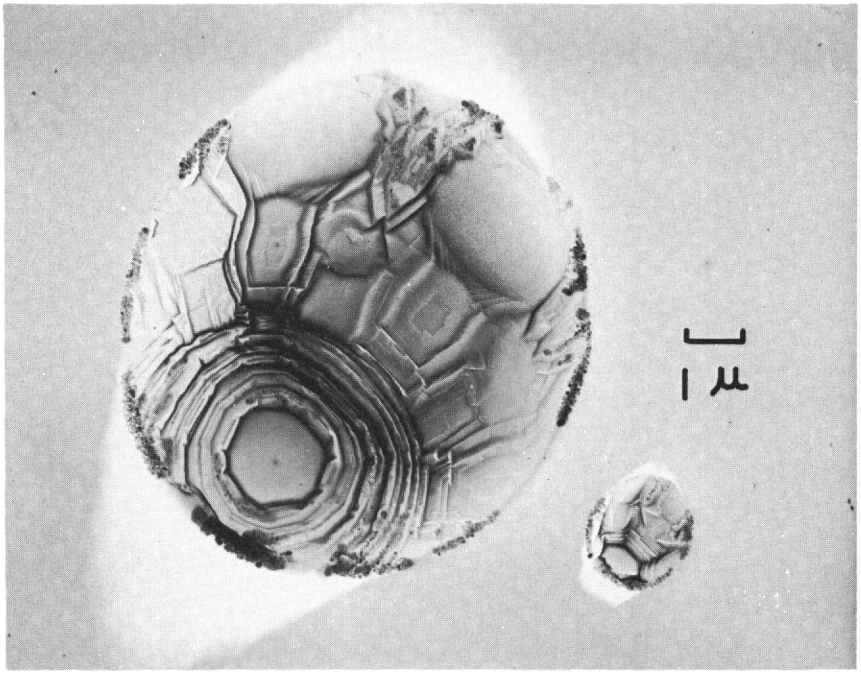

(Neg. 494E) (b) As-polished 7,500 X

Fig. 3.2-3 – Pore shape in sintered BeO
(a) Pores filled with polishing debris exhibit the usual spherical-elliptical shape as well as the comparatively rare hexagonal shape.
(b) Pores in an as-polished, ultrasonically cleaned section show negative crystal structure within the elliptical outline.

TABLE 3.2-2

LATTICE PARAMETERS OF BeO SPECIMENS

Material	Number Of Samples	Nominal Grain Size, microns	a-Axis, angstroms	Standard Deviation, angstroms	c-Axis, angstroms	Standard Deviation, angstroms	Ratio, c-Axis To a-Axis
AOX	26	20	2.6980	0.00015	4.3780	0.00123	1.6227
AOX	9	50	2.6979	0.00015	4.3776	0.00073	1.6226
UOX	8	20	2.6979	0.00013	4.3778	0.00057	1.6227
UOX+MgO	12	20	2.6982	0.00027	4.3780	0.00084	1.6226
UOX+ZrO_2	7	20	2.6980	0.00012	4.3780	0.00064	1.6227
HPA	7	20	2.6979	0.00014	4.3777	0.00077	1.6226
HPA+MgO	9	20	2.6981	0.00012	4.3779	0.00033	1.6226

Elastic Constants - Data on Young's modulus, shear modulus, Poisson's Ratio, and internal friction (logarithmic decrement) are summarized in Table 3.2-3 for specimens of the composition series and for two types of specimens of the grain-size - density series. The values reported are the dynamic constants determined from resonant frequency measurements using a Magnetest Elastomat instrument. The standard equations cited by Pickett* are used in computing the elastic constants, including a geometrical correction factor.†

Three specimens used as standards are run with each group of sample specimens to guard against instrumentation drift. These measurements, listed in Table 3.2-4, indicate that the precision of the moduli data is within 0.3 percent and the Poisson's Ratio data within 2 percent. The precision of the logarithmic decrement data is about ±40 percent, the variability being ascribed to the relatively small size of the specimens and the difficulty, inherent in the wave-decay method, of suspending specimens exactly on the nodal points.

TABLE 3.2-3

SUMMARY OF ELASTIC CONSTANTS OF BeO SPECIMENS

Specimen Composition	Number Of Rods Averaged	Nominal Grain Size, microns	Density, gm/cm^3	Young's Modulus, 10^6 psi	Shear Modulus, 10^6 psi	Poisson's Ratio	Log Decrement x 10^3
HPA	83	20	2.8900	52.52	20.06	0.317	1.83
UOX+MgO	422	20	2.9177	55.81	21.10	0.321	2.77
AOX	86	20	2.7667	47.26	17.90	0.320	1.54
AOX	234	20	2.9030	52.69	20.20	0.317	1.75
AOX	211	50	2.9245	53.64	20.63	0.316	2.82
HPA+MgO	66	20	2.8992	52.46	19.98	0.312	1.05
UOX	135	20	2.9041	55.48	21.00	0.320	2.73
UOX+ZrO_2	182	20	2.9498	54.83	20.64	0.326	1.22

*G. Pickett, "Equations for Computing Elastic Constants from Flexural and Torsional Resonant Frequencies of Vibration of Prisma and Cylinders," ASTM Proc. 45, 846, 1945.

†The correction factor K_1^t, influences E (Young's modulus) and ν (Poisson's Ratio). The corrected E value is calculated by multiplying the value obtained for E, in the standard equation, by K_1 where:

$$K_1^t = 1 + \frac{d^2}{\ell^2}\left(3.092 + 0.854\frac{E}{G}\right) - \frac{d^4}{\ell^4}\left(2.172\frac{E}{G}\right)\text{; thus}$$

$E_{corrected} = E_1 K_1^t$. (G = Shear Modulus) Poisson's Ratio then becomes $\nu = \frac{E_{corrected}}{2G} - 1$

TABLE 3.2-4

PRECISION OF ELASTIC CONSTANTS MEASUREMENTS

Parameter	Young's Modulus, 10^6 psi Rod Number[a]			Shear Modulus, 10^6 psi Rod Number[a]			Poisson's Ratio Rod Number[a]			Log Decrement, x 10^3 Rod Number[a]		
	A	B	C	A	B	C	A	B	C	A	B	C
Average value, $\bar{X}$	52.83	54.63	54.84	20.05	20.63	20.76	0.318	0.324	0.321	2.17	1.32	2.47
Standard deviation of readings, S_X	0.076	0.078	0.066	0.047	0.066	0.040	0.003	0.004	0.003	1.65	0.54	1.58
Standard deviation of average value, $S_{\bar{X}}$[b]	0.011	0.017	0.010	0.007	0.014	0.006	0.0004	0.0008	0.0004	0.24	0.12	0.24
95% of all readings fall within average, ±	0.15	0.15	0.13	0.09	0.13	0.08	0.006	0.008	0.006	3.2	1.1	3.1

[a]Number of readings: A-47, B-21, C-45.

[b]$S_{\bar{X}}$ = Standard deviation divided by $\sqrt{n}$, where n = number of observations.

Data on the variation of Young's modulus with density were obtained for the AOX and HPA compositions. The equation relating Young's modulus to resonant frequency predicts a linear relationship between Young's modulus and density (or porosity); a least-squares fit of the experimental data yielded the straight lines shown in Figure 3.2-4. Porosity values used in the figures were calculated from measured densities versus the theoretical density of 3.011 g/cm^3. Of interest is the fact that the two curves extrapolate to a value of about 57.2 x 10^6 psi as the Young's modulus of BeO of theoretical density.

Variation of the elastic constants with temperature was determined for AOX specimens of 50-micron grain size and a density of 2.90 g/cm^3. These data, shown in Figure 3.2-5, are consistent with existing information.

Modulus of Rupture - Modulus-of-rupture values obtained for various compositions and densities are summarized in Table 3.2-5, and Figure 3.2-6. The values are based on 4-point loading over a 3-inch span at a head travel of 0.060 inch per minute. The data are incomplete, particularly at elevated temperatures; measurements of 30 specimens at room temperature and 15 specimens at each of the elevated temperatures are planned. Table 3.2-6 includes a tabulation of the mean, maximum, and minimum values, and standard deviation for the room-temperature measurements. A standard deviation of 2500 to 3500 psi applies to all of the compositions.

In an effort to obtain additional data from a given number of specimens, modulus-of-rupture measurements were made on the fragments produced from rupture of the standard 3.5-inch specimens. Two specimen sizes and testing configurations were examined: 4-point loading on a 1.75-inch span, and 3-point loading on a 1.25-inch span. For the latter, the moment calculations were based on the point of fracture. The distribution curves from rupture of 60 specimens and the fragments, shown in Figure 3.2-7, are quite comparable for the 2 spans with 4-point loading. The values from the fragments can be normalized to the values for the full-size specimen with the following equations:

For the 3-inch span versus the 1.75-inch span, 4-point loading

$$M_3 = 0.856\ M_{1.75} + 2.878;$$

and for the 4-point, 3-inch span versus the 3-point, 1.25-inch span

$$M_3 = 0.736\ M_{1.25} + 4.211;$$

where M represents the modulus of rupture for the specimen size denoted in the subscript. Verification of such relationships for irradiated specimens will permit extension of the data where the number of specimens is limited.

Thermal Expansion - The thermal expansion of the UOX+MgO composition was measured at temperatures up to 1200°C using specimens 2 inches long in a conventional dilatometer apparatus. These data, in combination with prior data obtained on extruded pieces of other shapes, yielded the following equation for α, the mean coefficient of thermal expansion for the temperature range from 25° to T°C:

$$\alpha \times 10^6 = 4.804614 + 5.6398 \times 10^{-3}\ T - 1.72165 \times 10^{-6}\ T^2$$

based on measurements in the range from 200° to 1200°C. Values of α are summarized in Table 3.2-7. Limited additional measurements on the AOX and UOX compositions agree within ±3 percent of the values for UOX+MgO. Additional measurements are planned.

Dimensional Stability and Compressive Creep - The compressive-creep measurements completed to date have included specimens of the composition series together with a few specimens of other densities and grain sizes. All tests were in dry air at 1200°C for a period of 500 hours. The specimens were 1.0 inch long by 0.238 inch in diameter with

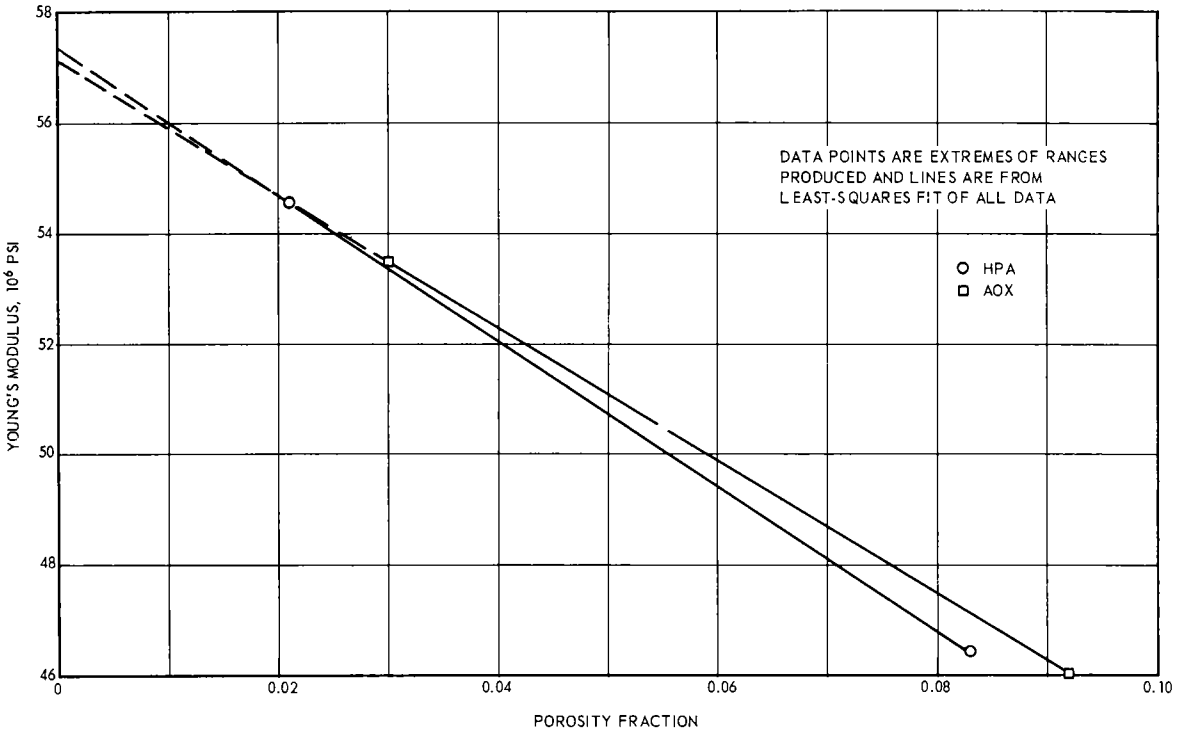

Fig. 3.2-4 – Young's modulus versus porosity fraction for HPA and AOX grades of BeO

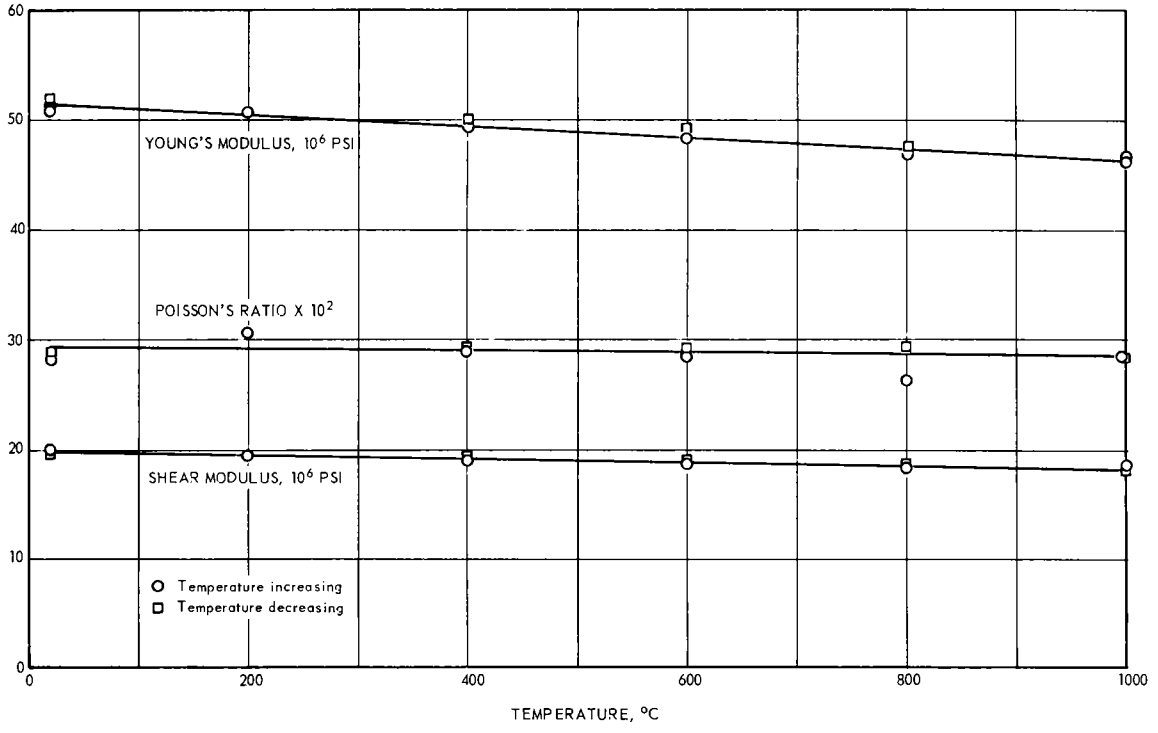

Fig. 3.2-5 – Young's modulus, shear modulus, and Poisson's Ratio of AOX-grade BeO as a function of temperature

TABLE 3.2-5

BeO MODULUS OF RUPTURE DATA

Specimen[a] Composition	Modulus Of Rupture, psi															
	Room Temperature						Elevated Temperatures, 4-Point, 3-Inch Span									
	4-Point 3-Inch Span		4-Point 1.75-Inch Span		3-Point 1.25-Inch Span		300°C		500°C		800°C		1000°C		1200°C	
	N[b]	X[b]	N	X	N	X	N	X	N	X	N	X	N	X	N	X
HPA	25	25,000	4	24,200	5	29,100	3	22,300	2	26,200	2	25,800	1	22,100	2	19,800
UOX+MgO	40	31,700	35	31,000	31	34,600	8	27,800	6	31,600	7	37,200	7	37,300	7	27,900
AOX	44	34,800	27	35,600	16	39,100	12	33,700	10	33,700	9	32,500	10	24,200	10	18,900
AOX[c]	31	19,500	29	18,800	27	20,200	5	9,900	5	18,200	5	24,100	4	26,200	4	23,800
AOX[d]	13	27,000														
HPA+MgO	37	29,800	17	31,700	16	37,200	2	29,600	2	25,800	3	32,500	2	32,800	3	21,200
UOX	41	30,300	38	31,800	35	33,800	7	30,400	7	31,800	6	35,200	7	36,600	8	29,400
UOX+ZrO_2	36	30,300	44	32,800	30	35,300	7	33,500	6	34,200	6	37,800	6	36,900	6	32,900

[a]Specimens were of nominal 20-micron grain size and 2.90 to 2.95 g/cm^3 density except for UOX+ZrO_2 whose density was 2.94 to 2.98 g/cm^3. Other exceptions are noted.

[b]N = number of specimens tested; $\overline{X}$ = average value of N specimens.

[c]Specimens were 50 microns in grain size, with a density of 2.90 to 2.95 g/cm^3.

[d]Specimens were 20 microns in grain size, with a density of 2.75 to 2.80 g/cm^3.

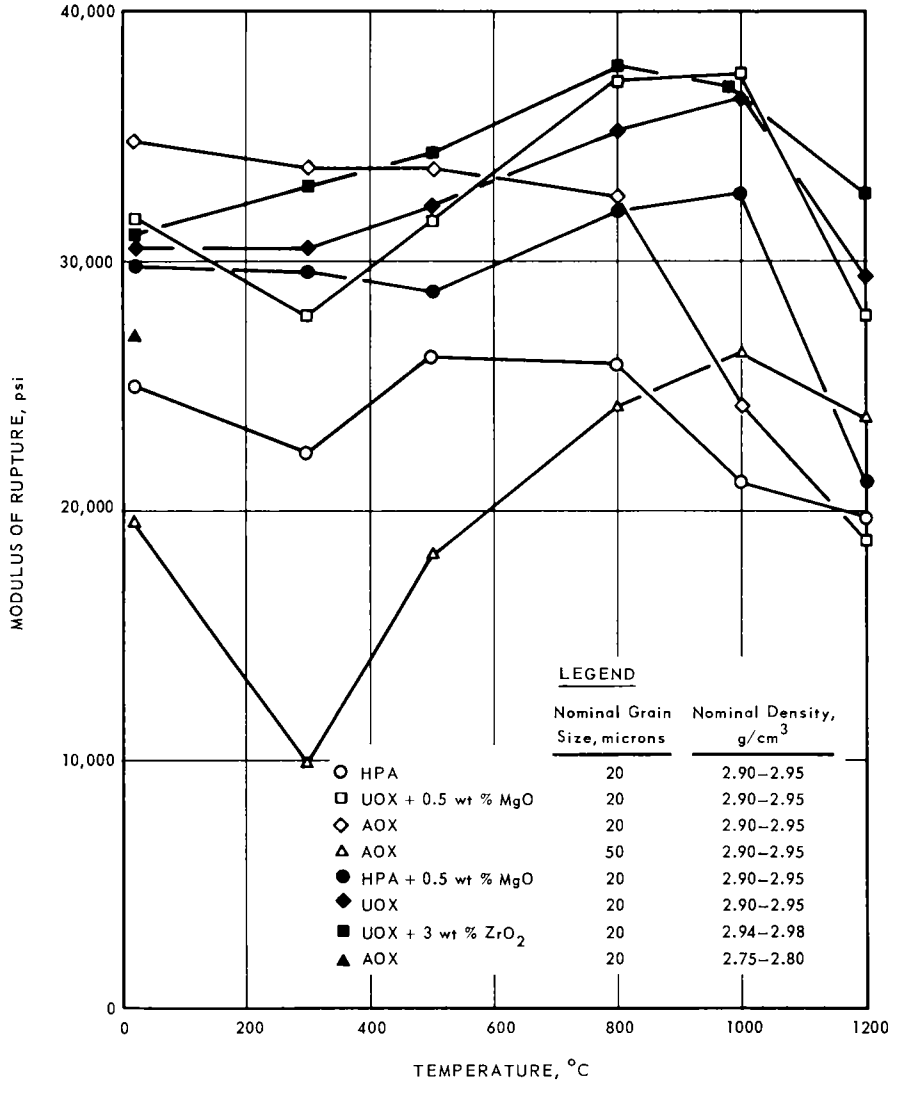

Fig. 3.2-6 – Modulus of rupture as a function of temperature

TABLE 3.2-6

STATISTICS OF MODULUS OF RUPTURE MEASUREMENTS ON BeO SPECIMENS OF COMPOSITION SERIES[a]

Specimen[b] Composition	Number Of Specimens	Modulus Of Rupture,[c] psi				Standard Deviation, psi
		Average	Maximum	Minimum	Range	
HPA	25	25,000	31,200	18,100	13,100	3,300
HPA+MgO	37	29,800	35,100	24,000	11,100	3,600
UOX	41	30,300	34,400	23,800	10,600	2,600
UOX+MgO	40	31,700	37,600	19,200	6,400	2,800
UOX+ZrO_2[d]	36	30,300	35,400	24,700	10,700	2,600
AOX	44	34,800	41,400	26,000	15,400	2,900
AOX[e]	31	19,500	23,200	15,300	7,900	2,200
AOX[f]	13	27,000	29,800	24,700	5,100	

[a]All measurements were made at room temperature.
[b]Nominal grain size of the specimens was 20 microns and the nominal density was 2.90 to 2.95 g/cm^3. Exceptions are noted.
[c]4-point loading on 3-inch span, 0.060-inch minimum head travel.
[d]Density - 2.94 to 2.98 g/cm^3.
[e]50-micron grain size.
[f]Density - 2.75 to 2.80 g/cm^3.

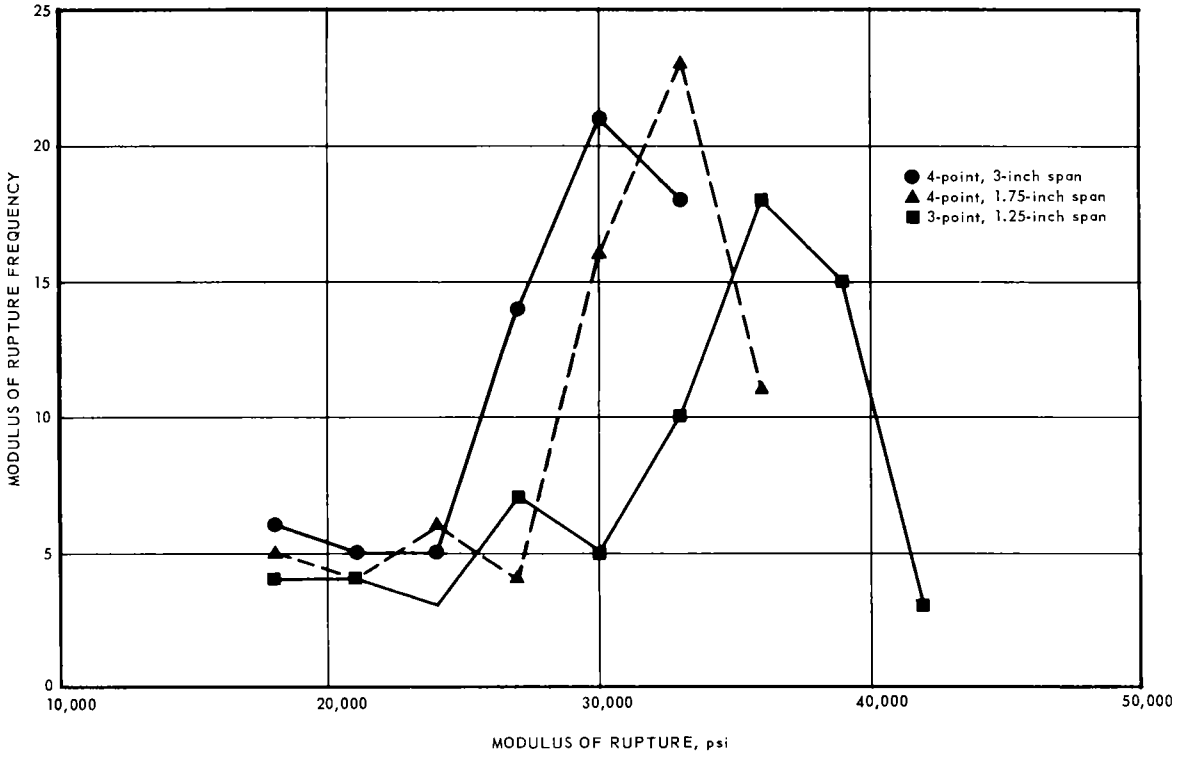

Fig. 3.2-7 – Modulus of rupture frequency distribution for 69 BeO rods of various composition, grain size, and density

TABLE 3.2-7

COEFFICIENT OF THERMAL EXPANSION OF BeO[a]

Mean Coefficient Of Expansion (α), microin./in.-°C	Temperature Range, °C
6.34	25 - 300
7.56	25 - 600
8.21	25 - 800
8.73	25 - 1000
9.09	25 - 1200

[a]Composition - UOX + 0.5 w/o MgO, density - 2.9 to 2.95 g/cm^3, grain size - 20 microns.

plane parallel ends, and were tested under column loading. The results listed in Table 3.2-8 appear to fall within the range of creep values observed heretofore. There is some indication, as shown in Figure 3.2-8, that the logarithm of the percentage of creep is linearly related to the percentage of theoretical density.

As a point of reference, a number of specimens were thermally aged in slowly moving dry air at 1200°C for 500 hours. The results, recorded in Table 3.2-9, indicate a high degree of stability under these test conditions.

Property Data of Irradiated BeO

A few measurements of irradiated specimens of the composition series were completed at the time of this report. Specimens examined were from the first two irradiations as outlined in Table 3.2-1.*

Microstructure - Changes in the microstructure of the UOX+MgO and AOX compositions after irradiation to approximately 2 x 10^{20} n/cm^2 were apparent only by electron microscopy. Some of the grain boundary separation arising from the anisotropic expansion of the BeO crystal could be detected. Figure 3.2-9 shows electron micrographs of unirradiated and irradiated AOX in the as-polished condition. In the unirradiated specimen, Figure 3.2-9a, grain boundaries are barely detectable and are most readily found by noting the elliptical shape of pores in the grain boundary. In the irradiated specimen, Figure 3.2-9b, grain boundaries are quite prominent and have separated enough that polishing debris could accumulate in the gap. The specimens had a grain size of 20 microns and a density of 2.9 g/cm^3 before irradiation.

By optical microscopy, the AOX and UOX+MgO materials were found to be single phase and of the original grain size.

Lattice Constants - Expansion of the BeO lattice dimensions in the AOX and UOX+MgO compositions amounted to approximately 0.53 percent in the c-axis and 0.07 percent in the a-axis at a dosage of 2 x 10^{20} n/cm^2. Differences in the c-axis expansion between the two

*Data on BeO specimens irradiated prior to 1961 were reported in the first progress report under this program, NMP-HTMP-1, "High Temperature Materials Program Progress Report No. 1," GE-NMPO, May 1, 1961 – June 30, 1961. These data have been omitted from this report because of uncertainty in dosages.

TABLE 3.2-8

COMPRESSIVE CREEP OF BeO COMPOSITIONS AT 1200°C

Material	Grain Size,[a] microns	Density, g/cm^3	Percent Of Theoretical Density	Load, psi	Creep[b] In 500 Hours, %
AOX	16.3	2.88	95.6	1000	0.18
AOX	14.8	2.867	95.2	3000	0.62
AOX	45.6	2.97	98.6	2000	0.03
AOX	42.7	2.97	98.6	3000	0.03
AOX	42.7	2.907	96.5	6000	0.09
UOX	22.3	2.903	96.4	3000	0.09
UOX+MgO	17.2	2.897	96.2	3000	0.23
UOX+MgO	(16)	2.937	97.5	6000	0.25
UOX+ZrO_2	(17)	2.941	96.7	3000	0.05
HPA	(20)	2.895	96.1	6000	0.22
HPA	(15)	2.901	96.3	3000	0.18
HPA	(15)	2.832	94.0	3000	0.68
HPA+MgO	(19)	2.937	97.5	3000	0.14

[a]Measured on actual pieces tested except where values are in parentheses; such pieces are from other rods in the same sintering batches.

[b]Column loading on specimens 1 inch long and 0.238 inch in diameter; test run in dry air.

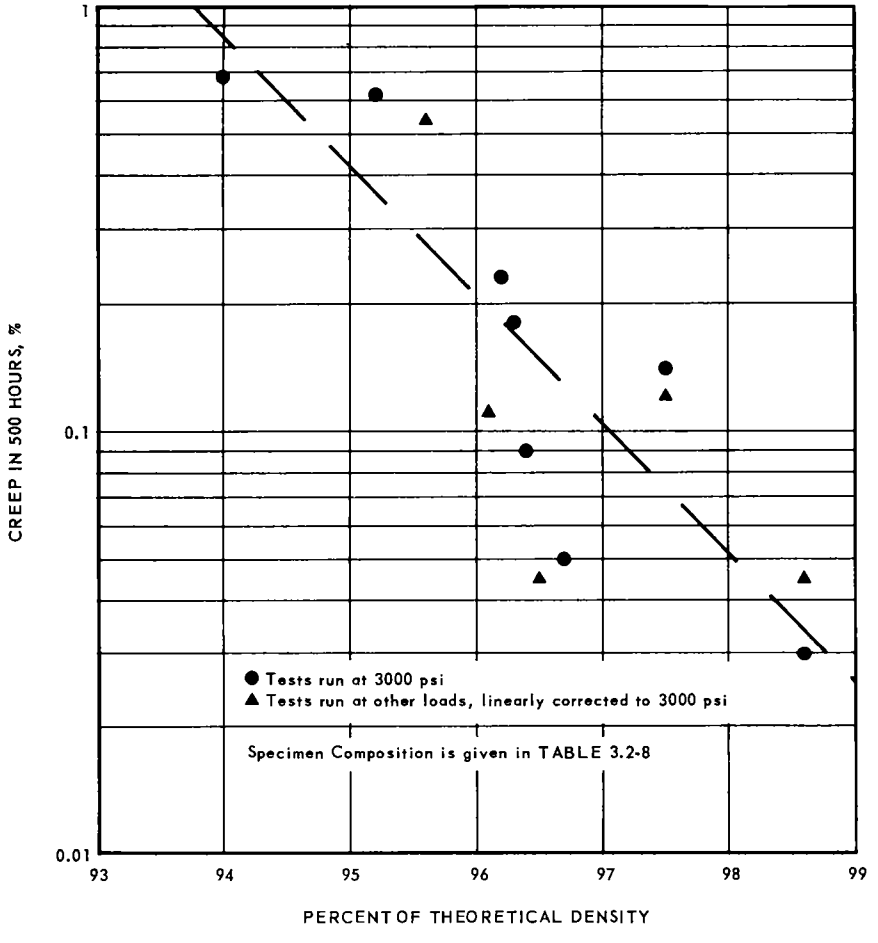

Fig. 3.2-8 – Compressive creep of BeO at 1200°C

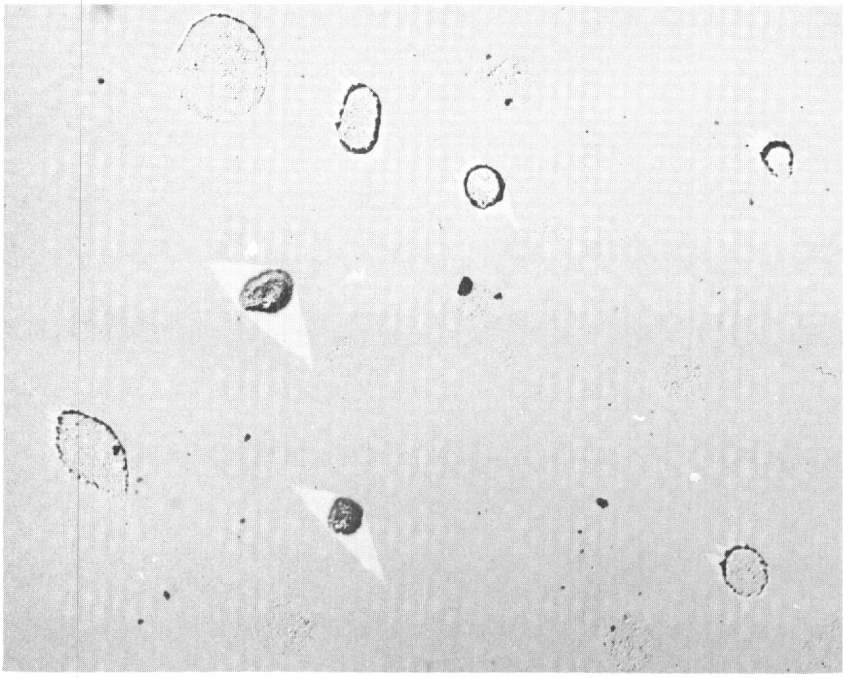

(Neg. 529E) a. Unirradiated 7,500 X

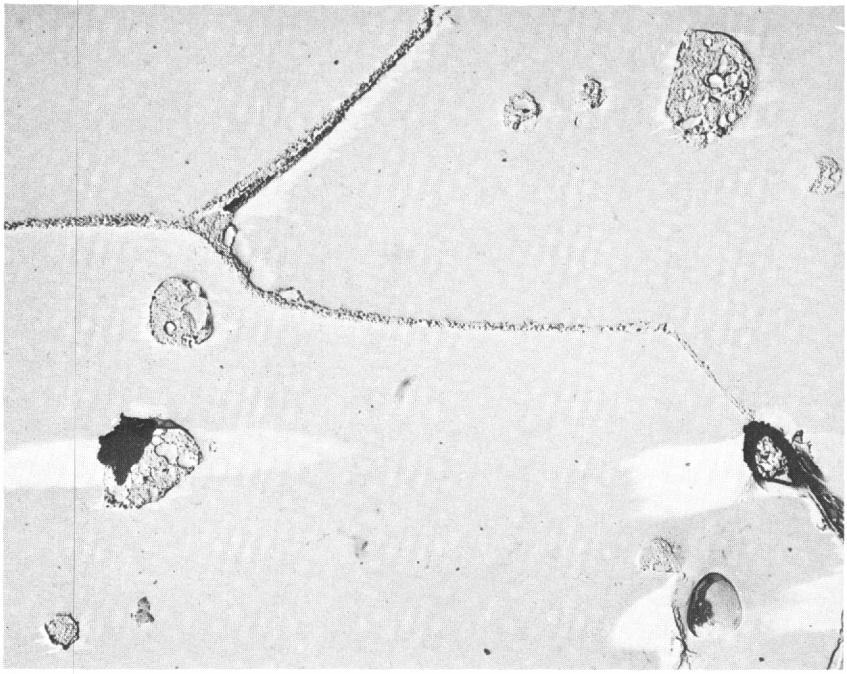

(Neg. 532C) b. Irradiated 7,500 X

Fig. 3.2-9 – Electron micrographs of AOX-grade BeO before and after irradiation. As-polished.

TABLE 3.2-9

DIMENSIONAL STABILITY OF BeO SPECIMENS IN THERMAL AGING TESTS

Specimen[a] Composition	Density, g/cm^3	Change, %		
		Length	Weight	Density
HPA	2.8846	0.00	0.02	0.07
UOX+MgO	2.8906	-0.01	-0.18	-0.02
AOX	2.8832	-0.01	0.01	-0.09
AOX	2.8142	0.00	0.03	0.02
AOX	2.9646	0.00	0.04	0.01
HPA+MgO	2.8961	-0.02	0.02	0.14
UOX	2.8824	0.01	0.02	0.05
UOX+ZrO_2	2.9345	0.01	0.03	0.07

[a]Exposure - 500 hours at 1200°C in slowly moving dry air.
Specimens - 3.5 inches long, 0.238 inch in diameter, 20-micron grain size.

compositions, shown in Table 3.2-10, can probably be ascribed to the different dosages. The expansion in the a-axis, however, is greater in the UOX+MgO composition and may be indicative of an effect of the MgO additive. Further information on this possibility will be available from other dosages and compositions of this series.

Radiation-Induced Expansion - The expansion of the BeO lattice resulted in increased dimensions, volume, and porosity and in decreased density. As indicated in Table 3.2-11, the volume and density changed ranged from 0.57 to 1.7 percent in the AOX and UOX+MgO compositions at dosages from 1×10^{20} to 2×10^{20} n/cm^2 ($\geq$ 1 Mev). The changes were slightly larger in the AOX material. For these two compositions, the measured volume change exceeded that calculated from the lattice parameters (at the 2×10^{20} dosage) by a factor of about 2; hence, roughly half of the measured expansion occurs as increased porosity. The maximum volume expansion measured in the specimens examined to date was 5.76 percent in the UOX+ZrO_2 composition at a dosage of approximately 3.5×10^{20} n/cm^2 ($\geq$ 1 Mev).

The corresponding dimensional changes are summarized in Table 3.2-12. In the AOX and UOX+MgO compositions, the expansion ranged from 0.14 to 0.6 percent in the dosage range from 1×10^{20} to 2×10^{20} n/cm^2 ($\geq$ 1 Mev). The maximum dimensional change observed was 2.08 percent in the UOX+ZrO_2 composition at about 3.5×10^{20} n/cm^2 ($\geq$ 1 Mev). The dimensional expansion of the different compositions was not equally distributed between the length and diameter. This discrepancy is readily apparent in the column listing the ratio of the fractional changes in length versus diameter. Although small differences in the ratio are not considered significant because of its sensitivity to small errors in the diameter measurements, the values of the ratio clearly show a difference between AOX and the other compositions.

Differences in the dimensional and volume expansion in the AOX and UOX+MgO compositions can apparently be explained on the basis of orientation. Randomly oriented grains expanding anisotropically cannot maintain contiguous grain boundaries; in contrast, grains with the same crystal orientation can do so since the expansion in the two grain boundary surfaces is the same. Thus, randomly oriented specimens should exhibit larger volume and dimensional changes than those with preferred crystal orientation because of greater

TABLE 3.2-10

LATTICE PARAMETER CHANGES IN BeO IRRADIATED AT 100°C

BeO Grade	Dosage, n/cm^2 (≧ 1 Mev)	Lattice Parameters, angstroms a-Axis	Δa	c-Axis	Δc	Δa/a x 10^3	Δc/c x 10^3	% Δc / % Δa	ΔV/V[a] x 10^3
AOX	none	2.6980		4.3780					
AOX	1.8×10^{20}	2.6998	0.0018	4.4000	0.0220	0.667	5.03	7.54	6.37
AOX	2.1×10^{20}	2.6998	0.0018	4.4011	0.0231	0.667	5.28	7.92	6.62
UOX+MgO	none	2.6982		4.3780					
UOX+MgO	2.05×10^{20}	2.7002	0.0020	4.4007	0.0227	0.741	5.19	7.0	6.67
UOX+MgO	2.2×10^{20}	2.7004	0.0022	4.4031	0.0251	0.815	5.73	7.03	7.38

[a]V = volume.

grain boundary separation. Similarly, perferred orientation in the radial direction, i.e., crystals oriented such that the c-axis or its major projection is normal to the longitudinal axis of the specimen should result in a greater percentage change in the diameter than in the length, while the reverse would be true for preferred orientation in the longitudinal direction. Thus the ratio of $\Delta l/l$ to $\Delta d/d$ would vary from less than 1 to greater than 1 as the preferred orientation changes from radial to longitudinal.

Qualitatively, the changes in the irradiated specimens are in the direction expected from the orientation measurements made prior to irradiation. The AOX, which exhibited greater diametral than length expansion, was the only composition which appeared to contain an excess of radially oriented crystals. The UOX+MgO, which expanded more in length than in the diameter, definitely was preferentially oriented in the longitudinal direction. Both the UOX and UOX+ZrO_2 are believed to be oriented in a manner similar to the UOX+MgO composition, as the expansion data indicate.

The dimensional changes in the HPA composition are somewhat anomalous but do not necessarily contradict the concepts of the effects of preferred orientation. The ratio of the fractional changes in length versus diameter of the irradiated HPA specimens indicates that they are longitudinally oriented to a degree comparable to the UOX+MgO. In contrast, the unirradiated HPA appeared randomly oriented. The volume change in HPA is about 2.7 times that in UOX+MgO for a relatively small increment of dosage, and this large volume change conforms to expectations for randomly oriented samples. This discrepancy can be explained by a nonisotropic separation of the grain boundaries, which is not distributed proportionally in the radial and longitudinal directions.

Preferred orientation of crystals is unquestionably a significant factor in the radiation stability of BeO because of its direct influence on grain boundary separation and the consequent influence on other properties of the material. Intensive efforts are currently being devoted to detailed measurements on various compositions.

Elastic Constants - The elastic constants of the irradiated BeO specimens have not been clearly defined to date. In unirradiated specimens, the transverse and torsional frequencies are apparent on the Elastomat as well-defined, high-amplitude peaks at the resonant frequency, and harmonics of the fundamental frequencies can be detected. In the irradiated specimens, in contrast, a series of moderate amplitude peaks are found at a number of frequencies. It appears possible, from an analysis of these frequencies, to define the fundamental transverse frequency but not the torsional frequency. Detection of the resonant frequencies was not improved in specimens in which approximately 30 percent of the ex-

TABLE 3.2-11

DENSITY VOLUME AND POROSITY CHANGES IN BeO IRRADIATED AT 100°C

Material Composition	Nominal Grain Size, microns	Dosage, n/cm^2 ($\geq$1 Mev)	Bulk Density			Volume			Total Porosity		
			Unirradiated, g/cm^3	Irradiated, g/cm^3	Decrease, %	Unirradiated, cm^3	Irradiated, cm^3	Increase, %	Unirradiated, %	Irradiated, %	Increase, %
AOX	20	1.24×10^{20}	2.9196	2.8984	0.73	2.5495	2.5676	0.71	3.00	3.71	0.71
AOX	20	1.61×10^{20}	2.9209	2.8925	0.98	2.5495	2.5764	1.05	2.96	3.90	0.94
AOX	20	1.75×10^{20}	2.9173	2.8814	1.24	2.5432	2.5758	1.28	3.08	4.27	1.19
AOX	20	1.96×10^{20}	2.9148	2.8776	1.28	2.5495	2.5834	1.33	3.17	4.40	1.23
AOX	20	2.00×10^{20}	2.9197	2.8743	1.56	2.5432	2.5849	1.64	3.00	4.51	1.51
AOX	20	2.09×10^{20}	2.9123	2.8693	1.48	2.5509	2.5914	1.59	3.25	4.68	1.43
AOX	50	1.76×10^{20}	2.9460	2.8951	1.73	2.5419	2.5840	1.66	2.13	3.82	1.69
UOX+MgO	20	1.30×10^{20}	2.9101	2.8912	0.65	2.5581	2.5759	0.70	3.32	3.95	0.63
UOX+MgO	20	1.78×10^{20}	2.9103	2.8817	0.99	2.5587	2.5850	1.03	3.31	4.26	0.95
UOX+MgO	20	1.82×10^{20}	2.9030	2.8771	0.90	2.5595	2.5844	0.97	3.56	4.42	0.86
UOX+MgO	20	2.12×10^{20}	2.9027	2.8698	1.14	2.5635	2.5954	1.24	3.50	4.59	1.09
UOX+MgO	20	2.17×10^{20}	2.9024	2.8696	1.14	2.5590	2.5902	1.22	3.58	4.66	1.08
UOX+MgO	20	2.25×10^{20}	2.9025	2.8645	1.31	2.5620	2.5982	1.41	3.57	4.84	1.26
HPA	20	2.4×10^{20}[a]	2.9139	2.8079	3.64	2.5430	2.6390	3.77	3.19	6.72	3.53
UOX	20	3.2×10^{20}[a]	2.9044	2.7825	4.20	2.5483	2.6617	4.45	3.46	7.56	4.10
UOX+ZrO_2	20	3.5×10^{20}[a]	2.9597	2.7988	5.44	2.5441	2.6906	5.76	1.67	7.02	5.35

[a]Dosages estimated on the basis of megawatt-hour exposure; dosimetry to be completed.

TABLE 3.2-12

DIMENSIONAL CHANGES IN BeO COMPOSITIONS IRRADIATED AT 100°C

Type Of BeO[a]	Dosage, n/cm^2 (≥ 1 Mev)	Increase,[b] % Length	Increase,[b] % Diameter	%Δ1 Ratio: %Δd
AOX	1.24 x 10^{20}	0.160	0.23	0.7
AOX	1.61 x 10^{20}	0.212	0.29	0.7
AOX	1.75 x 10^{20}	0.297	0.40	0.7
AOX	1.96 x 10^{20}	0.356	0.47	0.8
AOX	2.00 x 10^{20}	0.411	0.51	0.8
AOX	2.09 x 10^{20}	0.435	0.59	0.7
AOX[c]	1.76 x 10^{20}	0.436	0.61	0.8
UOX+MgO	1.30 x 10^{20}	0.233	0.14	1.7
UOX+MgO	1.78 x 10^{20}	0.358	0.23	1.6
UOX+MgO	1.82 x 10^{20}	0.403	0.30	1.3
UOX+MgO	2.12 x 10^{20}	0.499	0.35	1.4
UOX+MgO	2.17 x 10^{20}	0.532	0.36	1.5
UOX+MgO	2.25 x 10^{20}	0.553	0.43	1.3
UOX	3.2[d] x 10^{20}	1.779	1.31	1.4
HPA	2.4[d] x 10^{20}	1.623	1.03	1.6
UOX+ZrO_2[e]	3.5[d] x 10^{20}	2.077	1.72	1.2

[a]20-Micron grain size and a density of 2.90 to 2.95 g/cm^3 exceptions where noted.
[b]Values listed are the average of measurements on six specimens.
[c]50-Micron grain size.
[d]Dosages estimated on basis of megawatt-hour exposure; dosimetry to be completed.
[e]Density of 2.94 to 2.98 g/cm^3.

pansion had been thermally annealed. The French investigators Elston and Caillat reported similar difficulties with their irradiated BeO specimens.* Efforts are continuing to determine the frequencies related to the shear modulus by other techniques and by extension of the frequency range of the Elastomat.

On the basis of the deduced transverse frequency, a Young's modulus of 19.2 x 10^6 psi is tentatively assigned to UOX+MgO specimens irradiated to 2.12 x 10^{20} n/cm^2 (≥1 Mev). This value represents a decrease of 36 x 10^6 psi, or about 63 percent, from the unirradiated value. One of the factors contributing to decreased amplitude of the resonant frequencies was a large increase in the internal friction, shown in Table 3.2-13. As noted previously, the precision of the internal friction measurements is relatively poor; however, increases by as much as two orders of magnitude in the irradiated specimens leave no doubt of the effect. Internal friction is apparently a very sensitive measure of radiation effects in BeO.

*J. Elston and R. Caillat, "Physical and Mechanical Properties of Sintered BeO Under Irradiation," P/1159, Proceedings of the Second United Nations International Conference on the Peaceful Uses of Atomic Energy, Vol. 5, 1958.

TABLE 3.2-13

INTERNAL FRICTION CHANGES IN BeO IRRADIATED AT 100°C

Type Of BeO	Dosage, n/cm^2 (≧ 1 Mev)	Logarithmic Decrement (δ)		Change, %
		Original	Irradiated	
AOX	1.24 x 10^{20}	0.009	0.028	211
AOX	1.61 x 10^{20}	0.004	0.006	50
AOX	1.75 x 10^{20}	0.003	0.125	4060
AOX	1.96 x 10^{20}	0.006	0.102	1600
AOX	2.00 x 10^{20}	0.004	0.090	2150
AOX	2.09 x 10^{20}	0.002	0.172	8500
UOX+MgO	1.30 x 10^{20}	0.002	0.003	50
UOX+MgO	1.78 x 10^{20}	0.003	0.087	2800
UOX+MgO	1.82 x 10^{20}	0.002	0.125	6150
UOX+MgO	2.12 x 10^{20}	0.003	0.120	3900
UOX+MgO	2.17 x 10^{20}	0.001	0.086	8500
UOX+MgO	2.25 x 10^{20}	0.002	0.139	6850

Modulus of Rupture - The modulus of rupture of the specimens was decreased significantly by irradiation. As indicated in Table 3.2-14, the room-temperature modulus of rupture decreased to 20 to 30 percent of the unirradiated value at approximately 2 x 10^{20} n/cm^2 (≧ 1 Mev) and to about 2 to 3 percent at about 3 x 10^{20}. These initial measurements also indicate that appreciable differences exist in the strength-retention properties of the various compositions. For comparable exposure, UOX+MgO is clearly superior to AOX, and the UOX and UOX+ZrO_2 compositions appear more stable than the HPA material. The strength differences may be related more to the degree of preferred orientation in the specimens than to compositional differences. The smaller volume expansion and the correspondingly smaller amount of grain-boundary separation in a strongly oriented specimen should contribute less to the decrease in strength in comparison to specimens of random orientation and hence with greater grain-boundary separation.

An indication of greater strength retention in small-grain-size material is apparent in the comparison of the modulus-of-rupture values for the AOX specimens with two different grain sizes.

Thermal Annealing of Radiation Effects - The thermal annealing studies completed at the time of this report consisted of measurements of the length changes at temperatures of 600° to 1100°C. Specimens examined were UOX+MgO and AOX compositions irradiated at dosages of approximately 1 x 10^{20} and 2 x 10^{20} n/cm^2 (≧ 1 Mev).

Curves of the percent of the radiation-induced expansion annealed as a function of time indicated that a number of processes occur. Typical curves are shown in Figures 3.2-10 and 3.2-11. At 600°C, the major portion of the annealing occurred in the first 5 minutes; very little subsequent change took place. At 800°, 1000°, and 1100°C, the percentage annealed was linear with the logarithm of time, indicating that the annealing follows Tammann's law* which is applicable to diffusion processes. From the slope of the lines, an activation energy on the order of 110 kilocalories was obtained for specimens irradiated at 1.2 x 10^{20} to 1.3 x 10^{20} n/cm^2 (≧ 1 Mev), as shown in Figure 3.2-12. Annealing in specimens irradiated to the 2 x 10^{20} dosage, while apparently of the same activation energy at 1000°C and 1100°C, differed considerably at 800°C. Additional measurements are being completed at intermediate temperatures to define the annealing kinetics.

* G. Tammann, *Z. angew. Chem.*, 39, 869, 1926.

TABLE 3.2-14

MODULUS OF RUPTURE OF IRRADIATED BeO

Type Of BeO	Nominal Grain Size, microns	Density, g/cm^3	Dosage,[a] n/cm^2 (≧ 1 Mev)	Modulus Of Rupture[c]		
				Preirradiation Average, psi	Postirradiation Average, psi	Postirradiation Average, % of original
UOX+MgO	20	2.90	2.12×10^{20}	31,700	11,800	37.2
AOX	20	2.90	1.96×10^{20}	34,800	7,800	22.1
AOX	50	2.90	1.76×10^{20}	19,500	3,000	15.4
HPA	20	2.90	2.4×10^{20}[b]	25,000	1,700	6.8
UOX	20	2.90	3.2×10^{20}[b]	30,300	700	2.3
UOX+ZrO_2	20	2.94	3.5×10^{20}[c]	30,300	1,000	3.3

[a]Irradiated at 100°C.
[b]Dosage estimated from megawatt-hour exposure; dosimetry to be completed.
[c]Preirradiation values are the average of 30 specimens.
Postirradiation values are the average of 6 specimens.
Measured with 4-point loading on 3-inch span at 0.060-inch-per-minute load rate.

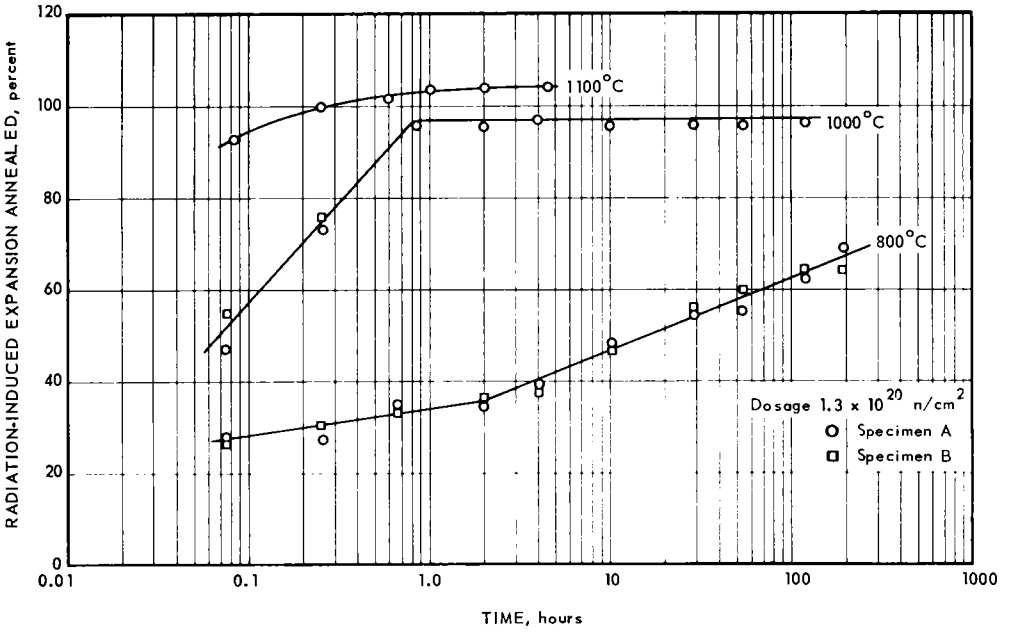

Fig. 3.2-10 – Thermal annealing of radiation-induced expansion in UOX + MgO

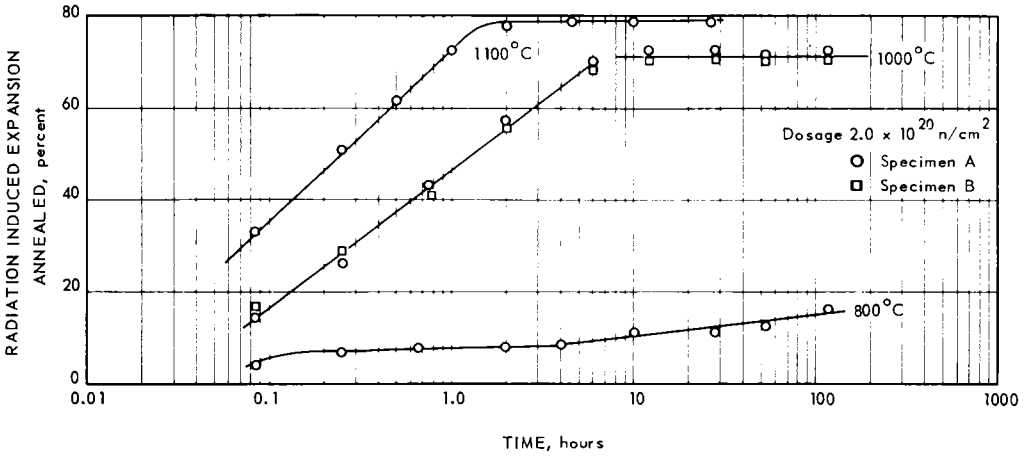

Fig. 3.2-11 – Thermal annealing of radiation-induced expansion in AOX

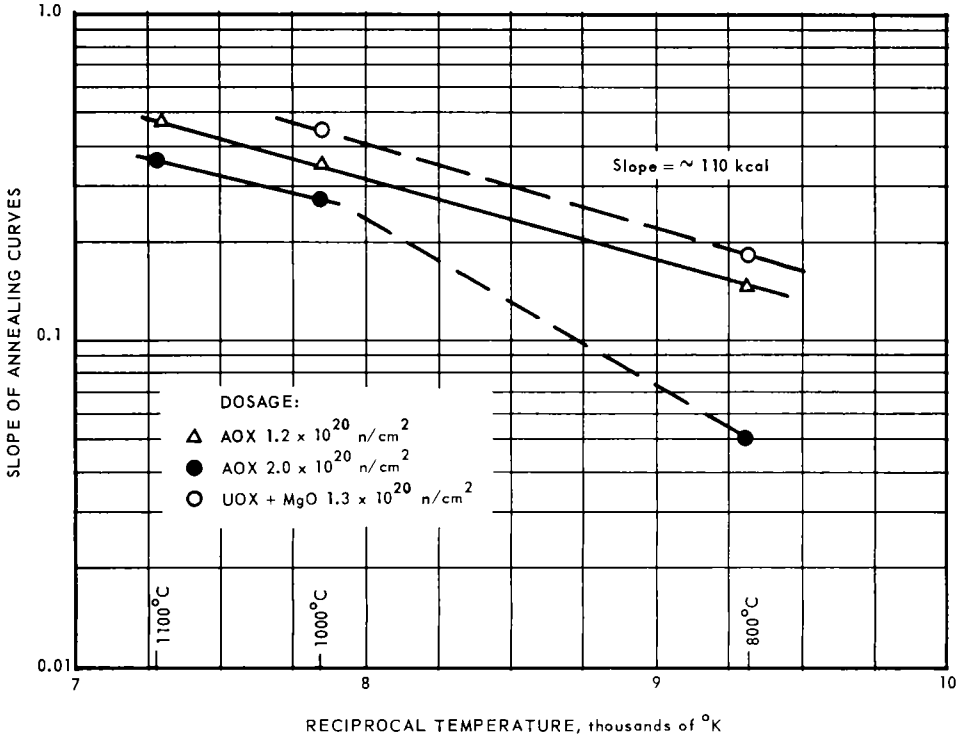

Fig. 3.2-12 – Activation energy of thermal annealing in irradiated BeO

The extent of annealing of the length changes varied with the specimen composition, the temperature, and the dosage. As indicated in Table 3.2-15, annealing, at the same times and temperatures of heating, was more complete in the samples subjected to the lower irradiation. Annealing was less complete in the AOX specimens than in the UOX+MgO at both 1000°C and 1100°C; this may also be indicative of an effect of orientation in the specimens.

Summary and Conclusions

The primary emphasis of the work to date has been on the composition series of tests. Specimens of the six compositions of this series were prepared by extrusion and sintering techniques and fairly extensive physical property measurements and microscopic examinations were completed. Approximately 80 percent of the irradiations at 100°C were completed and the first of the elevated-temperature irradiations is in progress. Initial post-irradiation data were obtained on five of the six compositions. In a secondary effort, methods were established for the preparation of most of the specimens to be used in the grain-size - density series.

Significant results of tests on irradiated specimens include a dimensional expansion of 1.5 to 2.0 percent and a decrease of the room-temperature modulus of rupture to about 3 percent of the unirradiated value at a dosage of 3×10^{20} n/cm^2 (≧ 1 Mev). Thermal annealing of the radiation-induced expansion appeared to follow the kinetics of the logarithmic rate law, and the total amount of annealing appeared to be dependent on the dosage. There was definite evidence, based on the limited number of measurements completed, that preferred grain orientation in specimens is a significant factor in the radiation stability of BeO bodies.

Plans and Recommendations

The following work is planned for the various phases of this program.

1. Complete the irradiations and measurements on the composition series specimens.
2. Complete the irradiations and measurements of the grain-size - density series as outlined in Figure 3.2-13. Two revisions have been made to the initial program on this series:
   a. The addition of specimens with grain sizes of approximately 5 microns and 10 microns in each of the density ranges. This addition is based on the limited available evidence of greater stability in materials of small grain size, and on the con-

TABLE 3.2-15

THERMAL ANNEALING OF RADIATION-INDUCED EXPANSION IN BeO

Specimen Composition	Dosage,[a] n/cm^2 (≧ 1 Mev)	Nominal Length Expansion, in.	Maximum Annealing,[b] %			
			600°C	800°C	1000°C	1100°C
AOX	1.24×10^{20}	0.0049	33	42	98	105
UOX+MgO	1.3×10^{20}	0.0077	40	64	98	105
AOX	2.0×10^{20}	0.0159	13	16	71	79
UOX+MgO	2.17×10^{20}	0.0195	19	34	94	99

[a] Irradiated at 100°C.

[b] Values quoted are an average of 2 specimens. Values shown for 800°C were measured after 180 hours, at which time annealing appeared to be continuing.

Compositions

1. AOX
2. UOX + 0.5 wt percent MgO
3. HPA

Grain size and density combinations

Density, g/cm^3	Grain size, microns
2.95 – 3.00	5, 20
2.90 – 2.95	5, 10, 20, 50, 80, 100
2.75 – 2.80	5, 10, 20, 50, 80
2.60 – 2.65	10, 20, 50, 80

(Not all of the listed combinations are used in all three compositions.)

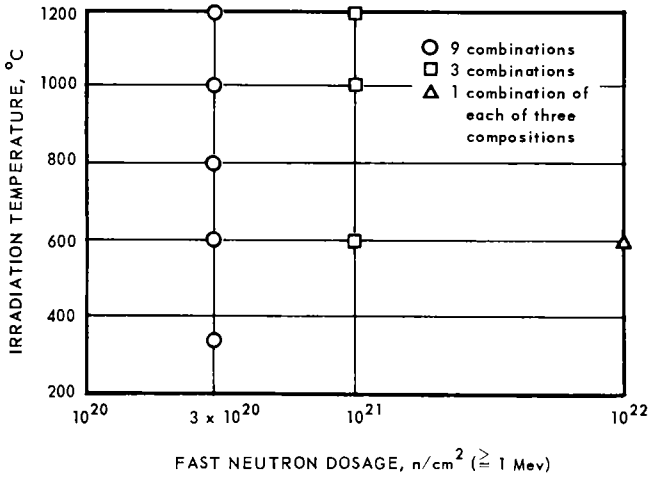

Fig. 3.2-13 – Irradiation and measurement conditions of the grain-size – density series

cept that very small grains may adjust to radiation-induced expansion with less deterioration of the physical properties of the material.

b. The addition of oriented specimens to the program as soon as possible, including samples with the maximum and minimum degree of crystal orientation achievable with modified sample-preparation techniques. In concept, specimens with a high degree of orientation should experience less separation at the grain boundaries than those with random orientation. Dimensional stability in two dimensions and greater strength retention appear possible in longitudinally oriented specimens at the expense of instability in the third dimension.

3. Conduct experiments, in the category of special studies, to determine creep under combined stress and irradiation conditions by suspending weights from BeO coil springs. Davidson and Losty* utilized this spring method in studies of graphite. Two BeO springs of UOX+MgO fabricated by grinding sintered tubes are shown in Figure 3.2-14. The square cross sections of the springs are 0.0185 inch and 0.035 inch, and the diameters are 0.3 inch and 0.325 inch, respectively. Stresses to determine the modulus of rupture of such springs can be induced by suspending weights ranging from 0.25 to 2 pounds, a range which appears feasible in irradiation capsules. Experiments of this type should also constitute an excellent method of detecting differences in radiation effects under different neutron fluxes or neutron spectra. The Young's and shear moduli and internal friction are also measurable with springs. In preliminary tests with the small spring, shown in Figure 3.2-14, a shear-modulus value was obtained that agreed within 2 percent with the value obtained by the resonant frequency method. Thus, experiments with springs permit examination of several important properties of the BeO as well as of flux and spectrum effects.

*H. W. Davidson and H. H. W. Losty, "The Effect of Neutron Irradiation on the Mechanical Properties of Graphite," Second United Nations Conference on the Peaceful Uses of Atomic Energy, Geneva, 1958, P-28, p. 307.

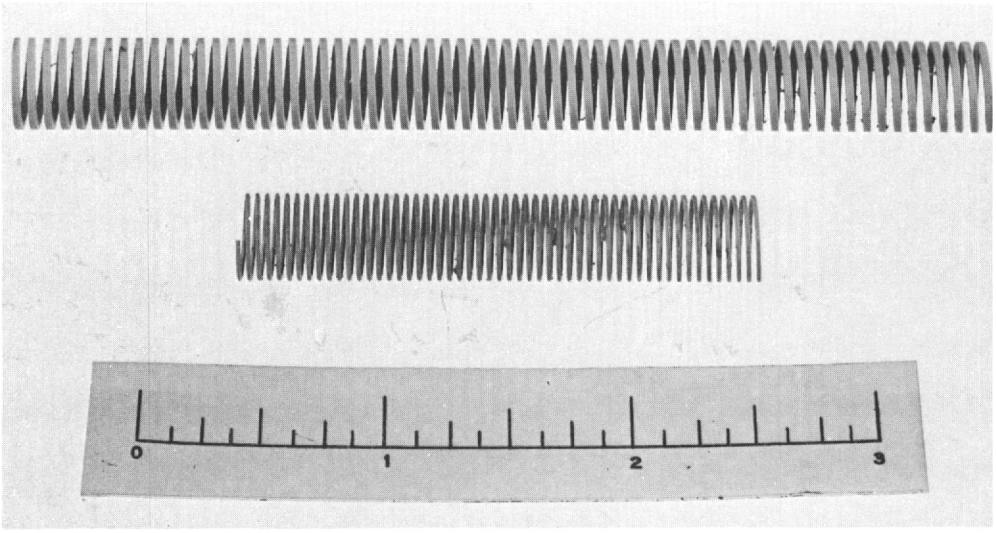

Fig. 3.2-14 – Helical springs of sintered BeO (P61-11-11)

ADDENDUM TO SECTION 3.2 "RADIATION EFFECTS ON BeO" (57063)

EXPERIMENTAL PROCEDURES

Specimen preparation procedures and the irradiation test facilities, irradiation assemblies, and dosimetry are summarized in the remainder of this section.

PREPARATION OF BeO SPECIMENS

As noted previously, the 3.5-inch long by 0.238-inch-diameter specimens used in this program are prepared by extrusion and machining. Commercially available grades of BeO in powder form are combined with aqueous organic plasticizers and then extruded, dried, prefired, sintered, ground to size, and finally inspected. Figure 3.2-15 illustrates the over-all preparation process; details of the process are described in the following steps.

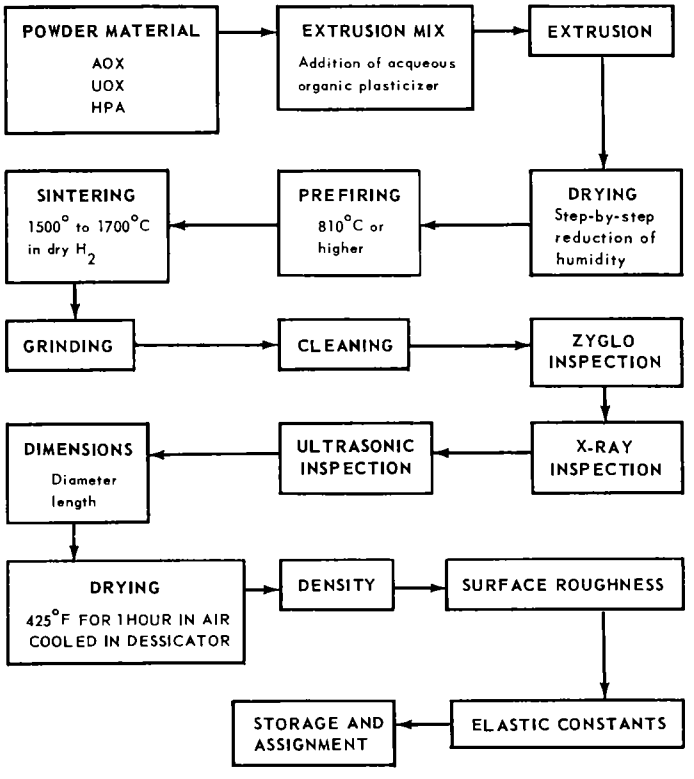

Fig. 3.2-15 – Preparation and inspection procedures for BeO specimens

1. Powder preparation and extrusion

Raw Materials - The three grades of BeO, utilized in specimens AOX, UOX, and HPA, differ in method of preparation, total impurity content, and crystallite size. Further information on the impurities present in the powders is shown in Table 3.2-16. Crystallite photomicrographs of the three powders are illustrated in Figures 3.2-16 and 3.2-17. Figure 3.2-18 gives the results of Coulter Counter particle-size analysis of the three grades of BeO.

Extrusion - As the first step in specimen preparation, the powdered BeO and the various additives are blended with a plasticizer-binder to produce the plastic mixture required for extrusion. Two compositions of plasticizer have been used; one consists of an aqueous solution of 10 weight percent starch, 10 weight percent polyvinyl alcohol, and 1 weight percent glycerine, and the other consists of a 10.7 weight percent aqueous solution of Penford Gum 300, a hydroxyethyl ether derivative of starch. The latter composition yields greater uniformity in the extrusions and is currently being used.

Additives, when used, are mixed with the plasticizer prior to its incorporation in the BeO. Additives such as MgO and ZrO_2 are mixed with the dry starch before the addition of water. An organic resin additive, used to increase the porosity of the sintered specimens, is first separately dispersed in a portion of the water specified for the gum solution and then added to the hydrated gum. The plasticizer-additive mixture is blended with the BeO powder in a wet-pass (Simpson Muller) mixer. The quantity of plasticizer added is determined in trial extrusions and usually amounts to about 33 weight percent of the mix.

TABLE 3.2-16

IMPURITY LEVELS IN THREE GRADES OF BeO POWDERS

Impurity Element	Impurity Concentration, ppm		
	AOX[a]	UOX[b]	HPA[c]
C	290	110	[d]
F	320	<10	13
P		10	12
S	9	430	28
Al	10	30	23
B	<3	<3	<3
Ca	40	100	<10
Cr	20	<10	<10
Fe	40	15	23
Li	50	1	
Mg	90	20	<10
Mn	100	<10	
Na	500	20	<10
Si	300	25	22
Sr	60	<10	
Zn	60	<20	

[a]AOX Lot 10.
[b]UOX Lot 200 W111.
[c]Average of HPA Lots K96 and 121, K111 and K123.
[d]Not determined.

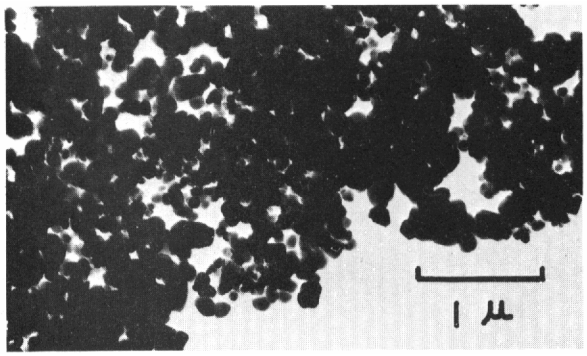

UOX

(Neg. 480D)

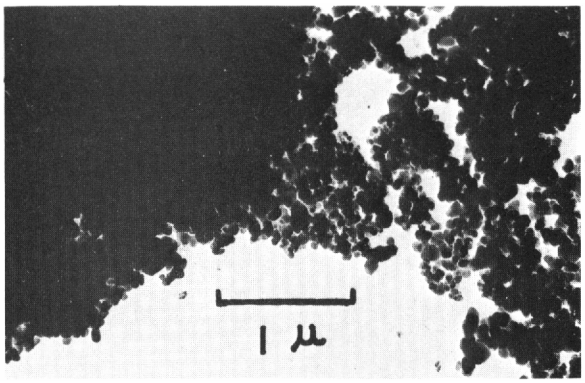

AOX

(Neg. 479B)

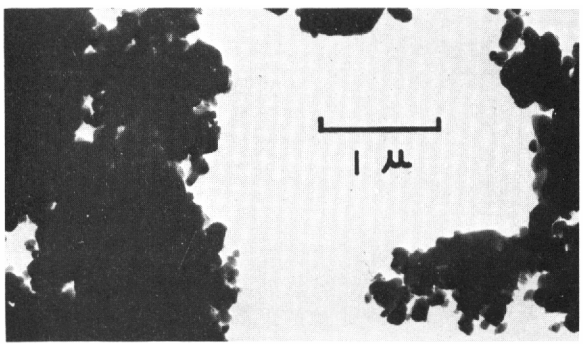

HPA

(Neg. 481B)

Fig. 3.2-16 – Photomicrographs showing crystallite size in AOX, UOX, and HPA grades of BeO powders. 20,000 X

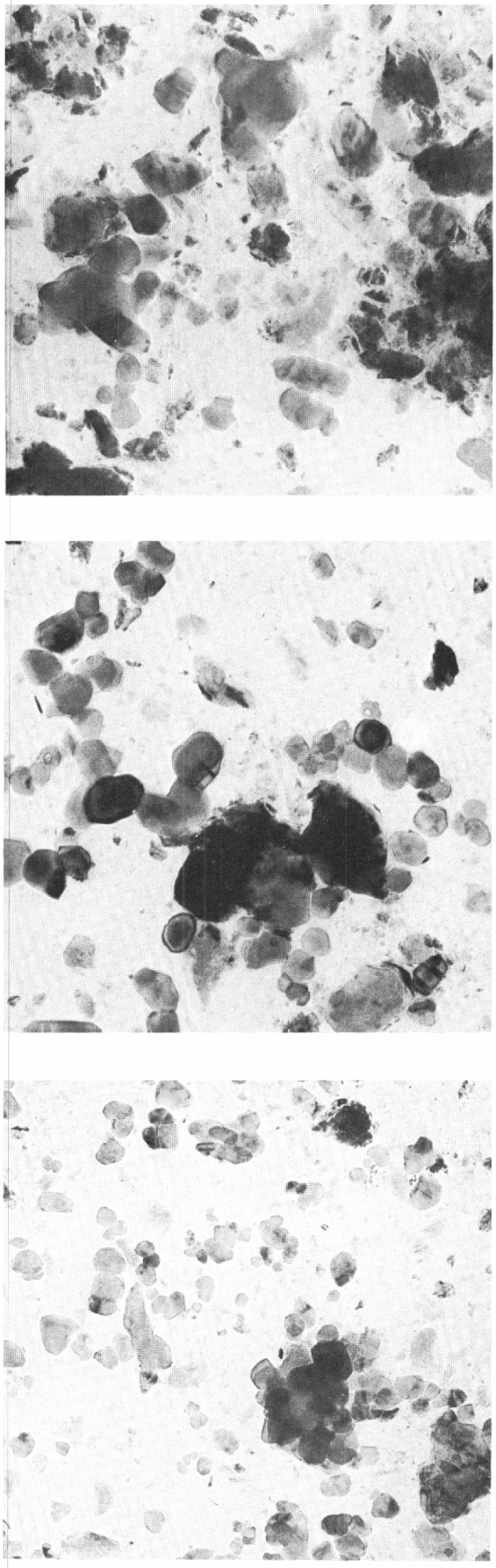

Fig. 3.2-17 – Crystallite size in AOX, UOX, and HPA grades of BeO powders (50,000 X)

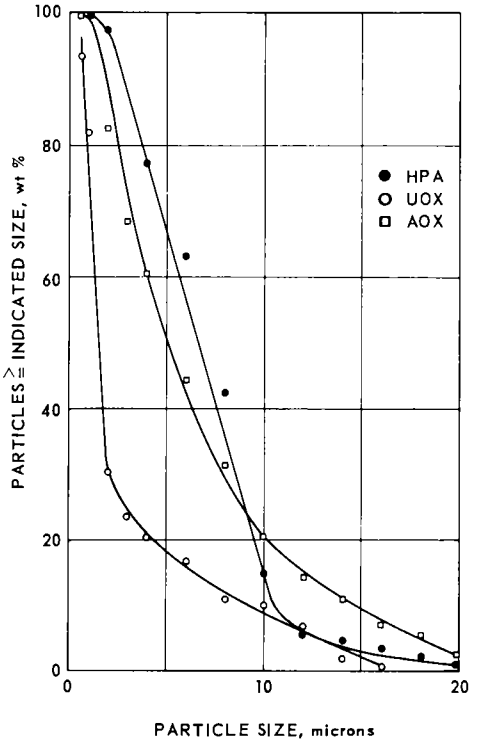

Fig. 3.2-18 – Coulter Counter particle size analysis of BeO source powders

The mix is extruded as rods at 5000 to 6000 psi with a 3.75-inch-diameter ram after de-airing at 18 mm pressure for 15 minutes. The rods are then dried at 60°C under a controlled, step-by-step reduction of the humidity.

2. Sintering

After drying, the rods are heated in air to 810°C or above to remove the binder, and are then loaded into molybdenum sintering fixtures in lots of 36 and sintered in a hydrogen atmosphere. Approximately 25 cubic feet of hydrogen per hour passes through the 1.5-cubic-foot hot zone of the furnace. Dry hydrogen is used to minimize the evaporation-condensation process of $Be(OH)_2$ transport that leads to low sintered density. The dew point of the gas rises from -45°C to about -12°C in passing through the furnace. The furnace temperature is changed at about 3°C per minute during heating and cooling.

Selection of Sintering Conditions - The density and grain size obtained in specimens are governed by prior treatment of the powder, such as calcining or the use of additives, and by the time and temperature of the sintering operation. The time and temperature required to obtain a desired grain size and density are determined from graphs of grain size versus density, density versus time, and grain size versus time. Typical charts of these relationships are shown in Figures 3.2-19 through 3.2-21 for AOX-grade BeO.

Figure 3.2-19 shows the grain sizes and densities obtained in four batches of powder with different treatments or additives. The top curve is typical for AOX-grade BeO. The position of the curve will vary slightly depending on the green density of the extruded rod and relative particle size for a given composition (constant impurity level). Changes in impurity level (such as the addition of 0.5 weight percent MgO to UOX-grade BeO) and sinterability not only change the position of the curve but change its relative shape as well. The second and third curves show the extent to which calcining part of the powder for 2 hours at 1290°C decreases density at a given grain size. The bottom curve shows the low density obtained in this material when 8 weight percent phenolic resin powder was added to the extrusion mix.

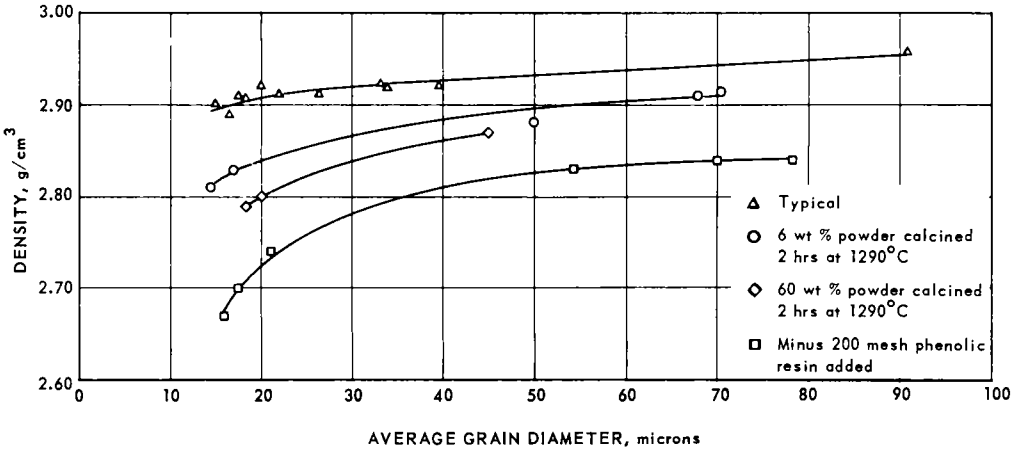

Fig. 3.2-19 – Sintered density versus grain size for AOX-grade BeO

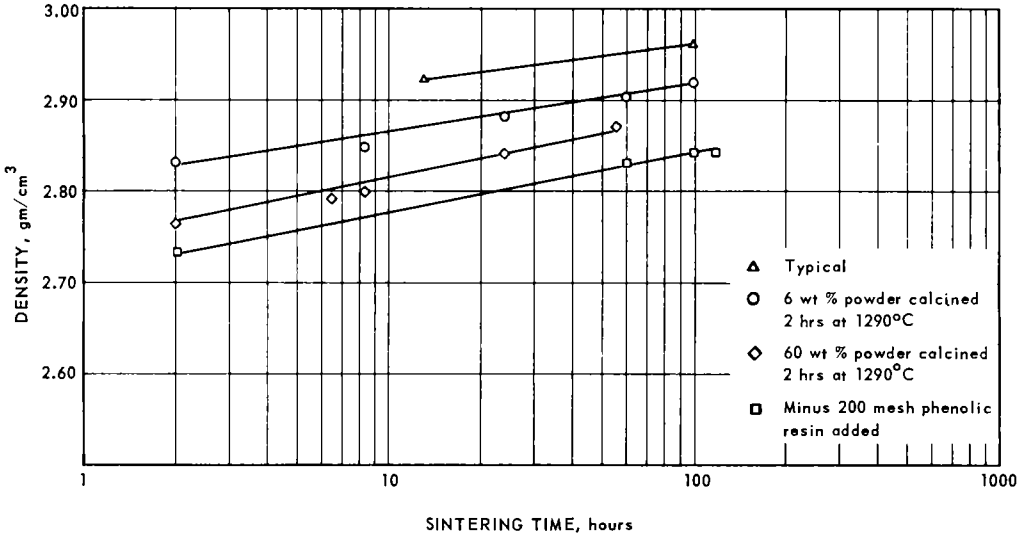

Fig. 3.2-20 – Density of AOX-grade BeO versus sintering time at 1700°C in hydrogen

Figure 3.2-20 shows the relationship between sintered density and sintering time at 1700°C in hydrogen, and illustrates the wide range of densities obtainable by varying the calcining temperature of the powder and by adding small quantities of insoluble organics to the extrusion batch.

Figure 3.2-21 shows the relationship between grain size and sintering time at 1700°C. Prediction of sintering time and temperature for specified sample characteristics may be interpolated from these graphs for each material at several temperatures.

Table 3.2-17 is a summary of the sintering conditions established to date for preparation of specimens of the composition or grain-size - density series.

3. Machining and inspection

Machining - The sintered rods, about 0.265 inch in diameter, are machined by centerless grinding to a diameter of 0.238 ± 0.001 inch by removing about 0.005 inch per pass

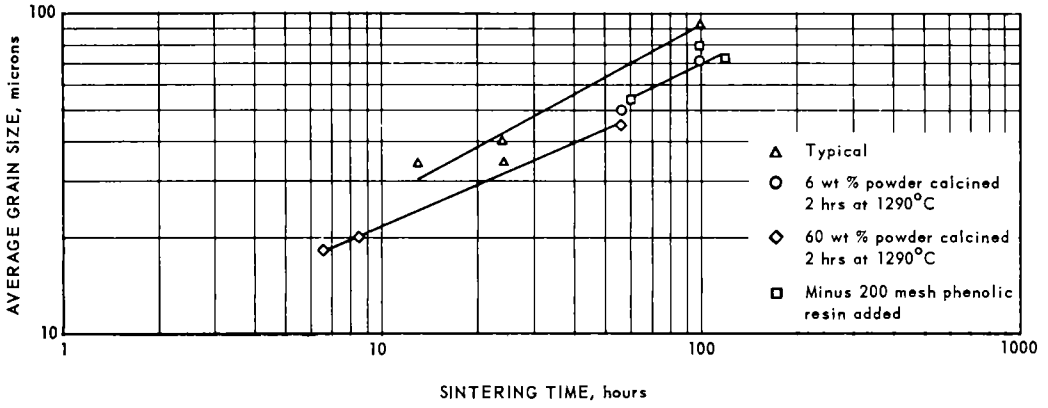

Fig. 3.2-21 – Grain size of AOX-grade BeO versus sintering time at 1700°C in hydrogen

TABLE 3.2-17

TYPICAL SINTERING CONDITIONS FOR TARGET DENSITIES AND GRAIN SIZE

Composition	Grain Size, microns	Density Range, gm/cm^3	Sintering Conditions
HPA	20	2.90 - 2.95	4 hours at 1700°C
HPA	50	2.90 - 2.95	24 hours at 1700°C
HPA	80	2.90 - 2.95	35 hours at 1700°C
HPA	120	2.90 - 2.95	64 hours at 1700°C
UOX+MgO	20	2.90 - 2.95	2 hours at 1480°C
UOX+MgO	50	2.90 - 2.95	24 hours at 1700°C
UOX+MgO	80	2.90 - 2.95	60 hours at 1700°C
AOX	20	2.90 - 2.95	3 hours at 1540°C
AOX	50	2.90 - 2.95	24 hours at 1700°C
AOX	80	2.90 - 2.95	60 hours at 1700°C
AOX	80[a]	2.90 - 2.95	100 hours at 1700°C
AOX	120	2.90 - 2.95	120 hours at 1700°C
AOX	20[b]	2.75 - 2.80	6 hours at 1700°C
HPA+MgO	20	2.90 - 2.95	2 hours at 1540°C
UOX	20	2.90 - 2.95	1 hour at 1700°C
UOX+ZrO_2	20	2.90 - 2.95	1 hour at 1700°C

[a]Batch contained 6 weight percent AOX powder calcined for 2 hours at 1290°C.
[b]Batch contained 60 weight percent AOX powder calcined for 2 hours at 1290°C.

down to 0.240 inch, and only 0.001 inch per pass thereafter. Silicon carbide wheels (60-grit, J-hardness) and Johnston's Cold Stream Coolant (a water-soluble vegetable oil) are used in all grinding operations. After centerless grinding, the rods are cut to a length of 3.500 ± 0.003 inches using metal-bonded diamond cutoff wheels. Cutoff pieces approximately 1/2 inch long are saved to be used as needed for ceramographic and chemical analyses. The rods and the small cutoff pieces are ultrasonically cleaned in a warm detergent solution, cleaned in perchlorethylene, dried, and packaged in clean plastic bags.

Inspection - The rods are inspected by Zyglo, X-ray, and ultrasonic transmission; they are rejected if defects exceeding 0.030 inch, such as cracks, chips, porous areas, or foreign inclusions are observed. Measurements of maximum and minimum diameter are taken 1/2 inch from each end and in the center of each rod. Five rods from each lot of about 36 rods are inspected for surface roughness with a Profilometer. Weight and density measurements are made on all rods that pass the above inspections. Samples are selected for test based on this density and the grain size reported after sintering.

The impurity content of sintered rods of the various compositions differs very little, as indicated in Table 3.2-18. A comparison of these values with those of the BeO powder in Table 3.2-16 shows that the concentration of elements such as carbon, sulfer and sodium is lower in the sintered rods that in the starting material. Although the concentration of some other elements increases slightly, the largest impurity pickup during processing is iron which generally increases approximately 100 ppm.

TABLE 3.2-18

IMPURITY LEVELS IN BeO RODS OF SIX COMPOSITIONS AFTER SINTERING

	Impurities, ppm					
Impurity Element	AOX (2)[a]	UOX (4)[a]	UOX+MgO (2)[a]	UOX+ZrO_2 (4)[a]	HPA (2)[a]	HPA+MgO (2)[a]
C	115	160	125	186	145	86
F		20	20	10	15	20
P		27	23	16	25	22
S	15	23	60	26	35	30
Al	25	50	45	50	30	83
B	<3	<3	<3	<3	<3	<3
Ca	80	130	150	125	25	28
Cr	10	24	35	20	18	45
Fe	103	240	215	140	118	205
Li	<1	<1	<1	<1	<1	<1
Mg	110	80		72	85	
Mn		<10	20	<10	<10	<10
Na	25	17	10	15	25	12
Ni	33	35	33	30	<10	50
Si	83	90	95	113	125	180
Sr		<10	<10	<10	<10	<10
Zn		<20	<20	<20	<20	<20

[a]Number of determinations.

IRRADIATIONS

Facilities

The facilities utilized for irradiations of BeO specimens are located in the Engineering Test Reactor (ETR) at the National Reactor Testing Station in Idaho. The facilities available on a continuous basis consist of a 3 by 3-inch core filler-block piece and a large through-loop. In addition, lower flux level reflector positions have been used for low-dosage experiments and a request has been submitted for additional high-flux space to be used for a long-term irradiation to extend to an exposure of 10^{22} nvt ($E_n \geq 1$ Mev).

Filler-Block Facilities - Interspersed in the ETR core and the aluminum reflector are 3 by 3-inch aluminum filler blocks used for irradiation experiments. The most common filler blocks contain four holes which can accommodate samples 1.125 inches in diameter and 36 inches long.

The experiments conducted in the filler-block facilities are of two basic types:

a. Capsule-type experiments in which no instrumentation to the outside of the reactor is provided and ETR water provides coolant for the experiment.
b. Lead-tube experiments in which instrumentation and/or mixed gases are provided at the specimens for recording and control of the temperature. In this category, equipment has been provided to supply either air at pressures up to 300 psig and flows up to 150 scfm or mixtures of helium and nitrogen in any desired proportions at flows up to 2 scfh per cartridge.

GE-NMPO utilizes core position I-13 for high-flux experiments of the filler-block type. The peak neutron flux is approximately 6 x 10^{14} n/cm^2-sec thermal and 3 x 10^{14} n/cm^2-sec fast ($E_n \geq 1$ Mev) in this position.

Loop Facility - A 6 by 6-inch (66) facility was requested for use in the High-Temperature Materials Program. This loop has not yet been installed in the reactor and, in the interim, a 9 by 9-inch (99) facility formerly assigned to GE-ANPD has been used. The two facilities are similar except for the maximum diameter of the assembly which can be irradiated (5.16 inches in the 66 and 7.263 inches in the 99). Both are vertical through-loops surrounded by fuel elements whose longitudinal axes are parallel to the experimental holes. The active lattice has a height of 36 inches; however, the neutron flux decreases by about a factor of 5 from reactor midplane to the top or bottom of the core. The piping, coolant flow, pressurization, and data gathering of the two loops are independent of each other, so that simultaneous experiments under differing conditions can be conducted. High-pressure, preheated air can be passed independently through each experimental loop to obtain the desired operating conditions.

Air is furnished by two compressors, each capable of delivering 15 pounds of air per second at 320 psig. The air from the compressors passes through two receivers and into three oil-fired heat exchangers that can heat it up to temperatures of approximately 600°C. Leaving the heaters, the air enters the reactor building, penetrates the reactor pressure vessel, and enters the in-pile tube. It then flows downward past the test sample in the active core, exits from the pressure vessel at the bottom of the reactor and is subsequently discharged to the atmosphere through the ETR exhaust stack.

The average neutron flux in the loop facilities is approximately 2 x 10^{14} n/cm^2-sec for both thermal and fast neutrons ($E_n \geq 1$ Mev).

A more complete description of these facilities is contained in APEX 716.*

*R. J. Harry and R. C. Fries, "Engineering Capabilities of In-Pile Irradiation Facilities Used by GE-ANPD," GE-NMPO, APEX-716, October 1961.

Irradiation Cartridges

Irradiation cartridges have been prepared for lead-tube experiments and loop-facility experiments.

1. Lead-tube experiments

Low-temperature irradiation cartridges - Cartridges for irradiations at about 100°C are comprised of three assemblies of six capsules each. The capsules are aluminum tubes 0.0625 inch in outside diameter with 0.035-inch-thick walls. Each capsule contains two BeO rods 0.238 inch in diameter and 3.5 inches long. Figure 3.2-22 shows the components and assembly of these cartridges. Heat removal is achieved by direct contact of the capsules with the reactor water moderator-coolant. To insure that specimen temperatures were less than 200°C during these irradiations, one of the cartridges was instrumented with four chromel-alumel thermocouples placed in the specimen ends and irradiated in the upstream position in the X-basket. The temperatures recorded during the irradiation were 66° ± 5°C; extrapolating these temperatures to the peak of the power profile, a maximum temperature of approximately 100°C is indicated.

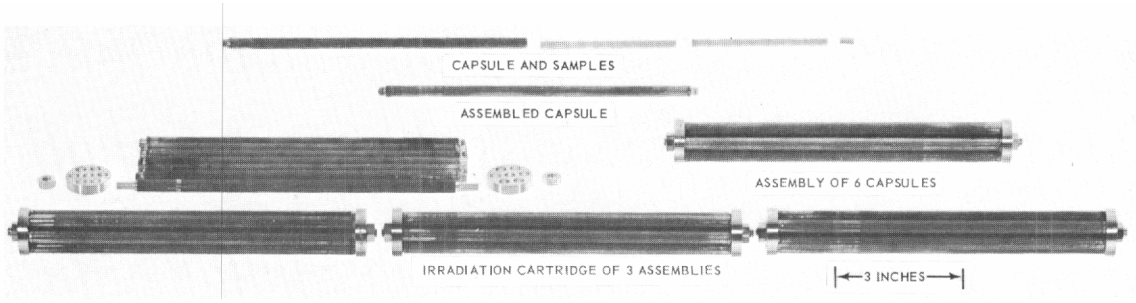

Fig. 3.2-22 – Rig for low temperature irradiation of BeO specimens (Neg. P61-7-6)

Elevated-temperature irradiation cartridges - A series of cartridges has been designed for irradiation of BeO specimens at temperatures above 200°C. The cartridges are similar in that specimen temperatures are maintained by conduction and radiation across a gas annulus between the specimen and an outside steel tube cooled by reactor water. Mixtures of helium and nitrogen gases are used for temperature control by varying the conductivity of the gas. The effect of the variable power profile from end to end in the cartridge has been compensated for by varying the thickness of the gas gap. Typical examples of this design are shown in Figure 3.2-23. In the 1000°C cartridge it was necessary to encapsulate the specimens in a radiation shield consisting of an inconel tube of 0.029-inch-wall thickness as shown in Figure 3.2-23. A summary of the pertinent parameters for the various cartridge designs appears in Table 3.2-19.

2. Loop-facility experiments

Each test assembly for the loop experiments consists of a test sample, in X-drawbar, the upper neutron scatterer, a tubular drawbar, and the shield plug. In addition, a stuffing box, a gear-drive mechanism, and a junction box are required for the 99 facility in which the drawbar penetrates the top cap of the reactor. The test sample is designed to fit the facility, although due to uncertainty in the schedule for removal of the 99 facility and installation of the 66 facility, the samples have been designed to fit the 66 size and, where it has been necessary to use the 99, they have been fitted to the larger size hole by means

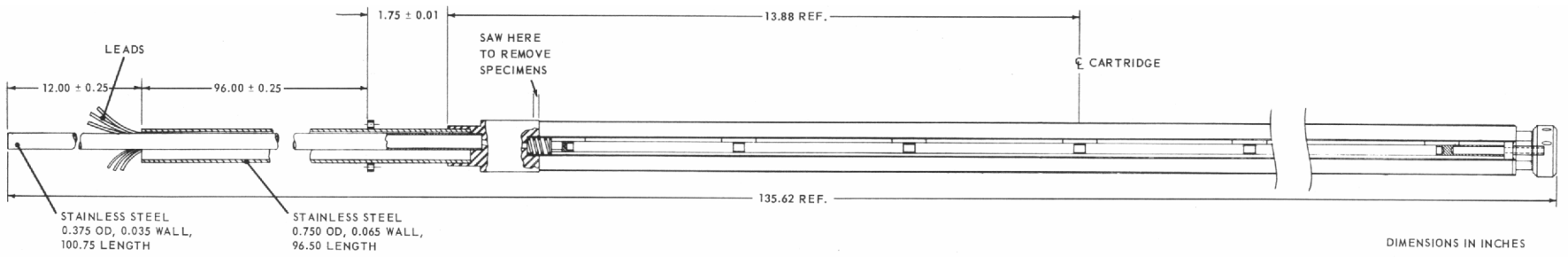

Cartridge design for BeO irradiations at 600°C (692E113)

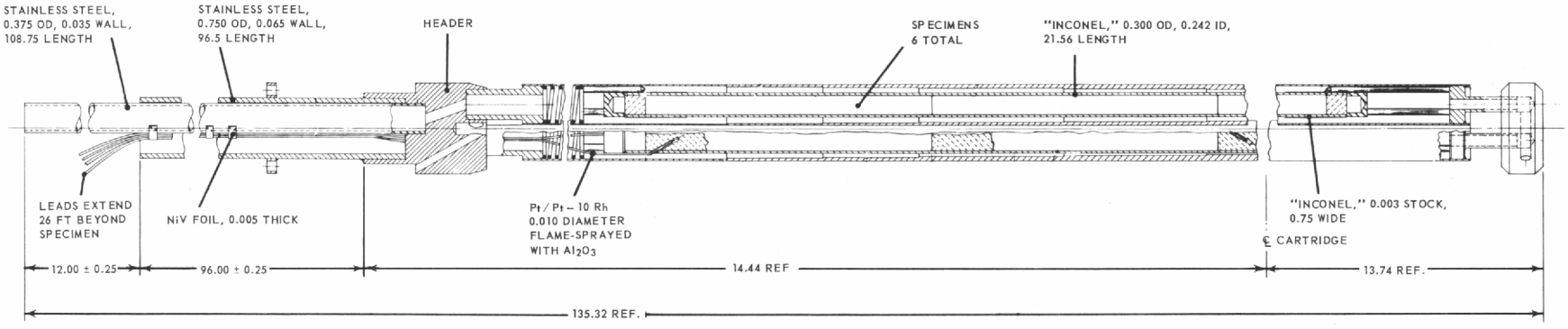

Cartridge design for BeO irradiations at 1000°C (692E117)

Fig. 3.2-23 – Typical designs of cartridges for BeO irradiations at temperatures of 600°C and 1000°C

TABLE 3.2-19

DESIGN PARAMETERS OF ELEVATED TEMPERATURE IRRADIATION CARTRIDGES

Specimen Temperature, °C	Number Of Specimens Per Cartridge	Gas Mixture, nitrogen mole fraction	Gap Thickness, Inches
600	24	0.4	0.058 - 0.085
1000	18	0.5	0.0555 - 0.0825
800	24	0.6	0.036 - 0.052
300	24	0.25	0.026 - 0.032

of adaptors. The test sample can be of any shape within the maximum dimensions of the facility. The test sample is suspended from a drawbar which provides a means of sample orientation and a means for routing instrumentation to the outside of the reactor.

The size of the 66 hole makes possible the simultaneous irradiation of many specimens. Two types of samples have been considered for irradiation: a thermal-conductivity test specimen 0.975 inch in outside diameter and 3.5 inches long, and a solid rod, 0.238 inch in outside diameter and 3.5 inches long, which is utilized for other physical property measurements. A cartridge that contains specimens of both types is shown in Figure 3.2-24. In this cartridge, 14 thermal-conductivity specimens are placed in two stages of 7 each at the upstream end of the cartridge. The temperature of the specimens is maintained at 800°C by means of the film temperature drop from the surface of the specimen to the coolant air stream. A total coolant flow of 4.2 pounds of air per second, of which approximately 1.3 pounds per second flows over the specimens, preheated to 590°C at an inlet pressure of 200 psia is provided to maintain specimen temperatures. The thermal-conductivity specimens are in tapered tubes to provide increased mass velocity of the coolant in the region of increased power generation towards the downstream end of the specimens. After passing the conductivity specimens in the cartridge, the coolant air reaches a mixing plenum and then the rear test section of the cartridge. The rear section of the cartridge contains 183 BeO test rods, 0.238 inch in diameter and 3.5 inches long, in 61 stainless steel tubes. The test specimens are maintained at a temperature of 1000°C by conduction and radiation across a stagnant air gap of 0.065 inch, and conduction through the steel wall to the air stream outside. Fifteen Pt / Pt - 10Rh thermocouples are imbedded in the specimens to measure temperature distribution.

Dosimetry - Readings of neutron dosages during the irradiations of the BeO specimens are obtained with commercially available cobalt-nickel alloy dosimeters (containing less than 1 percent cobalt). The combination yields, from the active-species Co^{60} and Co^{58}, a measure of the thermal and fast neutron fluxes.

The use of the (Ni, Co^{58}) reaction, for fast neutron dosimetry in reactors which have a high thermal flux, has been subject to criticism due to the large effective absorption cross sections for pile neutrons of the Co^{58}. The use of these detectors is further complicated by the fact that the (Ni^{58}, n) reaction can result in direct production of two isomers, a 72-day isomer and a 9-hour isomer which decays to the 72-day isomer. The cross sections of these isomers, and in particular the energy dependence of the cross sections, are not precisely known at present. Some recent measurements have been reported by Hogg;* for

*C. H. Hogg, et al., "MTR-ETR Technical Branches Quarterly Report, January 1 – March 31, 1961," IDO 16695.

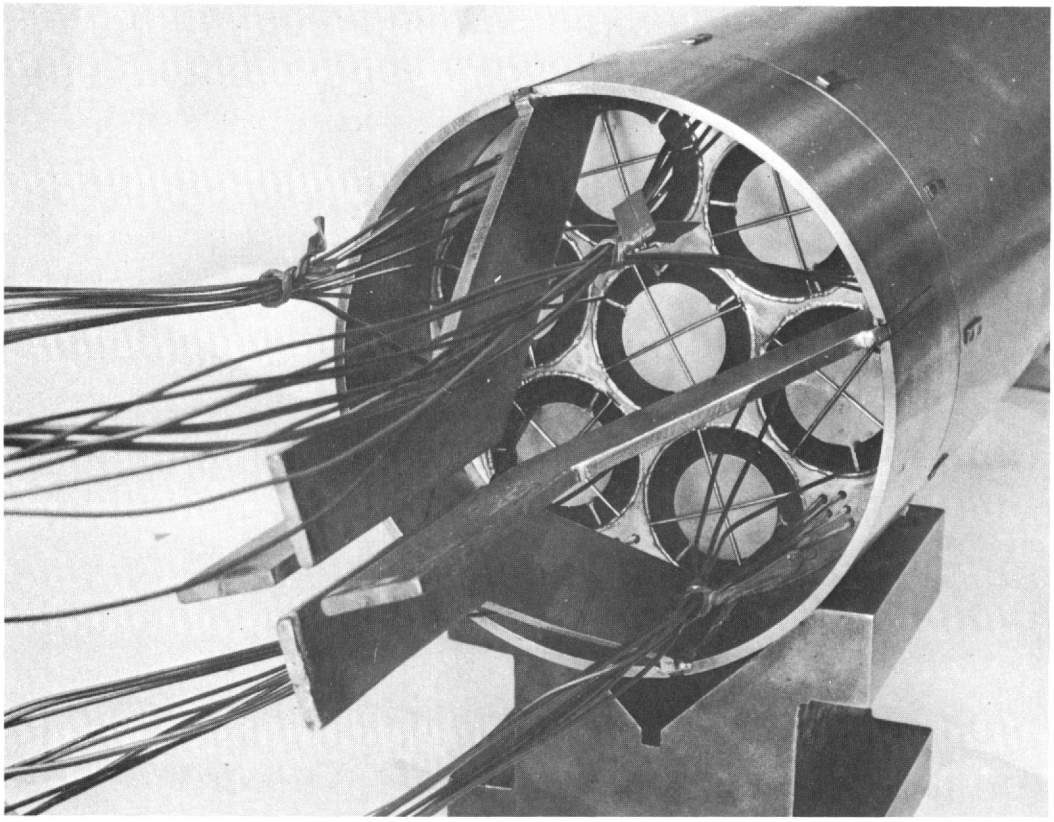

(Neg. P62-1-8B)

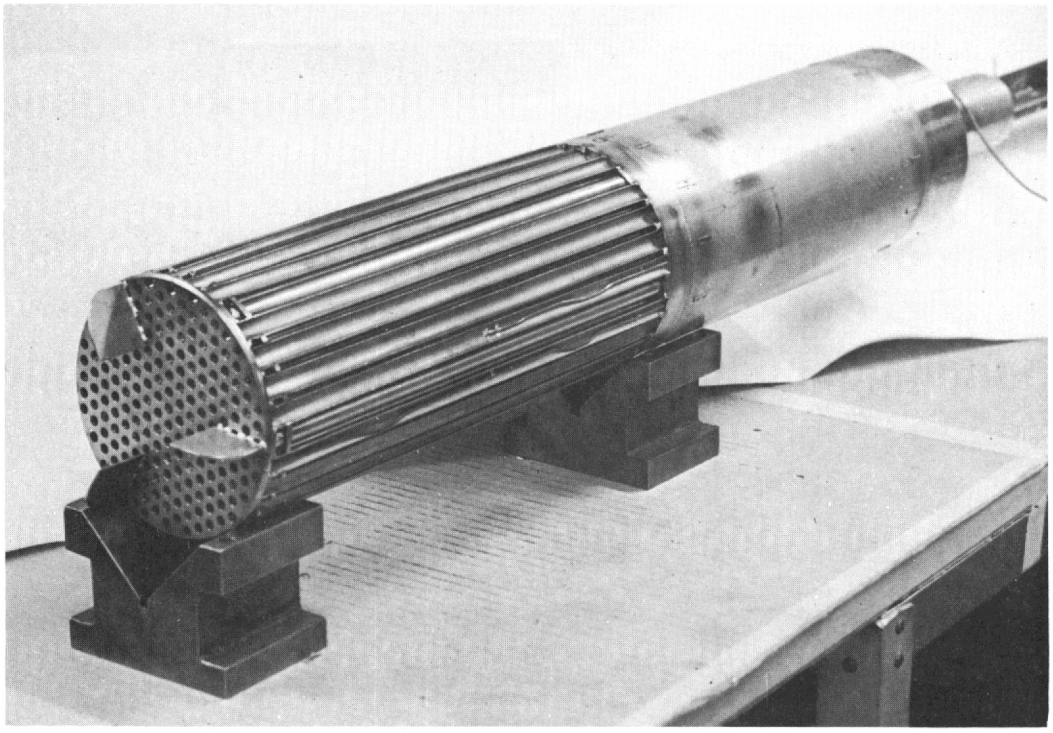

(Neg. P62-1-8C)

Fig. 3.2-24 – Cartridge for elevated temperature irradiation of BeO specimens in loop facilities

purposes of calculating the fast flux from the data, the values in Equation (1) have been used. Due to lack of specific information about the energy dependence of the cross sections of the Co^{58} isomers, it is assumed that the energy dependence is identical to Co^{59}, and burnout calculations are made with the "pile effective" flux as determined from the Co^{60} total activity.

Equation and Parameters for:

$$A_c = \lambda_c N = N_{ao}\lambda_c\phi_f \left(\sigma_f'' \left\{ \frac{\exp\left[-(\sigma_{ta}\phi_t)\,t\right] - \exp\left[-(\sigma_{tc}\phi_t + \lambda_c)\,t\right]}{(\sigma_{tc}\phi_t + \lambda_c - \sigma_{ta}\phi_t)} \right\} \right.$$

$$+ \lambda_b\sigma_f' \left\{ \frac{\exp\left[-(\sigma_{tb} + \lambda_b)\,t\right]}{(\sigma_{tb} + \lambda_b - \sigma_{ta}\phi_t)\,(\sigma_{tb}\phi_t + \lambda_b - \sigma_{tc} - \lambda_c)} \right. \qquad (1)$$

$$\left. \left. + \frac{\exp\left[-(\sigma_{ta}\phi_b)\,t\right]}{(\sigma_{tb}\phi_t + \lambda_b - \sigma_{ta}\phi_t)\,(\sigma_{tc}\phi_t + \lambda_c - \sigma_{ta}\phi_t)} - \frac{\exp\left[-(\sigma_{tc}\phi_t + \lambda_c)\,t\right]}{(\sigma_{tc}\phi_t + \lambda_c - \sigma_{ta}\phi_t)\,(\sigma_{tb}\phi_t + \lambda_b - \sigma_{tc}\phi_t - \lambda_c)} \right\} \right)$$

Where:

A_c is the Co^{58} activity corrected to the end of irradiation time, disintegrations/sec-gm
N_c is the concentration of Co^{58} nuclei, atoms/gm
N_{ao} is the initial concentration of Ni^{58} nuclei, atoms/gm
λ_c is the decay constant of 72-day Co^{58}, 1.1142×10^{-7}/sec
λ_b is the decay constant of 9-hour Co^{58}, 2.1394×10^{-5}/sec
σ_f'' is 64 millibarns, the fast neutron cross section of Ni^{58} for direct conversion to 72-day Co^{58}
σ_f' is 28 millibarns, the fast neutron cross section of Ni^{58} for direct conversion to 9-hour Co^{58}
σ_{ta} is 4.2 barns, the thermal neutron cross section of Ni^{58}
σ_{tb} is 150,000 barns, the thermal neutron cross section of 72-day Co^{58}
σ_{tc} is 1650 barns, the thermal neutron cross section of 9-hour Co^{58}
ϕ_f is the fast flux to be determined, n/cm^2-sec
ϕ_t is the thermal flux determined from Co^{60} total activity using 37 barns for Co^{59} cross section, n/cm^2-sec
t is the irradiation time, sec

Data from the neutron dosimeters activated during the initial irradiation of specimens in a core filler-block position have been reduced to fast neutron dosages, and are plotted in Figure 3.2-25. The use of a total cross section of 92 millibarns for production of Co^{58} infers that the neutron flux value obtained by means of Equation (1) is the Watt-fission spectrum "equivalent" neutron flux. The fraction of neutrons greater than 1 Mev in this spectrum is

$$\frac{\int_{1\ \text{Mev}}^{\infty} \phi\,(E)dE}{\int_0^{\infty} \phi\,(E)dE} = 0.693$$

where ϕ (E) is the energy dependence of the Watt-fission spectrum. The curves in Figure 3.2-25 do not contain the 0.693 factor.

Currently, iron dosimeters are being used in conjunction with the cobalt-nickel dosimeters. The (Fe^{54}, Mn^{54}) reaction is considered a better fast neutron detector than the (Ni^{58}, Co^{58}) reaction, especially for long-term irradiations. However, the cross sections and interfering reactions are not well established. Use of both types of dosimeters will permit correlation of dosages in the particular facilities used and facilitate transition to the iron dosimeters.

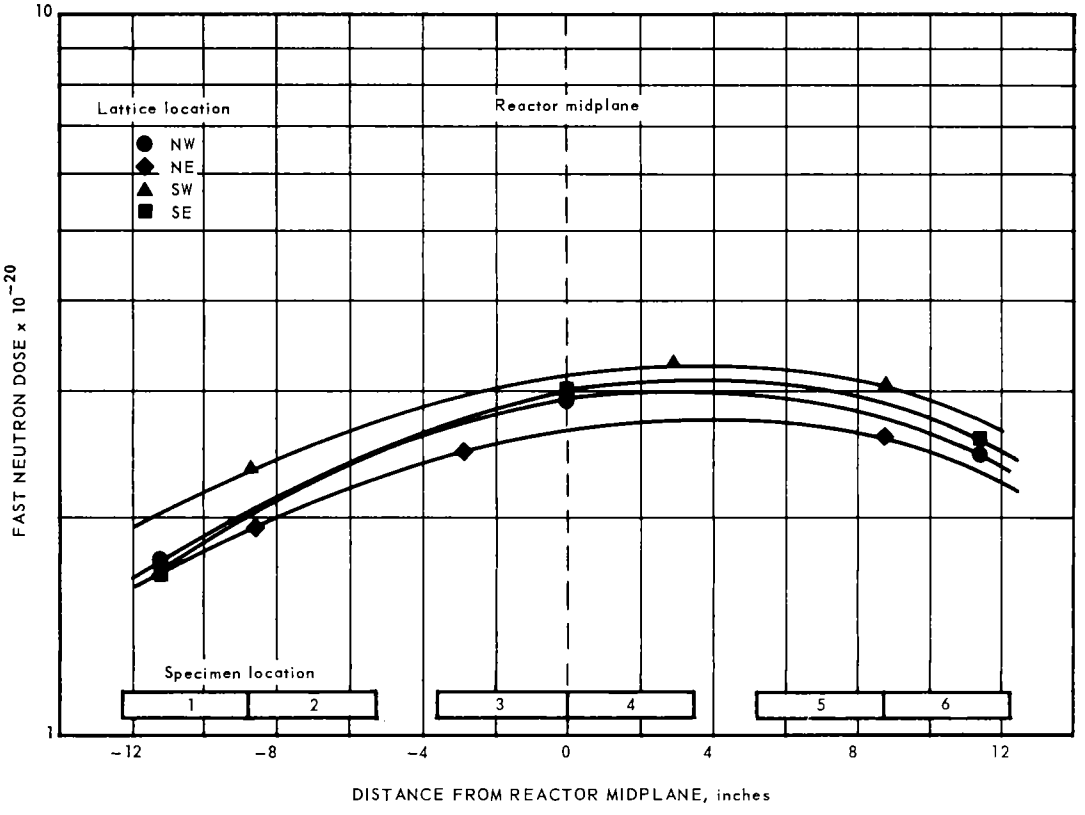

Fig. 3.2-25 – Fast neutron dosages of specimens irradiated in a core filler-block, using Co-Ni dosimeters

APPENDIX

REPORTS ISSUED DURING CALENDAR YEAR 1961

NMP-HTMP-1

High Temperature Materials Program Progress Report No. 1, May 1961 - June 30, 1961

GEMP-2

High Temperature Materials Program Progress Report No. 2, July 1, 1961 - July 31, 1961

GEMP-3A

High Temperature Materials Program Progress Report No. 3, Part A, July 1, 1961 - August 31, 1961, Unclassified

GEMP-3B

High Temperature Materials Program Progress Report No. 3, Part B, July 1, 1961 - August 31, 1961, Classified

GEMP-4A

High Temperature Materials Program Progress Report No. 4, Part A, August 1, 1961 - September 30, 1961, Unclassified

GEMP-4B

High Temperature Materials Program Progress Report No. 4, Part B, August 1, 1961 - September 30, 1961, Classified

GEMP-5A

High Temperature Materials Program Progress Report No. 5, Part A, November 15, 1961, Unclassified

GEMP-5B

High Temperature Materials Program Progress Report No. 5, Part B, November 15, 1961, Classified

GEMP-6A

High Temperature Materials Program Progress Report No. 6, Part A, December 15, 1961, Unclassified

GEMP-6B

High Temperature Materials Program Progress Report No. 6, Part B, December 15, 1961, Classified

GEMP-7A

High Temperature Materials Program Progress Report No. 7, Part A, January 15, 1962, Unclassified

GEMP-7B

High Temperature Materials Program Progress Report No. 7, Part B, January 15, 1962, Classified

GEMP-70

High Temperature Materials Program Progress Report No. 70, January 19, 1962, Unclassified

GEMP-101

A Method for Computing Primary Knock-On Spectra and Populations in Polyatomic Material Irradiated by Neutrons, October 1961, Unclassified

GEMP-102

Specialized Reactor - Shield Monte Carlo Program 18-0, October 1961, Unclassified

GEMP-103A

Summary of High Temperature Materials Work Performed in FY 61, Part A, May 1, 1961 - June 30, 1961, Confidential

GEMP-104

Testing of Fueled BeO at High Pressure in Five Different Environments, January 1962, Confidential

GEMP-105

Properties of Beryllium Intermetallic Compounds, Unclassified

E. A. Aitken, P. K. Conn, E. S. Collins, R. E. Honnell, "Studies of Fission Gas Release from In-Pile Tests: I - Recoil Loss from Ceramic Fuel Elements," Paper presented at "Joint Conferences - Nuclear Reactor Chemistry - Analytical Chemistry in Nuclear Reactor Technology," Gatlinburg, Tennessee, October 1961. To be published in the procedings of this meeting.

D. G. Besco and J. R. Beeler, "Bombardment of 'Two-Dimensional' BeO With Iodine," Bull. Am. Phys. Soc., 7, 48 (1962), (Nov.-Jan.)

FLIGHT PROPULSION LABORATORY DEPARTMENT

GENERAL ELECTRIC